Comparison of GNSS Processing Methodologies for Subsidence Monitoring
NAM GNSS Alternative Processing Method Project

van der Marel, H.

Publication date
2020

Document Version
Final published version

Citation (APA)
van der Marel, H. (2020). *Comparison of GNSS Processing Methodologies for Subsidence Monitoring: NAM GNSS Alternative Processing Method Project*. Nederlandse Aardolie Maatschappij.

NAM

Comparison of GNSS Processing Methodologies for Subsidence Monitoring, NAM GNSS Alternative Processing Method Project

Hans van der Marel

Delft University of Technology

Datum April 2020

Editors Jan van Elk & Dirk Doornhof

General Introduction

Gas production and the resulting reduction of reservoir pressure cause compaction of the reservoir formation. This is expressed as subsidence at surface, which e.g. requires measures to maintain the ground water level in the area above the Groningen gas field. Subsidence measurements are also used to determine the compaction of the gas reservoir, which drives seismicity in the Groningen area. Monitoring of subsidence is therefore an important activity for NAM. Different techniques are used to monitor subsidence: levelling surveys, GNNS-measurements and InSAR satellite observations.

The Study and Data Acquisition Plan for Winningsplan 2016 (Ref. 1 and 2) included a research program into the monitoring of subsidence aiming to improve the processing and interpretation of the GNSS (Ref. 3 and 4) and In-SAR technologies (Ref. 5 and 6).

The goal of the NAM GNSS Alternative Processing Methodologies project is to compare existing GNSS processing methodologies, to investigate potential biases in the solutions and to obtain transparent time series estimates (decomposition of signals) for NAM monitoring stations, with the final aim to detect deformation trend changes with predefined confidence levels.

In the current report three GNSS processing methods have been investigated: State Space modeling (SSR, currently used by NAM), regional network processing with the Bernese GNSS Software (BSW), and Precise Point Positioning (PPP).

References

1. Study and Data Acquisition Plan – Winningsplan 2016, NAM, Jan van Elk and Dirk Doornhof, April 2016
2. Study and Data Acquisition Plan update 2019, NAM, Jan van Elk and Dirk Doornhof, January 2019
3. Comparison of GNSS Processing Methodologies for Subsidence Monitoring, NAM GNSS APM Project Report, Hans van der Marel, TU Delft, Apr 2020.
4. GNSS-Processing in context with the 'Study and Data Acquisition Plan' related to the Production plan 'Winningsplan' Groningen, K. Hoentjen and L. Huisman, Geo-Information Services Kadaster, Mar 2019.
5. High resolution InSAR in the Groningen area - 2018-2019 Advanced Services, Yuxiao Qin, Jacqueline Salzer, Hanno Maljaars and Pieter Bas Leezenberg, SkyGeo, Nov 2019.
6. Improving the Functional and Stochastic Model of In-SAR, NAM INSAR FM SM Project Report, F.J. van Leijen, S. Samiei-Esfahany, H. van der Marel and R.F. Hanssen, TU Delft, Apr 2020.
7. Ensemble Based Subsidence application to the Ameland gas field – long term subsidence study part two (LTS-II) continued study. Technical report, 2017, NAM, Assen, Netherlands.

NAM

Title	**Comparison of GNSS Processing Methodologies for Subsidence Monitoring, NAM GNSS Alternative Processing Method Project**	**Date**	April 2020
		Initiator	NAM
Autor(s)	Hans van der Marel	**Editors**	Jan van Elk Dirk Doornhof
Organisation	Delft University of Technology	**Organisation**	NAM
Place in the Study and Data Acquisition Plan	Study Theme: Reservoir Compaction Comment: Gas production and the resulting reduction of reservoir pressure cause compaction of the reservoir formation. This is expressed as subsidence at surface, which e.g. requires measures to maintain the ground water level in the area above the Groningen gas field. Subsidence measurements are also used to determine the compaction of the gas reservoir, which drives seismicity in the Groningen area. Monitoring of subsidence is therefore an important activity for NAM. Different techniques are used to monitor subsidence: levelling surveys, GNNS-measurements and InSAR satellite observations. The Study and Data Acquisition Plan for Winningsplan 2016 included a research program into the monitoring of subsidence aiming to improve the processing and interpretation of the GNSS and In-SAR technologies. The goal of the NAM GNSS Alternative Processing Methodologies project is to compare existing GNSS processing methodologies, to investigate potential biases in the solutions and to obtain transparent time series estimates (decomposition of signals) for NAM monitoring stations, with the final aim to detect deformation trend changes with predefined confidence levels.		
Associated research	(1) Development of compaction models based on core measurements. (2) Inversion of subsidence to derive compaction estimates. (3) Seismological modelling.		
Used data	Measurements from GNNS stations.		
Associated organisations	06-GPS		
Assurance	Internal.		

Delft University of Technology

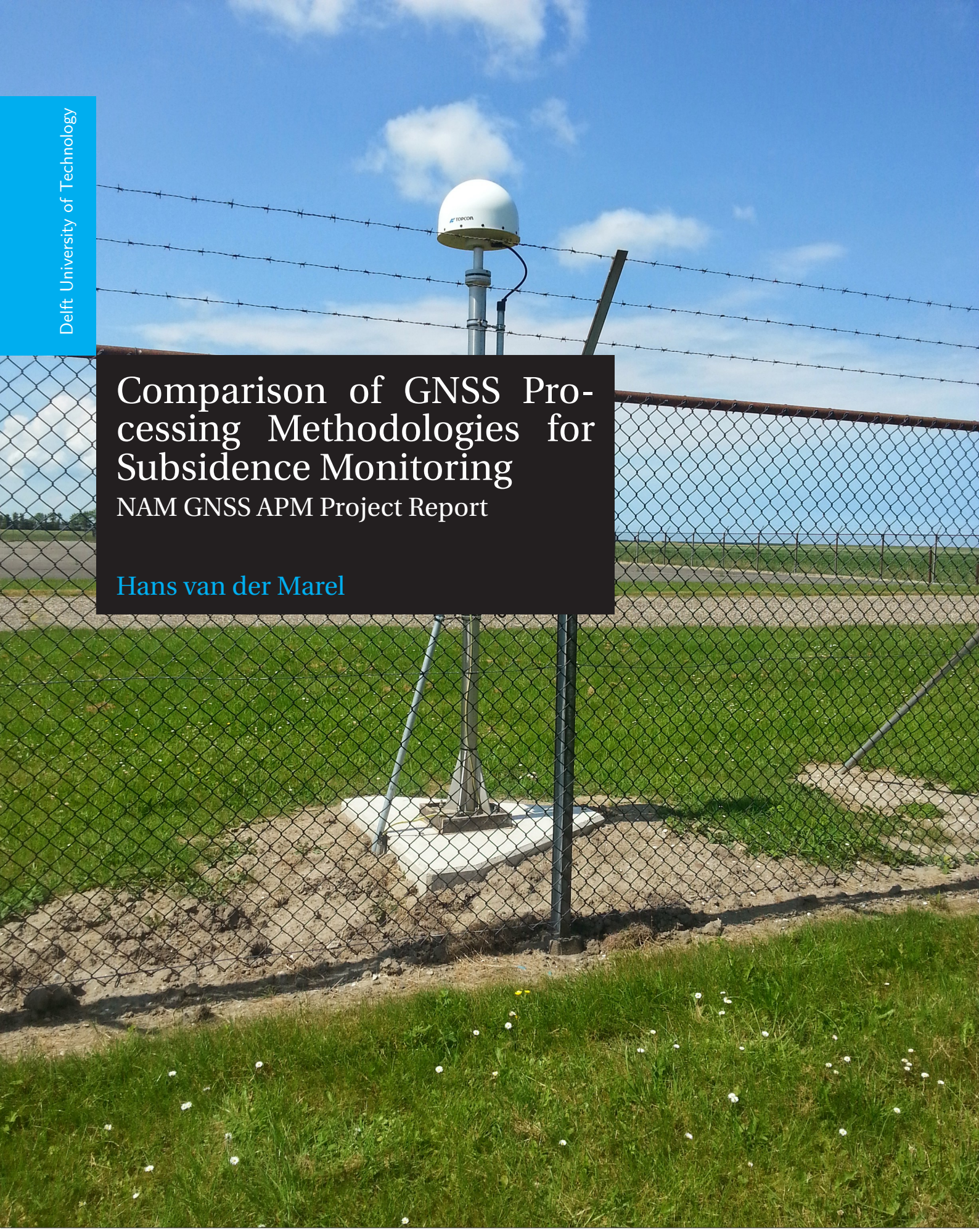

Comparison of GNSS Processing Methodologies for Subsidence Monitoring

NAM GNSS APM Project Report

Hans van der Marel

TU Delft Delft University of Technology

Challenge the future

The front cover shows the GNSS antenna of the NAM monitoring station at Usquert (picture NAM).

H. van der Marel

Comparison of GNSS Processing Methodologies for Subsidence Monitoring
NAM GNSS APM Project Report

17 April 2020

Final report for the Nederlandse Aardolie Maatschappij (NAM), GNSS Alternative Processing Methodologies (APM) project, Geodetic Studies TU Delft 2018/2019 (WO/NT No: 60301048 0020).

Publisher:
Faculty of Civil Engineering and Geosciences
Delft University of Technology
P.O. Box 5048
Stevinweg 1
2628 CN Delft
The Netherlands

The text has been type set using the MikTex 2.9 implementation of LaTeX. Graphs and diagrams were produced, if not mentioned otherwise, with Matlab and Inkscape.

CONTENTS

1

INTRODUCTION

The goal of the NAM GNSS Alternative Processing Methodologies (GNSS APM) project is to compare existing GNSS processing methodologies, to investigate potential biases in the solutions and to obtain transparent time series estimates (decomposition of signals) for NAM monitoring stations, with the final aim to detect deformation trend changes with predefined confidence levels.

In the project three different processing methodologies are investigated: State–Space modeling (SSR), EUREF standard regional network processing (BSW), and Precise Point Positioning (PPP). An overview of the main characteristics for each method is given in Table 1.1. For a more in–depth description of the methodologies the reader is referred to section 3.

Table 1.1: GNSS processing methodologies.

Name	Methodology	Main characteristics	Reference frame
SSR	State–Space Representation Kalman Filter	Undifferenced processing; local reference stations; state–space modeling.	Constrained to local reference stations with incremental coordinate updates.
BSW	EUREF standard regional network processing (Bernese software)	Double–differences; Ionosphere free linear combination; zenith troposphere delay (ZTD) estimation; IGS/EPN reference stations; precise IGS orbits.	Unconstrained (undistorted) best fit to selected IGS/EUREF reference stations in ITRF2008.
PPP	Precise Point Positioning	Precise IGS orbits and clocks; Ionosphere free linear combination; zenith troposphere delay (ZTD) estimation.	ITRF2008 provided by the satellite orbits and clocks.

The three processing methodologies have each been tested on the NAM monitoring stations in the North of the Netherlands. The NAM monitoring stations, which are located in the Groningen, Ameland and Drenthe area, are shown in Figure 1.1.

The SSR method is the method that is used by NAM for reporting subsidence in the study area. The data is processed by 06-GPS, on behalf of NAM, using the SSR method implemented by the Geo++ GNSMART software [Wübbena, Bagge, and Schmitz, 2001; Henry and Dentz, 2016; Dentz and Henry, 2019]. The EUREF standard regional network (Bernese) processing [Dach et al., 2015; Hoentjen and Huisman, 2019] and Precise Point Positioning (PPP) [Zumberge et al., 1997; Blewitt, Hammond, and Kreemer, 2018] methods are the alternative processing methods that are investigated in this study, and compared with the SSR method. Each of the processing method involves a different

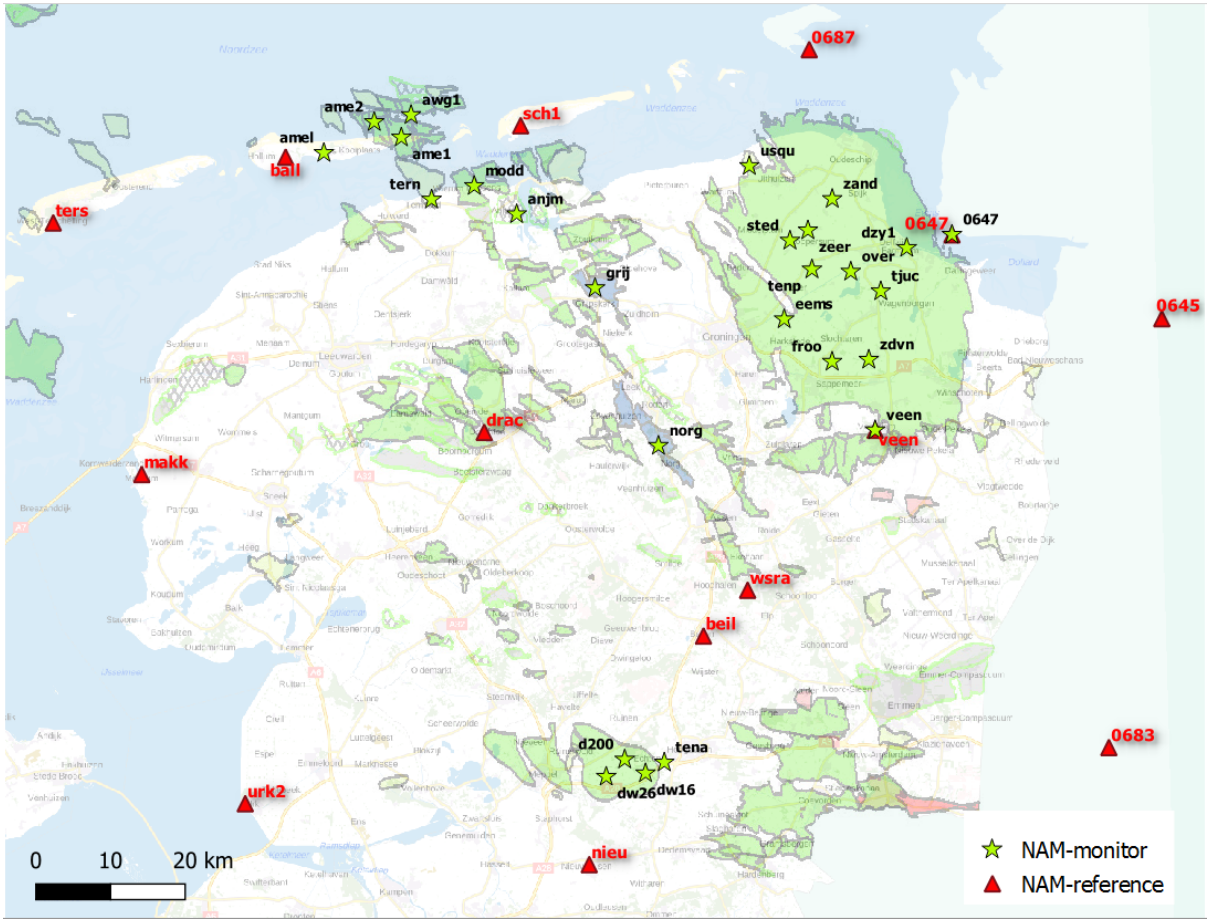

Figure 1.1: Network of NAM monitoring and reference stations.

data provider and processing software. This resulted in three completely independently processed GNSS time series datasets that are used as input for this study. An overview of the datasets, softwares and data providers is given in Table 1.2.

Table 1.2: GNSS datasets.

Name	Software	Data provider
SSR	Geo++ GNSMART v1.4.13	06–GPS, Sliedrecht, Netherlands
BSW	Bernese GNSS Software v5.2	Kadaster, Apeldoorn, Netherlands
PPP	Gipsy/Oasis v6.4	Nevada Geodetic Laboratory (NGL), Reno, Nevada, USA

The SSR dataset only includes the NAM monitoring stations. The BSW and PPP datasets, however, include many other stations in addition to the NAM monitoring stations, including the so–called NAM reference stations, of which the coordinates have been fixed (with incremental updates) in the SSR processing. Other groups of stations that have only been processed by the BSW and PPP methods are IGS and EUREF stations [Dow, Neilan, and Rizos, 2009; Bruyninx et al., 2019], which have been used by the BSW processing to best fit the solutions to the ITRF2008 reference frame [Altamimi, Collilieux, and Métivier, 2011; Altamimi et al., 2016], and the so–called AGRS stations and NETPOS stations in the Netherlands. The data from these stations plays a role in the analysis of the SSR reference station coordinates. The dataset are described in more detail in Section 4.

The time series in each input dataset is decomposed into several components [Marel, 2015; Williams, 2015]. The components are: long term trend using a spline function, annual and semi-annual components, temperature influence, atmospheric loading, time series steps, and residuals of the fit. Tem-

perature and pressure data from the Royal Netherlands Meteorological Institute (KNMI) is used in the estimation of the temperature influence and atmospheric loading. During a first iteration also two common mode components are estimated: (i) the common mode in the *residuals* (residual stack), and (ii) common mode of the *periodic parameters* (harmonics, temperature influence, and atmospheric loading). Common modes are signals that for a region of interest are the same, or, have a common cause, and are present in all the stations. For the estimation of the common mode however only a subset of well behaving stations is used. The common mode is removed in the second iteration, providing the final decomposition and common modes. It is important to note that the common modes do not affect the estimated long term trends, and only play a role in the comparison of the periodic components and stochastic properties of the solutions. This approach has been used before in Groningen [Marel, 2015], the Wadden Sea area [Leijen et al., 2017; Fokker et al., 2018] and the former mining area in Zuid-Limburg [Marel et al., 2016]. For more details on the procedure the reader is referred to Section 5. Results of the decomposition are given in Section 6.

In Section 7 the BSW and PPP time series for the NAM reference stations are used after a time series decomposition to analyze the coordinates that have been used as constraints in the SSR processing. The BSW and PPP time series for the NAM reference stations are also used to link the BSW and PPP solutions to a subset of the reference stations to provide a local correction to the ITRF2008 reference frame used by these solutions. The impact of these reference frame corrections on the estimated trend series of the NAM monitoring stations is analyzed in Section 8.

Finally in Section 9 the results are discussed in a broader context, and, conclusions and recommendations are given.

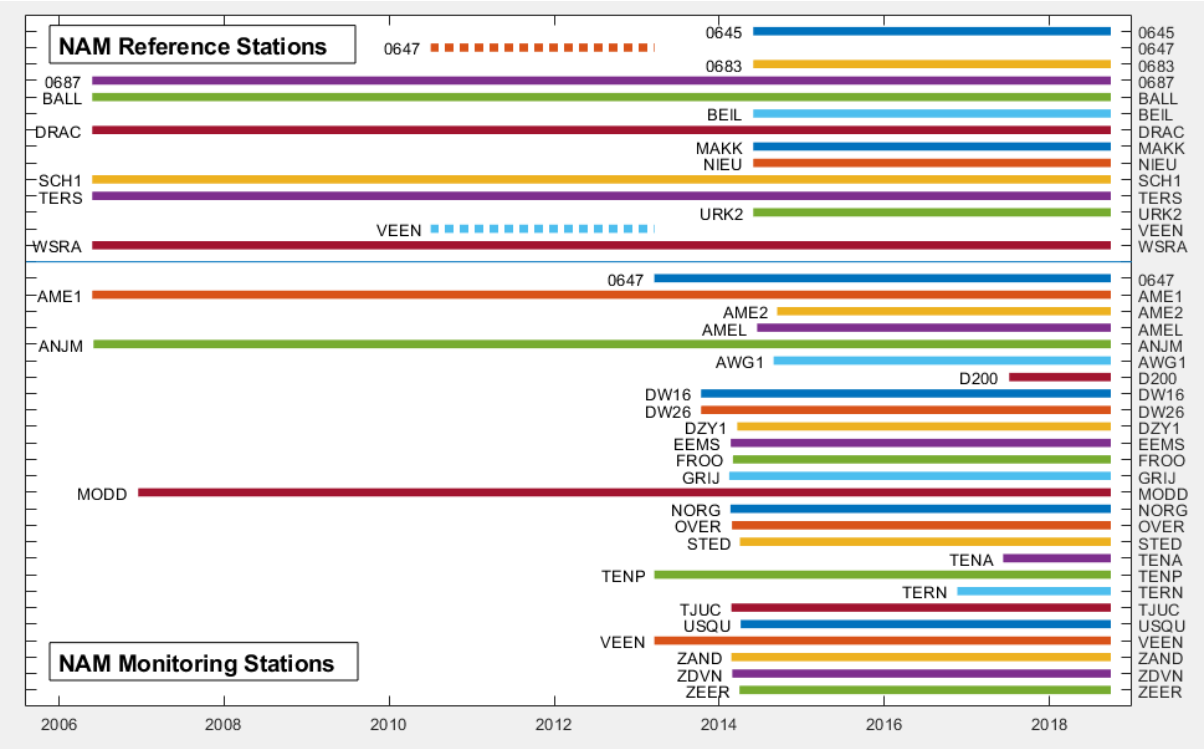

Figure 1.2: Timeline of NAM reference and monitoring stations. The stations VEEN and 0647 became monitoring stations in March 2013. Before March 2013 they were used as reference stations for GPS campaigns in the Waddenzee area, but, they have not been used as reference stations for the continuous stations AME1, ANJM or MODD.

2

NAM MONITORING AND REFERENCE STATION NETWORK

A map of the NAM monitoring and reference stations is shown in Figure 1.1, while the time history and status of the stations is shown in Figure 1.2.

2.1. NAM MONITORING STATIONS

In 2006 the first three NAM continuously operating GPS monitoring stations were installed in East-Ameland (AME1), Moddergat (MODD) and Anjum (ANJM) [Henry and Dentz, 2016]. For the processing by 06-GPS six reference stations were selected at the time.

On March 19, 2013, the first monitoring station in the Groningen area, Ten Post (TENP), was added to the network. At the same time the stations Veendam (VEEN) and Emden (0647), which were from 2010 until 2013 used as reference station for the GPS campaigns in the Waddenzee, became monitoring stations because of observed ground motions. Also, in October 2013 two monitoring stations near 'De Wijk' were added (DW16, DW26). In February and March 2014, ten more monitoring stations were added in the Groningen gas field area (DZY1, EEMS, FROO, OVER, STED, TJUC, USQU, ZAND, ZDVN, ZEER), bringing the number of monitoring stations in the Groningen gas field area to 11. At the same time two monitoring stations were installed at underground gas storage fields (NORG, GRIJ).

The reader should be aware that the station DZY1 (Delfzijl), is in called DZYL the 06-GPS reports [Henry and Dentz, 2016; Dentz and Henry, 2019]. However, in this report the name DZYL is used for the nearby NETPOS station and DZY1 for the 06-GPS station. This is confusing, but cannot be avoided when two operators use the same abbreviation for different stations, and since the NETPOS station became in service before the 06-GPS station it was decided – by convention – to rename the 06-GPS station in this report.

September 2014 two new monitoring stations were installed on platforms in the Noordzee (AME2, AWG1). The nature of the platforms is such that only the height components can be used for monitoring ground motions, and only after a correction for temperature related effects is applied. The horizontal components of the platforms should be interpreted with caution, as short term variations are likely related to structural changes and not ground motions, and only the long term trends in the horizontal components are maybe indicative of ground motion. In June 2014, the new AGRS.NL station in Nes Ameland (AMEL), just outside the gas-field, was added as monitoring station.

To facilitate the extension of the network also more reference stations were added. This brings the number of monitoring stations in 2014 to 23 and the number of reference stations to 12. At the end of 2016, and later in 2017, three more monitoring stations were added: two near 'De Wijk' (TENA, D200), and one in the Waddenzee area (TERN). This brings the total number of monitoring stations to 26 at the end of 2017. For a full list of monitoring stations with their commission date see Appendix A.1.

In 2018 twenty-six so–called Integrated Geodetic Reference Stations (IGRS) stations were installed in the Groningen area and added to the NAM monitoring network. The IGRS stations consist of a GNSS antenna and receiver, two backflipped 90cm triangular corner reflectors for InSAR, and a leveling bolts [Hanssen, 2019; Kamphuis, 2019]. The time series of these stations is, at the time of writing, too short to be useful for this project, and these stations are therefore not considered in this project, and not shown on the map or in the time line.

For all monitoring stations, except AGRS station Ameland (AMEL) and the station in Emden (0647), the same equipment is used: Topcon GB-1000/EG3_OEM GNSS receivers with a Topcon CR-3 choke ring antenna. For the station in Ameland (AMEL) initially a Leica GR25 receiver was used, but was replaced by a Trimble NETR9 in July 2016, for the antenna a Leica 3D choke-ring antenna (LEIAR25.R4 LEIT) was used over the full period. In Emden (0647) also a Leica 3D choke-ring antenna is used, but with a Leica GRX1200+GNSS receiver until June 2015, and a Septentrio PolaRx4 after June 2015. Further details are given in Appendix A.1. All antennas have been individually calibrated. For the GPS-processing raw observations per station are collected with an interval of 15 seconds.

2.2. NAM REFERENCE STATIONS

The network started in May 2006 with six reference stations, in Borkum (0687), Ballum (BALL), Drachten (DRAC), Schiermonnikoog (SCH1), West-Terschelling (TERS) and Westerbork (WSRA), with the focus on the Waddenzee area [Henry and Dentz, 2016]. The stations TERS in West-Terschelling and WSRA in Westerbork are part of the Dutch national GPS infrastructure (AGRS.NL) and the EUREF Permanent GPS Network (EPN). The station WSRA uses the same antenna as the EPN and IGS (International GNSS Service) station WSRT, but uses a different receiver. Because of this results for either WSRA or WSRT are very similar. The 06-GPS reference station in Schiermonnikoog (SCH1) is installed on the same building as the AGRS station Schiermonnikoog (SCHI), just 2.10 m away, but using different equipment. A word of warning, the 06-GPS reference station SCH1 is called SCHI in the 06-GPS reports [Henry and Dentz, 2016; Dentz and Henry, 2019], which can be confusing.

In July 2010 two already existing GPS stations were added to the list of NAM reference stations, in Emden (0647) and Veendam (VEEN) [Dentz and Henry, 2019]. However, 0647 and VEEN were only used as reference stations for the GPS campaigns[1] in the Waddenzee area, but not for the continuously operating stations AME1, ANJM or MODD that feature in this report. In March 2013, station VEEN and 0647 were removed from the list of reference stations, because of observed station motion, and are since then processed as NAM monitoring station.

To facilitate the extension of the network to the Groningen and De Wijk areas, five extra reference stations were added in October 2013, Makkum (MAKK), Urk (URK2), Beilen (BEIL), Nieuwleusen (NIEU) and Meppen (0683). In September 2014, one more reference station, in Leer (0645), was added. This brings the final number of reference stations since May 2014 to 12.

Since then no changes in the network of reference station occurred, except for a relocation of the reference station Nieuwleusen (NIEU) by roughly 50 m at the end of 2015.

The reference stations BALL, BEIL, DRAC, MAKK, NIEU, SCH1 and VEEN, which are operated directly by 06-GPS, use more or less the same equipment as the monitoring stations: Topcon GB-1000/EG3_OEM GNSS receivers with a Topcon CR-3 choke ring antenna. For the other stations, Borkum (0687), Emden (0647), Leer (0645), Meppen (0683), Terschelling (TERS) and Westerbork (WSRA) different equipment is used. A full overview of the equipment used is given in Appendix A.2. All antennas are individually calibrated, except for the antenna at Westerbork.

2.3. OTHER STATIONS

The BSW and PPP datasets include other stations besides the NAM monitoring and reference stations. These are

[1] These campaigns fall outside the scope of this report.

- All IGS and EUREF stations in the Netherlands, and several IGS and EUREF stations from Belgium, Germany, UK, Sweden and Switzerland. These stations have good coordinates in the ITRF2008 reference frame and have been used by the Bernese solutions to connect to ITRF. These stations have also been processed in the PPP processing, but in the PPP processing they are not used (directly) for the reference frame connection.
- All AGRS stations,
- All NETPOS stations.

The data from the IGS, EUREF and AGRS stations plays a role in the analysis of the coordinates that have been constrained in the SSR processing.

Some of the NETPOS and AGRS stations are located near NAM monitoring and reference stations: the NETPOS station Delfzijl (DZYL) is 425 m to the South-East from the NAM monitoring station DZY1, and the AGRS station Schiermonnikoog (SCHI) is installed on the same building as the NAM reference station SCH1, separated by just 2.10 m. The stations DZYL and SCHI have been added to the analysis in this report, but the reader should realize that these stations are only available in the BSW and PPP solutions as they and are not processed in the SSR solution. Confusing is that the 06-GPS stations DZY1 and SCH1 are actually called DZYL and SCHI in the 06-GPS reports.

The BSW and PPP processing include all other NETPOS stations and comparisons between the BSW and PPP solutions for these stations are possible. However, in this report we focus only on comparisons in the region of interest, using the subset of NETPOS stations DZYL and SCHI.

The AGRS station WSRA, which is one of the NAM reference stations, is not included in the PPP processing. Instead, the IGS station WSRT, which uses the same antenna as WSRA, has been processed. The BSW solutions for WSRT and WSRA are nearly identical, so for the PPP solutions, we can safely use WSRT instead of WSRA in the comparisons.

The meta data for the stations DZYL, SCHI and WSRT is given in Appendix A.3.

The PPP solution also includes some stations from LNR-GlobalCom (Lauwersoog, Delfzijl, Hoogezand-Sappermeer) in the region of interest, but they were not included in the analysis because there is no second solution to compare with. There is also a station in Roden that is operated by Geometius which hasn't been processed by any of the solutions.

The dataset are described in more detail in Section 4.

3

PROCESSING METHODOLOGIES

In this section the SSR, BSW and PPP processing methodologies are described. It is assumed that the reader is familiar with the basics of GNSS and GNSS data processing. For a comprehensive background on GNSS we refer to the Handbook of Global Navigation Satellite Systems [Teunissen and Montenbruck, 2017] or one of the many GNSS textbooks.

3.1. STATE–SPACE REPRESENTATION (SSR) METHOD

The data from the GPS monitoring stations is post-processed by 06-GPS using the GNSMART software of Geo++ GmbH, Hannover, Germany [Wübbena, Bagge, and Schmitz, 2001]. The Geo++ software is able to deliver a highly accurate result for the combination of fixed GPS reference stations and dynamic GPS monitoring stations in one single processing, with optimal use of antenna calibration models and state–space modeling of all GPS error sources. In 2005 successful tests were carried out with this software package at the Anjum site, where deliberate lowering of the GPS-antenna could be detected at the mm-level, within a few days of observation time [GeoService, 2006a; GeoService, 2006b].

3.1.1. GNSMART SOFTWARE

GNSMART stands for "GNSS State Monitoring and Representation Technique". A complete state space model (SSM) with millimeter-accuracy is implemented for the rigorous and simultaneous adjustment of GNSS observables, which is essential to resolve phase ambiguities, as well as to mitigate major GNSS error sources. To determine the (error) state of a GNSS system, GNSMART estimates the following state parameters:

- satellite clock error, satellite signal delays (group delays) and satellite orbit error (kinematic orbits)
- ionospheric and tropospheric signal propagation delays
- carrier phase ambiguities
- receiver clock error and receiver signal delays (group delays)
- receiver coordinates (fixed, dynamic or relaxed)
- receiver multipath (optional; not included in the 06–GPS processing)

For the receiver coordinates various models can be used in a single processing run: fixed coordinates for GPS reference stations, dynamic (filtered) for GPS monitoring stations and relaxed (unknown with a-priori sigma) for campaign stations and reference station coordinate updates.

The state-space modeling of GNSMART applies several corrections to the GNSS observations before the parameter estimation. The SSM model is set up for the following corrections:

- satellite-receiver phase wind-up effect (satellite attitude)
- (absolute) satellite and receiver antenna phase center variation (PCV) correction
- relativistic corrections (satellite clock error and orbit computation)
- site displacement effect (solid earth tide and ocean loading included; pole tide and atmospheric loading not included for current network)
- higher order ionospheric correction (not included for current network)

For the current network GNSMART does not correct for atmospheric loading effects and higher-order ionosphere. This is not necessary because of the small size of the network [GeoService, 2006a; Henry and Dentz, 2016] [1]. Ocean loading however cannot be neglected. The variation in ocean loading is significant over the extend of the network and is predominately present for stations near the coast. A correction for ocean loading is applied using the FES2004 model, with station dependent coefficients provided in by the free ocean tide loading provider, courtesy Onsala Space Observatory, Chalmers University, Sweden [Dentz, 2019].

The adjustment model is a Kalman filter for the simultaneous adjustment of all L1 and L2 observations. It results in one rigorous solution of all stations, fixed, dynamic or relaxed, with all correlations known in one run. The adjustment uses IGS Ultra rapid precise orbits [Henry and Dentz, 2016; Dow, Neilan, and Rizos, 2009]. The Kalman filter is run in post-processing mode over periods of five to six weeks, using all available reference, monitoring and campaign stations for that period. Each period overlaps by one week [Dentz, 2019]. The first week[2] is used for the Kalman filter to obtain a steady state and is not used for the final solution. Therefore, each run results in a one month final solution. The coordinates are computed with an interval of one hour.

The reference station coordinates in each run are kept fixed (not adjusted) using coordinates determined by a special procedure described in Section 3.1.2. For the monitoring stations a dynamics model is used. Two options have been investigated by Geo++ and 06-GPS [GeoService, 2006a]: the first uses dynamics of the coordinate residuals of 1mm/day, while the second uses dynamics of 1mm/hour. For the final processing a dynamics of the coordinate residuals of 1 mm/hour was selected [Henry and Dentz, 2016; Dentz, 2019].

The 06-GPS processing results give the height of each ARP (Antenna Reference Point), which is the bottom of the antenna pre-amplifier.

3.1.2. REFERENCE STATION COORDINATES

In order to obtain reliable results it is necessary to have accurate and homogeneous coordinates for the reference stations. Discrepancies between the reference station coordinates, which will be kept fixed in the processing, should be as small as possible.

To compute the initial coordinates of the reference stations 06-GPS processed a complete month (July 2006) of reference station data using the GNSMART software. In this processing run the coordinates of the AGRS.NL stations in Terschelling en Westerbork, and the station in Borkum, were fixed to values published in ETRS89 using the ETRF2000 realization [Dentz and Henry, 2019; Dentz, 2019]. The coordinates of the other reference stations were computed. This provided an initial set of coordinates for the NAM reference stations in ETRS89/ETRF2000.

The GNSMART software internally does all its computations in the International Terrestrial Reference Frame (ITRF). This is the reference frame used by the precise IGS satellite orbits that are used in the processing. The reference station coordinates are transformed into ITRF coordinates at the epoch of measurement, using a 14 parameter datum transformation. The internal processing is performed in ITRF. The estimated coordinates for the monitoring stations are transformed back into the reference frame of the reference stations before output [Dentz, 2019].

[1] That the effect for atmospheric loading is negligible is confirmed by the analysis in in this report.
[2] Currently a one week period is used, in the past also a two week period was used.

The data from the continuously operating NAM monitoring stations is processed by 06-GPS since 2006 on a monthly basis in a network with reference stations (see Figure 1.1). The coordinates of these reference stations are kept fixed (standard deviation of 0.0 mm) to the previously computed values. The coordinates of the monitoring stations get some freedom to move, using a dynamics model with a standard deviation of 1 mm/hour. However, there is always the possibility that the positions of the reference stations change as well. This can be due to physical movements or due to instrumental changes, such as an antenna replacement.

To detect changes in the reference station coordinates the reference station coordinates are checked periodically. In case movement is detected in one or more reference stations, the coordinates of the reference stations are updated. The reference station coordinates are checked by 06-GPS, starting 2009, once per year using the following procedure [Dentz and Henry, 2019; Dentz, 2019]:

a. Recalculation of all reference station coordinates using GNSMART by giving them an a-priori standard deviation of 1.0 mm for the horizontal position and 2.0 mm for the height. In this run only the reference stations are included (the monitor stations are not processed), using four weeks of data, of which the first 48 hours are not used to stabilize the filter [Dentz, 2019]. For the coordinates the “relaxed reference station with a-priori accuracy" option of the Geo++ software is used (This is different from the monitoring stations, for which a dynamics model with a standard deviation of 1 mm/hour is used). The coordinates, which are computed every hour, are averaged to obtain the final product of the run (the first 48 hours are not used in the averaging). The final result of this run are coordinates that are a best fit (in least squares sense) to the a-priori (previous) values of the coordinates and the state–space modeling of the error sources in GNSMART.

b. The coordinates of reference stations, with a deviation of more than 2.0 mm (in any of the components) compared to the existing coordinates, are changed.

c. The calculation of step a. is run again with the new coordinates to check that the coordinates remain within the 2.0 mm limit. If that is the case, the modified coordinates will be used in the subsequent computations of the monitoring stations [Dentz, 2019].

d. The network of monitoring stations is processed again with all reference stations fixed to the new coordinates, and the newly computed coordinates for the monitoring stations are compared to the previous values, in order to calculate the influence of the new reference station coordinates on the monitoring station coordinates.

The reference station coordinates have been checked every year from 2009 on-wards, usually in the month of May. Each check involved the analysis of four weeks of data. Typically there are only a few reference stations for which the coordinates exceed the limits. For instance, in 2009 and 2011 two reference stations needed updates, but in 2010 no updates were needed. The monitoring station coordinates over the reference station check period, usually the month of May, are thus computed twice. Once with the old reference station coordinates, and once with the new coordinates. The influence of the change in reference station coordinates on the GPS monitoring stations was always smaller than 1 mm, often even smaller than 0.5 mm, depending on the distance to the reference station for which the coordinates were changed.

In case there is an antenna change in one of reference stations, the coordinates of that station are recomputed immediately within the reference station network, keeping the reference station coordinates fixed except for the station with the antenna change. The coordinates of that station are fixed to the new coordinates in subsequent runs of the monitoring network, so that an antenna change at a reference station doesn't have any consequences for the monitoring stations [Dentz, 2019].

In Section 7 the time evolution of the fixed coordinates of the reference stations is shown and compared to values computed from the BSW and PPP processing.

3.2. BERNESE SOFTWARE PROCESSING (BSW) METHOD

The Bernese GNSS Software is a scientific, high-precision, multi-GNSS data processing software developed by the Astronomical Institute of the University of Bern (AIUB) [Dach et al., 2015]. The Bernese GNSS software can be used for a variety of applications, ranging from a single GPS short baseline, to high precision campaigns with baselines of several hundred to thousands of kilometers, up to the determination of precise orbits and Earth Rotation Parameters (ERP). The software is used by the Center for Orbit Determination in Europe (CODE) for the routine analysis of the global IGS network, including the computation of precise orbits, clocks, Earth rotation parameters and station coordinates. The software is also used by most analysis centers for the EUREF Permanent GNSS Network (EPN), which is the European densification of the global IGS network [Bruyninx et al., 2009], as well as by many national mapping agencies, scientific institutes and universities for the processing of GNSS campaigns and data from Continuously Observing Reference Stations (CORS).

The Bernese GPS program system consists of more than 30 Fortran programs. Most of these programs run in a batch mode and do not need any user interaction during execution time. The program options and lists of data and parameter files are prepared by the Bernese GPS Menu system, from which also the programs can be started in either interactive mode or batch mode. The batch mode processing can be highly automated, allowing to run more or less similar runs on a hourly to daily basis.

The Bernese GNSS software uses double differencing on the observations. In the double differencing approach the satellite and receiver clock parameters are eliminated on an epoch-by-epoch basis by forming differences of the observations. First, observations of two different receivers to the same satellite are subtracted, eliminating the satellite clock parameters, giving the so-called single difference. Next, two single differences are subtracted to eliminate the receiver clock parameter, giving the double difference. This greatly reduces the amount of parameters to be estimated in the batch least squares adjustment, leaving basically only station coordinates, phase ambiguities and Zenith Troposphere Delay (ZTD) to be estimated in regional sized networks. The ionosphere delay is eliminated by forming the ionosphere free linear combination from dual frequency observations, but the Bernese GNSS software also has options for local, regional and global ionosphere modeling. The double difference carrier phase ambiguities, which should be integer, are estimated initially as float numbers and then, in a separate process, using various techniques depending on the baseline length, fixed to integer values. The rate of success depends on the length of the baselines, but usually above 90% of the ambiguities is fixed to integers.

In the zero difference approach — used by GNSMART and Gipsy/Oasis for the two other processing methods that are investigated — the satellite and receiver clock parameters are estimated along with the other parameters, using a Kalman-filter type of approach. The zero difference and double difference approach give in theory identical results, although the implementation in software may result in small differences. The main advantage of the double difference approach, which uses weighted least squares, is that it results in normal equations, which later on can be combined to constrain the solution or combine different estimates. The main disadvantage of the double difference approach is that, because of correlations introduced in the double differencing process, the co–variance matrix of observations (which need to be inverted) is almost full, and albeit the software uses some sophisticated techniques to handle these matrices, it does have implications for the number of stations that can be processed. The main advantage of the zero difference approach is that it is a little bit more flexible with respect to changes in the tracking configuration, and that it can be used for processing single stations. The other advantage is that it is more easy to use a Kalman filter (although a Kalman filter is sometimes also used in single or double difference processing), and is therefore is a little more flexible in modeling the time-behavior of parameters such as ZTD.

The geographic reach or domain of the GNSS network is an important consideration in the processing. In a short baseline or local network only coordinates and ZTD differences between stations can be estimated; this is because the satellite clock parameters have to be estimated or eliminated. Coordinates of at least one station in the network, in the reference frame of the satellite orbits and

with a quality better than the satellite orbits, is needed to constrain the network. 'Absolute' ZTD's can be estimated only when the network is covering a sizable region, because then the same satellite is seen from different elevation angles at different stations that allow one to estimated both satellite clock parameters as well as absolute ZTD. Another important reason to extend the geographic reach is to include more than one reference, or fiducial, station, and use only those reference stations which are of high quality, have observations available in the public domain, and with reliable coordinates in the International Terrestrial Reference Frame (ITRF). The reference stations that fulfill these needs are notably IGS stations, EPN stations in Europe, and AGRS.NL stations in the Netherlands. When the network becomes global also the satellite orbit and Earth Rotation (ERP) parameters can be estimated along with station coordinates, zenith delays and other parameters. This is the type of processing that is used by IGS analysis centers.

The NAM data is processed by the Kadaster, using the Bernese GNSS Software Version 5.2, following the guidelines for the European Permanent Network (EPN) Analysis Centers [Hoentjen and Huisman, 2019]. This is a type of regional processing that has been standardized to a large extend in the Bernese GNSS software, and is used for a lot of the campaign processing and routine processing of continuously operating GNSS stations for the densification of the IGS and EPN networks [3]. This processing has been scripted in the BSW in a process called `RNX2SNX` (Rinex to Sinex) [Dach et al., 2015].

The network processed by the Kadaster consists of the following stations:

- IGS GNSS reference stations BRUS, BRUX, HERS, KOSG, MORP, ONSA, POTS, WSRT, WTZR and ZIMM,
- AGRS.NL stations, NETPOS stations, NAM monitoring and reference stations.

A total of 108 station have been processed for this study. All stations in the second category are processed in the same way. The AGRS.NL and NETPOS stations were included for reasons given in [Hoentjen and Huisman, 2019]. The availability of data and solutions is 99.5% on average. The data interval was 10 or 30 seconds (Rinex-2 file format).

The following external products and models were used in the processing:

- IGS precise satellite ephemerides, Earth rotation parameters, and satellite ANTEX antenna phase center models. No consistent set of products was available for the period from 01-01-2007 up to and including 01-07-2018, see Table 3.1 for details of the used products,
- CODE Differential code and phase biases, and ionosphere delay models,
- Global Mapping Function (GMF), the Global Pressure Temperature (GPT) model, as well as the gradient model of Chen and Herring (CHENHER),
- FES2004 model for the correction of ocean loading, with station depended parameters computed by the free ocean tide loading provider website of Chalmers University of Technology, Sweden.
- Individual receiver antenna calibrations, when available, if not (e.g. IGS reference stations) the values from I08.ATX or I14.ATX were used. See Table 3.1.

Following the EUREF guidelines, the station coordinates are estimated on a daily basis, troposphere ZTD parameters have been computed once per hour, and the troposphere gradient parameters once per day, following the general settings in the `RNX2SNX` script provided with the Bernese GNSS software. The ionospheric delay was eliminated using the ionospheric free linear combination, with a correction for the higher order ionospheric term. Baselines for the double differencing were formed

[3] The Bernese GNSS Software can also do a PPP solution, but this option is mainly used to obtain good approximate coordinates for a final processing in network mode

using an algorithm that maximizes the number of observations. Integer double difference carrier phase ambiguities were computed baseline by baseline, using several strategies, maximizing the number of resolved integer ambiguities. The double–difference residuals are checked for outliers, and if necessary, the computations are repeated without the detected outliers.

Table 3.1: IGS products used by the BSW processing [Hoentjen and Huisman, 2019].

		IGS satellite products		**IGS reference stations**	
From	To	Orbits, clocks and ERP	Satellite antenna models	ITRS realisation	Receiver antenna models
2007-01-01	2015-02-14	IGS repro2	I08.ATX	IGb08	I08.ATX
2015-02-15	2017-01-28	IGS final	I08.ATX	IGb08	I08.ATX
2017-01-29	2018-07-01	IGS final	I14.ATX	IGb08	I08.ATX *)

*) I14.ATX in alternative solutions.

The IGS stations BRUS, BRUX, HERS, KOSG, MORP, ONSA, POTS, WSRT, WTZR and ZIMM have been used in linking the daily coordinate solutions to the International Terrestrial Reference Frame 2008 (ITRF2008). The coordinates and velocities of the IGb08 realization of ITRF2008 have been used; the values, at epoch 2005-01-01, are given in Hoentjen and Huisman, 2019, and have been propagated to the epoch of measurement by the Bernese software. The connection to the IGb08 is made using the minimum number of constraints possible: only three shifts are estimated for each daily solution, using weighted least–squares to minimize the coordinates residuals of the IGS stations with respect to the IGb08. In this way, a so–called free network solution is obtained, that is aligned through IGb08 to the ITRF2008.

The main deliverable from the Kadaster to this project was the previously described dataset in IGb08. As secondary deliverable three more datasets were provided

- Free network solution, as with the main product, but as of 29 January 2017 in IGS14 instead of IGb08, using I14.ATX instead of I08.ATX for the receiver antenna model of the IGS stations,
- The previous solution, transformed into ETRS89 realization ETRF2000(R08), following EUREF guidelines,
- The previous solution, but now given in the Dutch realization of ETRS89, ETRF2000 based on AGRS.NL.

In this study only the main deliverable, the homogenized solution in IGb08, is used. Using I14.ATX instead of I08.ATX for the receiver antenna calibration after 29 January 2017, resulted otherwise in additional unwanted steps in the solution.

3.3. PRECISE POINT POSITIONING (PPP) METHOD

Precise Point Positioning (PPP) is a positioning technique aimed at processing un–differenced carrier phase and pseudo-range measurements from a stand-alone GNSS receiver to compute positions with a high, decimeter or centimeter, accuracy everywhere on the globe. To facilitate the PPP technique precise GNSS satellite orbit and clock solutions are required. Precise GNSS satellite orbit and clock solutions are available from the International GNSS Service (IGS) for post-processing applications, but also more and more real-time orbit and clock solutions are becoming available.

The PPP technique has become very popular in the scientific and research communities for applications that require high accuracy and in which latency was not important, but for which a full network solution is too complicated. With the advent of real-time orbit and clock solutions the PPP technique is now also used for a wide range of applications such as offshore positioning, aircraft navigation, high-precision farming and meteorology. The main problem so-far for real-time applications is the relatively long convergence time (in the order of 10-30 minutes) of the algorithm to the desired accuracy, especially when compared to RTK techniques.

So far high-precision PPP was geared towards users employing dual frequency receivers. More recently also high accuracy positioning using stand-alone single-frequency GPS receivers is investigated. Single frequency receivers, which are being used, for instance, in geo-referencing applications and precise agriculture, are becoming popular thanks to a lower price relative to their dual-frequency counterparts. The performance of the single frequency PPP is mainly driven by the quality of existing ionosphere models.

In the Precise Point Positioning (PPP) approach previously estimated satellite clock parameters from a global network are used, in addition to the satellite orbits and ERP that were needed for the network processing [Zumberge et al., 1997]. Therefore, for each station only station coordinates, epoch-wise receiver clock parameters, ZTD and phase ambiguities have to be estimated. One of the advantages of the PPP approach is that stations can be processed station by station, and that it is not necessary to process a regional network. The downside of the PPP approach that it is more difficult to estimate integer phase ambiguities, as is often done in the network approach. This is only possible in the PPP approach when several stations are processed together, or, using additional products from the global network processing.

It is essential in the PPP approach that orbits, ERP and satellite clock parameters come from the same source. These parameters are in general highly correlated. In order to get the best results the software and models used for PPP, must be the same as those used to generate orbit and clock products. It is essential that the PPP applications use the same correction models as those use to generate satellite orbits and clocks in the global network processing.

From a theoretical point of view the PPP solution is equivalent to a network solution using a step–wise processing. In the first step a global network is analyzed by a global analysis center, while in the second step the user receiver data is processed using products from the first step. This means that the PPP technique is capable of delivering the same millimeter accuracy as network solutions do, and also, that integer ambiguity resolution is possible. It is only because of a few practical limitations and choices that the performance of PPP is slightly below the performance of network solutions. It is important to understand these practical limitations, their impact and possible solutions. However, the main strength of the PPP lies in the volume of data that can be processed and scalability in term of number of stations. In the PPP processing processing times scale linearly with the number of stations because each user station can be processed by itself. In case of the network processing, because all stations have to be processed together, there is also a quadratic term involved. This makes it possible with PPP to process very large number of stations on a routine basis.

Nevada Geodetic Laboratory (NGL) provides a long-running service to the scientific community that includes data products for over 17,000 stations available online, including metadata, lists of stations, plots of position coordinates, tables of data holdings, and descriptions of new items relating to the products, benefiting many kinds of Earth science [Blewitt, Hammond, and Kreemer, 2018]. The products can be found on the NGL webpage `http://geodesy.unr.edu/`. In total, NGL scours more than 130 Internet archives in an attempt to find possible useful GPS data, including the Netherlands. Data for the Netherlands, including the AGRS.NL, NETPOS, 06-GPS and NAM monitoring and reference stations, is provided through the Dutch Permanent GNSS Array website, which collects the data from the different providers. Every week, NGL updates the daily position coordinates, and updates the computed velocities. NGL also provides a free GPS Data Processing and Data Products System for Earth Science, inviting people to contribute new data.

The GPS data analysis at NGL is carried out with the GISPY-OASIS-II software package v6.4 and analysis products provided to NGL by the Jet Propulsion Laboratory, Pasadena, California [Zumberge et al., 1997]. Starting November 2019 all data in the NGL holdings have been reprocessed with the new and improved GipsyX v1.0 software, using the IGS14 instead of IGb08. In this study we used the data processed in IGb08 using GIPSY-OASIS-II v6.4. The main characteristics of the processing are

- Undifferenced ionosphere-free carrier phase and un-differenced ionosphere-free pseudo-range, elevation angle cutoff 7 degrees, sampling rate 5 minutes, CA-P1 biases from CODE applied,

- Ionosphere 1st order effect removed by linear combinations, 2nd order effect modeled,
- A-priori wet and dry troposphere from GPT2 model, GPT2 mapping function, estimation of Zenith delay and gradients as random walk every 5 minutes,
- GPS satellite orbit position/velocity estimates, GPS satellite clock estimates, GPS satellite attitude parameters, WLPB estimates (widelane and phase biases) and daily transformation parameters from NNR to IGS14 from JPL,
- Solid earth and pole tide from IERS 2010 Conventions, permanent tide not removed from model
- Ocean Tide Loading diurnal, semi-diurnal, MF, and MM model FES2004, semi-annual self-consistent equilibrium model, hardisp.f from IERS2010,
- Satellite phase centers offsets and PCV model from igs14_wwww.pcm applied,
- Receiver antenna and radome types from RINEX header, receiver antenna PCV model from igs14_wwww.atx applied,

Starting November 2019 all data in the NGL holdings have been reprocessed with the new and improved GipsyX v1.0 software. The new results use improved models including the VMF1 mapping function and nominal troposphere, elevation weighted observations, and higher order ionospheric calibrations, improved JPL Repro 3 orbits, and the latest global reference frame IGS14. The updated products have not been used in this study.

4

INPUT DATASETS

The output of the GNSS processing is provided in different data formats. Before attempting the decomposition, the various datasets are read in Matlab and converted into a Matlab structure array that is input for the next phase: the decomposition of the signals. The format of the Matlab structure array is the same for each dataset. Each element of the structure array contains the data for a single station. The structure for each station contains a reference epoch and position, daily position time series in North, East and Up displacements (coordinate differences) with respect to the reference position in ETRF2000, with the date and time and precision of the coordinates, a list of events, as well as other meta data. In this section the import and conversion of the data is described.

4.1. STATE–SPACE REPRESENTATION (SSR) METHOD

4.1.1. NAM MONITORING STATIONS

Data from NAM monitoring stations is processed by 06-GPS using the Geo++ GNSMART software [Henry and Dentz, 2016]. The results of the processing are provided in the form of csv files (one per station) with the date, time, longitude, latitude and height. A data point is provided every hour. A Matlab script reads the csv files and converts these into a Matlab structure array. Each element of the structure array contains the data for a single station. The resulting structure array is saved to the mat file `tsSSR.mat`.

During the conversion several consistency checks are carried out: i) some parts of the dataset with invalid data need to be removed, and ii) duplicate epochs have to be detected and removed. Periods with missing data are still included in the input dataset, just repeating the last computed position until new data is included. This is a byproduct of the filter approach used by GNSMART. This data must be removed from the time series, this is a complicated process that has been implemented in a dedicated function. Of course, it would be much better if this data was not included in the first place.

The station `DZYL` was renamed to `DZY1` in order to use the same names as in the other solutions.

The latitude, longitude and height are converted into North, East and Up time series (in meters) with respect to a reference position and epoch. The reference position and epoch are computed as the mean of the positions and epochs. The reference epoch is rounded to the nearest start of the year. The North, East and Up displacements are computed from ellipsoidal coordinate time series $(\varphi, \lambda, h)_k$, with

$$\begin{aligned} dN_k &= (\bar{M}(\varphi_0) + h_0) \cdot (\varphi_k - \varphi_0) \\ dE_k &= (\bar{N}(\varphi_0) + h_0) \cdot \cos\varphi_0 \cdot (\lambda_k - \lambda_0) \\ dU_k &= h_k - h_0 \end{aligned} \tag{4.1}$$

with $(\varphi, \lambda, h)_0$ the latitude, longitude and height of the reference position, and $\bar{M}(\varphi_0)$ the meridian

radius of curvature and $\bar{N}(\varphi_0)$ the radius of curvature in the prime vertical,

$$\begin{aligned} \bar{N}(\varphi_0) &= \frac{a}{\sqrt{1-e^2\sin^2\varphi_0}} \\ \bar{M}(\varphi_0) &= \frac{a(1-e^2)}{(1-e^2\sin^2\varphi_0)^{3/2}} \end{aligned} \tag{4.2}$$

with radius of curvature $\bar{N}$ normal to $\bar{M}$. On the equator the radius of curvature in East-West is equal to the semi-major axis a, with $\bar{N}(0^0) = a$, while the radius of curvature in North-South is smaller than the semi-minor axis, with $\bar{M}(0^0) = a(1-e^2) = b(1-f) = b^2/a$. On the poles the radius of curvature $\bar{N}(\pm 90^0) = \bar{M}(\pm 90^0) = a/\sqrt{(1-e^2)} = a^2/b$ is larger than the semi-major axis a.

The hourly data interval is decimated to a daily interval using a moving mean of 24 hours. Decimation to daily intervals is necessary for direct comparison with the alternative processing methods, which use daily data intervals.

The csv files provided by 06-GPS do not include an estimate of the precision of the positions. Therefore, the standard deviations in the time series structure is set to a nominal value of 1 mm. The data provided by 06-GPS also does not include meta data with the antenna and receiver types.

The meta data information was at first extracted from the SINEX files provided by the Bernese GPS software from the alternative processing. This data was used to build a csv text file with events, called `allEventsNam.txt` and `allEventsEdited.txt`, that include lines with `station name`, `event date`, `event type`, `event name`, and `remarks`. Possible event types are antenna change, receiver change and known coordinates steps. The second file was hand edited and updated several times during the project to include the latest findings, in particular corrections for the meta data and freshly detected steps. The same file is used in the analysis of all three processing strategies. The meta data for the monitoring stations is given in Appendix A.1.

The resulting structure array for the NAM monitoring stations is saved to the mat file `tsSSR.mat`.

4.1.2. NAM REFERENCE STATIONS

The coordinates of the NAM reference stations are constrained to reference values during the processing of the NAM monitoring stations. The values for the reference station coordinates have been computed using the procedure described in section 3.1.2. There have been occasional updates of the reference station coordinates and changes in the set of reference stations [Dentz and Henry, 2019], with the aim to minimize the impact on the positions in the area of interest. These coordinates are provided by 06-GPS in an Microsoft Excel file. The reference station coordinates are read in a Matlab script and converted into the structure array format used for the other stations, so they can be analyzed and plotted as time series, although a decomposition makes no sense for this data (which we therefore won't do). The station `SCHI` was renamed to `SCH1` in order to use the same names as in the other solutions. The meta data is again provided by the hand-edited `allEventsEdited.txt` file, see also Appendix A.2 for the meta data for the NAM reference stations. The time series structure array with reference station coordinates and approximate coordinates for the monitoring stations is saved to the mat file `tsSSRref.mat`. The time of a coordinate step is also saved in an event file called `refEvents.txt`, which has the same format as the previous event file.

4.2. BERNESE SOFTWARE PROCESSING (BSW) METHOD

Data from the NAM monitor and reference stations, as well as many other stations, is processed by the Kadaster using the Bernese GNSS Software [Hoentjen and Huisman, 2019]. The results of the processing are provided in the Solution Independent Exchange Format (SINEX), an international standard for the exchange of position solutions, with full co-variance matrix and meta data. A SINEX file is provided for each day of processing, containing all the stations processed during that day.

The SINEX files are first converted into a Matlab structure array using a SINEX parser written by the author. Each structure array element is a (daily) solution. The structure array, and its elements,

are saved as a Matlab mat files for further processing. The mat files basically contains the same information as the SINEX files, but are much quicker to read than the original SINEX files. After 29 January 2017 two SINEX files are provided for each daily solution, using respectively IGb08 and IGS14 as reference frame. Both are converted, but it is the IGb08 that is used in the main analysis.

After the daily SINEX files have been converted to Matlab structures, the SINEX structures are converted into the time series structures that are used for the decomposition. The difference is that the SINEX structure array elements are daily solutions, with all stations processed during that day, whereas the time series structure is structured station by station (each station is a structure element) with for each station the North, East and Up time series, with precision information, events and meta data. The resulting structure array is saved to the mat file `tsBSWncIGb08.mat`.

The SINEX files contain Cartesian coordinates in an Earth Centered Earth Fixed frame. The Cartesian coordinates are converted into North, East and Up displacements with respect to a reference position. The reference position is the mean of the Cartesian coordinates. The resulting North, East, Up time series is in the IGb08 reference frame, thus the North and East displacements have a large component that is due to the velocity of the Eurasian plate. Therefore, for each station the nominal velocity of the Eurasian plate is computed, and the North and East displacements are corrected for that velocity. The nominal velocities are computed using the transformation from ETRF2000 to ITRF2014; the nominal velocities are thus the nominal station velocity in ITRF2014 with respect to ETRF2000[1]. The Up component is not corrected for the nominal velocity. The reason for this is that velocities in the Up component are already in a practical range, unlike the North and East component, which all have velocities around 24 mm/y. On the other hand, we observed a difference of 0.9 mm/y in vertical velocity between ITRF2008 and ETRF2000 over the North of the Netherlands, and considering that ITRF2008 is a much more recent realization than ETRF2000 (which is acutally tied to a very early realization of ITRF), we believe ITRF2008 is the better choice for the vertical component. See also Section 7.3 where we come back on this issue. The resulting North, East and Up time series are therefore in ETRF2000 for the horizontal component, and in IGb08 for the vertical component. The standard deviations for the North, East and Up components have been computed from the co-variance matrix of the Cartesian positions.

The meta data with antenna and receiver information is also used to build a csv text file with events, called `allEventsNam.txt` and `allEventsEdited.txt`, that include lines with `station name`, `event date`, `event type`, `event name`, and `remarks`. Possible event types are antenna change, receiver change and known coordinates steps. The second file was hand edited and updated several times during the project to include the latest findings, in particular corrections for the meta data and freshly detected steps. The same file is used in the analysis of all three processing strategies.

4.3. PRECISE POINT POSITIONING (PPP) METHOD

The PPP data has been downloaded from the NGL website on November 18, 2018. The NGL website provides the data is two different formats. For the analysis in this report the files `ssss.IGS08.tenv3` have been used, which give the time series of station `ssss` in IGS08 using the `tenv3` format, which provides the time series in latitude, longitude, height format. The `tenv3` format was selected because it contains more information than the alternative, `txyz2`, format.

The North, East and Up displacements have been computed using the exact same algorithm that was used for the SSR dataset, given in Eq. 4.1. The North and East displacements have been corrected for plate velocity using the exact same way as was used for the Bernese solution, resulting in North and East displacements in ETRF2000. The Up component was not corrected, and is in IGS08. The standard deviations for the North, East and Up displacements were taken from the file.

A couple of stations were renamed in order to use the same names as in the other two solutions: BLLM was renamed to BALL, BORK into 0687, D645 into 0645, EMDE into 0647 and MEPP into 0683.

[1] ITRF2014 is used instead of ITRF2008(IGb08). The idea was to use the most recent realization of ITRF to get the best possible result. So, strictly speaking the horizontal components are not in ETRF2000, but include an additional component related to the transformation between ITRF2008 (the reference frame of the solution) and ITRF2014.

The NAM stations DZY1 and SCH1 were not included in the NGL solutions, but the identically named and nearby stations DZYL and SCHI were included.

The receiver and antenna type information was copied from the Bernese solutions.

The resulting time series were stored in a structure array using the same format as for the other two solutions. The structure array was saved into a matfile `tsPPP.mat`.

5

TIME SERIES DECOMPOSITION

A GNSS time series decomposition is used to remove the effect of outliers and steps in the data, and to separate between periodic and environmental signals for the individual stations, common mode effects and station trends. The objective of the decomposition is to remove annual- and semi-annual harmonics, temperature related effects, atmospheric loading and common mode effects from the input time series, and in the process, detect and remove outliers and steps. The final outcome of the GNSS time series decomposition is the sum of the estimated trend (fitted spline function) and the (moving average of the) residuals, thus, effectively removing the periodic (harmonic) signal, temperature effects, atmospheric loading, common modes, steps and outliers in the data. The decomposition is performed in exactly the same way for all three datasets.

The raw GNSS input time series is influenced by a number of processes and observational effects. These are:

a. Long term station movement. This is what we are basically after.

b. Monument movement as result of the environmental conditions, residual Earth tides and loading, atmospheric loading, ground water effects, seasonal variations of gas production (and injection), etc.

   Tidal loading effects have been modeled in the software but small residual effects may remain. These residual effects, as well as effects of ground water fluctuations, seasonal variations in gas production (and injection), and other motions of the monument, for instance, under the influence of temperature changes, may still be present in the raw time series. Some of these signals may be of interest, e.g. seasonal variations in gas production, but others, depending on the application may just be a nuisance. Atmospheric loading has not been modeled in any of the three processing methods, but the different processing methodologies will respond in different ways to this effect. It is expected to cancel in the SSR processing, but not in the PPP and BSW processing.

c. Apparent motions, but no real motions, as the result of for instance un-modeled elevation and azimuth dependent antenna phase delays (can only be partly covered by antenna calibration), site multipath, and un-modeled atmosphere effects.

   The GPS processing, which include the estimation of rather correlated receiver clock, troposphere zenith delay and height parameters, is very sensitive to elevation dependent effects in the observations and models used by the processing. As result of the repeating GPS satellite constellation these effects can result into several harmonic effects in the time series.

d. Common mode signals.

   These are effects that are (more or less) the same for all stations, which can be due to the used reference frame, common atmosphere and loading effects, or errors in the used satellite orbits

and clocks. The common mode signal depends to a large extend on the used processing method. In case of PPP processing large common modes are expected, but in case of the SSR processing the common modes will be much smaller as these effects are already absorbed by the state–space modeling.

e. Steps due to equipment changes.

f. Measurement noise.

To separate these effects as much as possible a decomposition of the GPS time series is made.

The raw time series are decomposed into components including a secular trend, temperature influence, atmospheric loading, harmonic components, steps and noise components. Summing them returns the original time series. The time series decomposition is done using in-house developed Matlab software. Each component of the time series Δ, with Δ either ΔN, ΔE, ΔU (North, East, Up), can be described by the following model

$$\begin{aligned}\Delta(t) &= s(t) + \Delta_{\mathrm{AtmLd}}(P(t) - P_0) + \Delta_{\mathrm{TempI}}(T(t) - T_0) + \\ &\quad \sum_i (a_{si} \sin 2\pi f_i t + a_{ci} \cos 2\pi f_i t) + \Delta_{\mathrm{CM}}(t) + \sum_j \Gamma_{t_j}(t) + \epsilon\end{aligned}$$

with $s(t)$ the trend, Δ_{AtmLd} an atmospheric loading coefficient and Δ_{TempI} a temperature influence coefficient, a_{si} and a_{ci} harmonic coefficients, $\Delta_{\mathrm{CM}}(t)$ a common mode signal that is the same for all stations, $\sum_j \Gamma_{t_j}(t)$ the cumulative effect of steps, with $\Gamma_{t_j}(t|t < t_j) = 0$, and ϵ the residual noise, t time in decimal years and f_i frequency in cycles/year.

To illustrate the decomposition, in Figures 5.1, 5.2 and 5.3, the results of the time series decomposition for respectively the North, East and Up component, is shown for a set of selected stations, using solutions from the Bernese GNSS software as input. In these figures stations are plotted in a single sub-plot, off-setting each time series by a certain amount on the y-axis. Each sub-plot contains a component of the decomposed time series.

The trend model $s(t)$ can be a linear trend, higher order polynomial or spline function. In the current project a spline function is used. The spline consists of piece-wise polynomials of order k and a length of more than one year for each segment. The order k and nominal length can be selected. For this project we used default setting which proved to work well for many projects: splines of order two ($k = 2$) with a nominal period of two years. This is equivalent to using piece-wise continuous linear polynomials with nominal two year segments, as can be seen in in Figures 5.1, 5.2 and 5.3. The breakpoints between the individual segments are distributed evenly over the time series, such that period between two breakpoints is as close as possible to two years. If the time series is shorter than two years a single linear polynomial is used. The trend model is continuous, however, at each breakpoint there will be a discontinuity in the velocity. To prevent discontinuities in the first derivative (velocity) at the break points a higher order spline ($k \geq 3$) should be used, but, it is our experience, that this does not add much to the quality of the fit and makes it even a bit worse at the ends of the time series. Also, we find the piece-wise linear model easier to interpret; it basically amounts to estimating the velocity over (approximately) a two year period. In our experience estimating a single velocity over the full period is not a good idea. The reason for this is that the various time series all have different lengths, and for the decomposition we would like to be able to obtain the same quality of fit for each time series indepedent of it's length. Also, there are sometimes real changes in the velocity over the years, and we actually do observe these with the current model.

For each coordinate component an atmospheric loading coefficient and a coefficient for station deformation under influence of temperature are estimated, using observed atmospheric pressure P and temperature T from the KNMI meteo station in Eelde[1].

[1] Data from KNMI station Eelde has been used for all stations over the region of interest. For stations in the Ameland area and near De Wijk KNMI stations in Leeuwarden and Hoogeveen could have been used. We believe, from the results we obtained, that the impact of using data from more meteo stations will be very small, but this is definitely something that would be useful to investigate further.

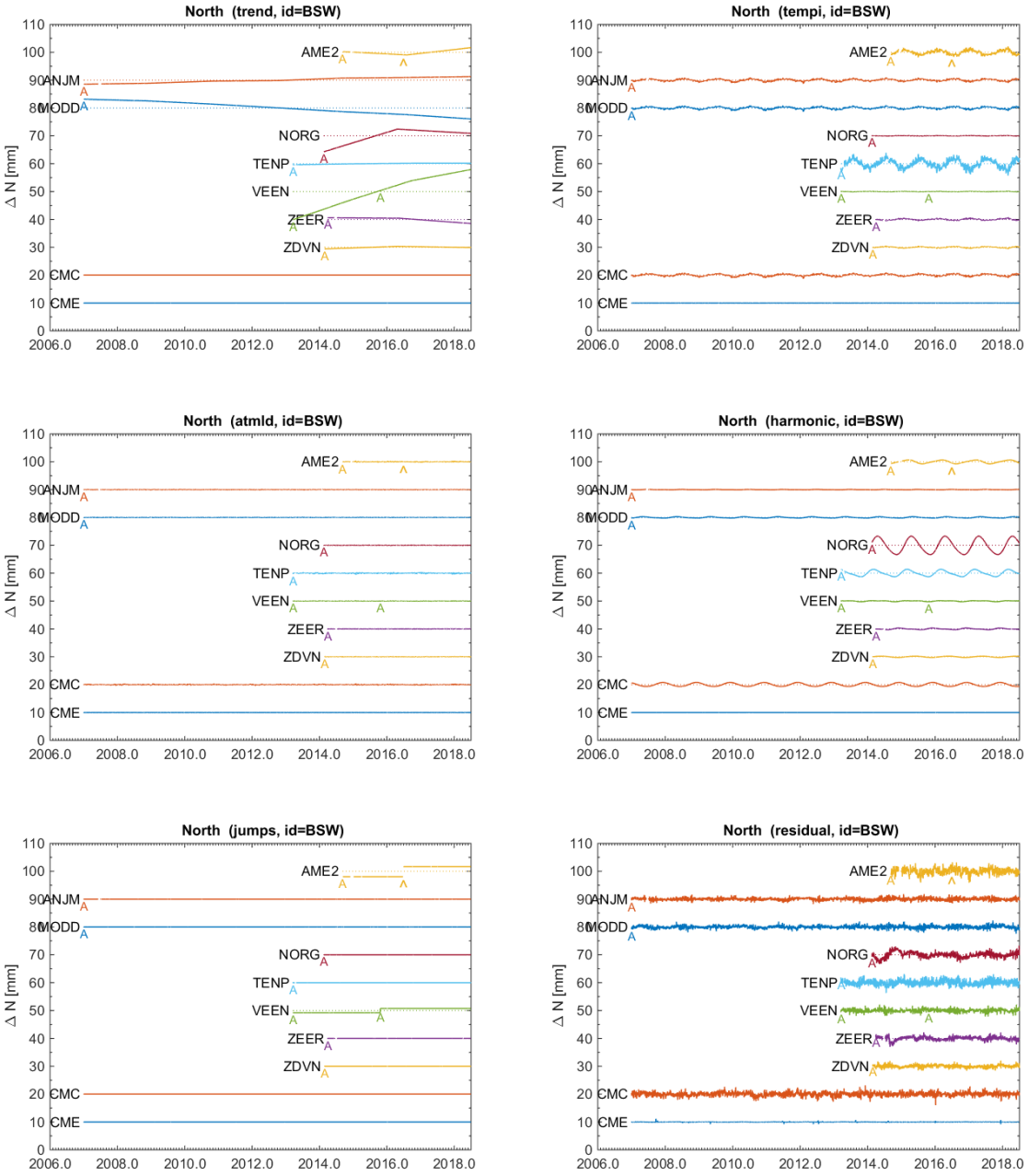

Figure 5.1: North time series components for selected NAM monitoring stations. From left to right, top to bottom, a) estimated trend function, b) temperature influence, c) atmospheric loading, d) annual and semi-annual harmonics, e) steps and f) residuals after fit. Data from 8 selected stations is shown using results from the decomposition of the Bernese GNSS Software (BSW) time series. Antenna changes are indicated by a "A", other steps by a "∧". The series marked by CMC is the common mode correction estimated from the previous iteration, which is the same for every station. The series marked by CME is the common mode estimated during this iteration. The common modes have been computed from more stations than shown in this figure. The original time series (not shown) is the sum of the station time series in each plot, with the CME and CMC components added.

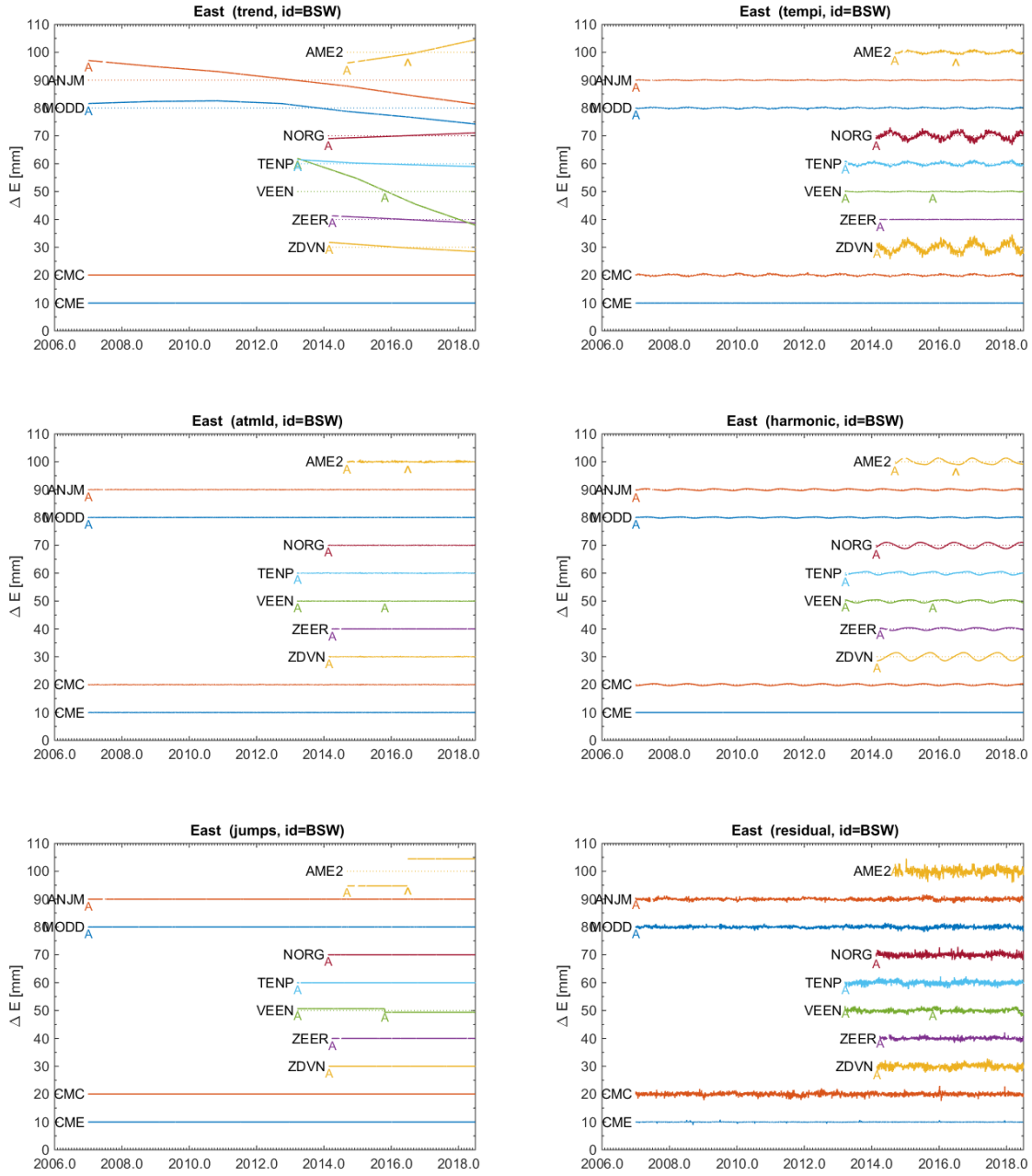

Figure 5.2: East time series components for selected NAM monitoring stations. From left to right, top to bottom, a) estimated trend function, b) temperature influence, c) atmospheric loading, d) annual and semi-annual harmonics, e) steps and f) residuals after fit. Data from 8 selected stations is shown using results from the decomposition of the Bernese GNSS Software (BSW) time series. Antenna changes are indicated by a "A", other steps by a "∧". The series marked by CMC is the common mode correction estimated from the previous iteration, which is the same for every station. The series marked by CME is the common mode estimated during this iteration. The common modes have been computed from more stations than shown in this figure. The original time series (not shown) is the sum of the station time series in each plot, with the CME and CMC components added.

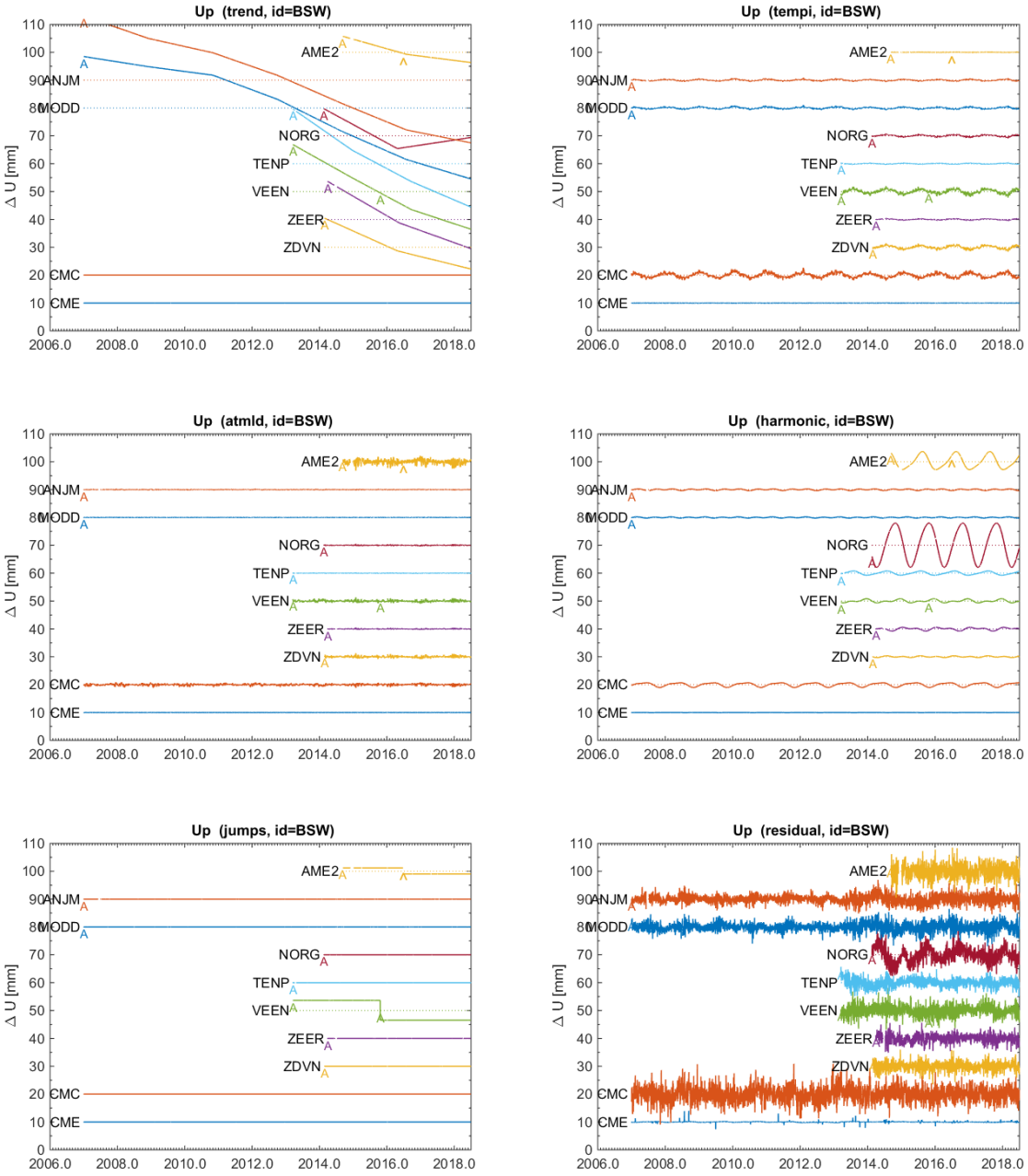

Figure 5.3: Height time series components for selected NAM monitoring stations. From left to right, top to bottom, a) estimated trend function, b) temperature influence, c) atmospheric loading, d) annual and semi-annual harmonics, e) steps and f) residuals after fit. Data from 8 selected stations is shown using results from the decomposition of the Bernese GNSS Software (BSW) time series. Antenna changes are indicated by a "A", other steps by a "∧". The series marked by CMC is the common mode correction estimated from the previous iteration, which is the same for every station. The series marked by CME is the common mode estimated during this iteration. The common modes have been computed from more stations than shown in this figure. The original time series (not shown) is the sum of the station time series in each plot, with the CME and CMC components added.

The harmonic terms that are estimated have periods of 1 cycle/year (annual) and 2 cycles/year (semi-annual). These periods are very common periods in GPS time series, but often not related to real motion. Apparent motions, as the result of for instance un-modeled elevation and azimuth dependent antenna phase delays, site multipath, and un-modeled atmosphere effects, often manifest themselves in GNSS time series with annual and semi-annual periods.

Multipath and antenna phase delays are related to GPS orbital period as they depend on the position of the GPS satellites relative to the observer. The orbital period of GPS satellites is slightly shorter than half a sidereal day. Hence, the GPS satellites appear in the same part of the sky with a period of slightly less than one sidereal day; to be more precise, the repeat time is about 246 seconds less than a solar day[2]. The result is that the error from multipath and un-modeled antenna phase delays repeats itself in high–rate positioning time series with periods of 23h55m50s. As we use for our time series a daily sampling, we will only observe an indirect effect due to aliasing with the daily sample rate. It takes about 351 days for the GPS satellite constellation to repeat at exact the same (solar) time of day. This is close to the GPS draconitic year of 351.6 days, which is the time it takes the Sun (as seen from the Earth) to complete one revolution with respect to the GPS ascending orbital nodes. It is this frequency, and higher harmonics, that are observed in almost all IGS products, whereby multipath, antenna phase patterns, but also orbital error and the effect of Earth shadow crossings, are contributing factors. On the other hand, for atmospheric effects we expect periods of one solar year and higher.

It could be possible to estimate harmonics with frequencies for both the solar and draconitic year (and higher) separately, but this is not a good idea since this would result in unwanted aliasing effects, especially in combination with the spline trend model we are using. This is the reason that we have chosen to estimate only annual and semi-annual periods of exactly 1 and 2 cycles/year. It is possible to estimate more harmonic components, but as we will see from the estimated periodograms in Section 6 there are, except for the PPP solution, no other significant harmonics present in the time series.

The harmonic components are usually artifacts from station multipath and antenna phase variations, although sometimes they may also be related to real displacements. Seasonal variations in ground water level and gas production (and injection) may result in real seasonal variations in the time series that are difficult to separate from the annual and semi-annual harmonic periods caused by site multipath, un-modeled antenna phase phase variations and un-modeled atmospheric effects. The best "give-away" for such real effects are usually the residuals after the fit; it is seldom the case that ground water level fluctuations and gas production (and injection) cause near perfect annual and semi-annual harmonics as is the case for site multipath and antenna phase variations. This can be seen quite well in Figures 5.1, 5.2 and 5.3 for the station `NORG`. However, it is undeniable that some of these real motions will leak into the harmonics.

Temperature related effects and atmospheric loading also have a clear seasonal component, but because of the strong correlation with meteorological parameters and shorter than seasonal periods in these parameters, it turns out that these effects can be separated quite well from the harmonic parameters. The estimated temperature effects say something about the monument stability; they usually occur in the horizontal direction for stations that are installed on buildings, as can be seen in Figures 5.1, 5.2 and 5.3 for stations `ZDVN`, `TENP` and `AME2`. The annual harmonics term and temperature coefficient can be estimated individually without any problems. These two parameters can be separated very well from an estimation point of view. Sometimes both terms amplify each other, in other cases the opposite may happen. Adding a term for the temperature effect gives a significant improvement in the fit.

Atmospheric loading has not been modeled in any of the three processing methods, but the dif-

[2]The general rule-of-thumb is that this advance is 4 minutes a day, or 240 seconds, the difference in duration between a sidereal and solar day. However, because of the ellipsoidal shape of the Earth the orbit plane is not fixed in space, resulting in a precession of the ascending node by about 14.66°/y and shorter orbital period. The exact repeat period depends on the location on Earth, but is is on average 246s less than a solar day.

ferent processing methodologies will respond in different ways to this effect. It is expected not to be present in the SSR processing because the effect is the same on the monitoring and reference stations, but, on the other hand we expect it will be present in the PPP and BSW processing. Atmospheric loading, as expected, manifests itself mainly in the vertical component, and is negligible in the horizontal components, as can be seen from Figures 5.1, 5.2 and 5.3. Nevertheless, the effect in the vertical is relatively small compared to the harmonics and temperature influence.

Tidal loading effects have been modeled in all three GNSS processing softwares. If this were not the case, this would probably show up with frequencies of half a Lunar Month (14.2 days/year) and higher in the time series.

Whenever there is a change of antenna a new step is introduced in the decomposition. The time the step starts is taken from the meta data. The size of the step is estimated as an extra parameter. There were a few instances where it was necessary to introduce an extra step. The reason for these extra steps is not always clear and can sometimes only be guessed from the observed pattern. For instance, AME2, one of the antenna's on a platform, was moved by a few decimeter for a single day, and was then re-located to almost the same position, but not exactly. Speculation has it that the antenna was moved for maintenance work (which was later confirmed by the station operator). These steps and outliers were detected using a moving median filter, with outlier and step detection, on the residuals of the time series decomposition.

Outlier detection takes place before and after each time series decomposition. Before the time series decomposition the very large outliers or data points with large formal standard deviations are removed. The main part of the outlier detection is done after the decomposition on the residuals of the fit. To find multiple outliers (and steps) in the same iteration a moving median filter with outlier and step detection is used. The moving median filter estimates a new filtered time series with the 21 day moving median and the standard deviation estimated from the median absolute deviation (MAD) over the 21 day period. The window length for the filter was based on the noise characteristics of the residuals, for periods larger than 21 days we observed a flicker noise behaviour, whereas for shorter periods there was (but not in all cases) it behaved more like white noise.

A data point is considered to be an potential outlier when the absolute value of the residual with the moving median is larger than 5 times the standard deviation computed from the MAD. The data point will be flagged, but is not yet considered an outlier. The MAD standard deviation for the outlier test is computed over the whole period; it turns out this is more stable than the MAD from the 21 day periods, but also there is no indication that the noise characteristics change over the time series. As each data point appears in 21 different moving median windows also the outlier test can be repeated 21 times. The final decision to mark a data point as outlier is taken using a voting mechanism; when the data point is flagged in more than half the windows it is considered an outlier. If not, the flags are probably false alarms as the result of an undetected step. The algorithm to detect steps is a bit more complicated; it is based on the the differences between two moving medians, one before, and one after, a suspected step. As steps happen only occasionally, the results from the step detection are not processed automatically, but reported to the user. When the user is convinced it is a real step, the step, with the time it starts, is added to the list of events (antenna and receiver changes are other events). The detected outliers on the other hand are removed automatically in a next iteration of the decomposition. Usually one (outlier) iteration (two runs) are sufficient to remove all outliers. The window length for the moving median (21 days), outlier rejection level (5) times the MAD standard deviation, and step detection level (5) are all input parameters. The 21 day period was selected based on the results of the periodograms. For the outlier rejection level a conservative value of 5 was selected in order to remove only a modest number of the most important outliers.

The common modes are estimated from a stack of stations. Two different types of common modes are computed

- residual stack
- common mode of the estimated harmonic, temperature influence and atmospheric loading

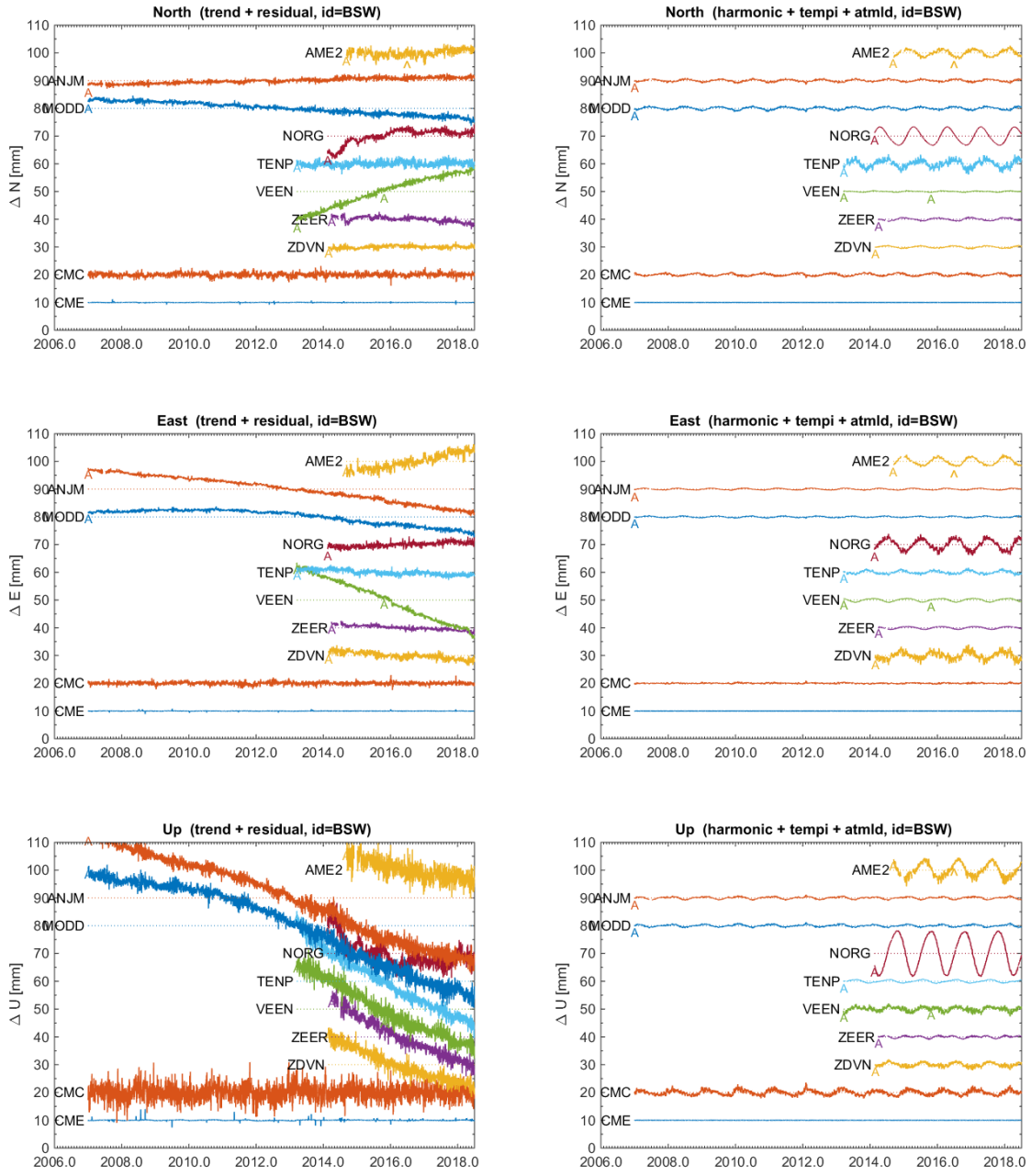

Figure 5.4: Height time series components for selected NAM monitoring stations. In the sub-plots on the left the estimated trend plus residuals are plotted for respectively the North, East and Up component. In the sub-plots on the right the "periodic" components, composed of the annual and semi-annual harmonics, temperature influence and atmospheric loading is plotted. Data from the 8 selected stations is shown using results from the decomposition of the Bernese GNSS Software (BSW) time series, the same as shown in Figures 5.1, 5.2 and 5.3. Antenna changes are indicated by a "A", other steps by a "∧". The series marked by CMC is the common mode correction estimated from the previous iteration, which is the same for every station. The series marked by CME is the common mode estimated during this iteration. The common modes have been computed from more stations than shown in this figure. The original time series for each component (not shown) is the sum of the sub-plot on the left and right, plus the steps of Figures 5.1, 5.2 and 5.3, plus the CME and CMC components.

parameters

The stations that participate in the stack are carefully selected, excluding stations from the stack for which the time series decomposition model doesn't fit. These are usually stations with un-modeled steps or discontinuities in the derivatives (velocity), or stations that are affected by processes (gas-storage, salt-mining, ground water fluctuations) that cannot be represented by annual and semi-annual harmonics . The common mode of the estimated harmonic, temperature influence and atmospheric loading parameters is computed by taking the average of the estimated parameters. The residual stack is computed by binning the residuals in daily bins and then averaging the residuals in each bin.

To correct the time series decomposition for the common modes it is necessary to iterate the decomposition (these are different iterations than for the outlier detection and removal). In the first run (iteration 1) the common modes are computed. Then in the second iteration the common modes (residuals stack and common mode parameters) are subtracted from the time series, before a new decomposition is estimated. Two iterations (runs) are sufficient to remove the common modes. The computed residual stack and common mode parameters are shown in Figures 5.1, 5.2 and 5.3 as time series labeled with CMC or CME. The series labeled with CMC is represents the common mode computed in the first iteration, CME is the common mode that is computed in the current iteration, which is in Figures 5.1, 5.2 and 5.3 the second and final iteration. The amplitude of the CME series is very small and is only plotted here as proof that two iterations are sufficient.

The common modes for the other two solutions are not shown in this section. What we can say here is that the common mode for the SSR solution is not significant. It is much smaller than the common mode for the BSW solution. On the other hand, the common mode for the PPP solution is larger than the common mode for the BSW solution. For a comparison of the estimated common modes see Section 6.

A final remark on the common modes is that they do not affect in any way the estimated trend functions.

From the individual components of the decomposition new products can be generated. For instance, for monitoring long term subsidence, one could decide to remove the harmonics, temperature effects, atmospheric loading, jumps and common modes to obtain a clean series. This gives you the same series as taking the estimated trend function and adding the residuals. This is illustrated in Figure 5.4, for the same stations and decomposition as used for Figures 5.1, 5.2 and 5.3. The subplots on the left show the final estimated trend, which is composed of the estimated trend function plus the residuals from the decomposition. The subplots on the right show the "periodic" components, the annual and semi-annual harmonics, temperature influence, and atmospheric loading, that has been removed from the series in order to obtain the result in the subplots on the left.

We believe that adding the residuals to the estimated trend function gives the best possible representation of the station trends. The trend alone will not do in case there is a sudden change in velocity, as is the case for instance in the East component of the station VEEN. The velocity change, caused by a sudden pressure drop in a salt cavern, is not captured by the estimated trend function, but it remains visible in the residuals. So adding the residuals to the estimated trend function makes sense, as it restores the any un-modeled component. Although, it would have been better to model the sudden velocity change in the trend function, e.g. by starting a new spline segment at this instance.

The station NORG is located above a sub-surface gas storage facility. This is an example where the current decomposition does not work well. Part of the station displacement is leaked into the estimated harmonic components. The estimated temperature influence and atmospheric loading components are all-right. A better representation of the station displacement would have been obtained by not removing the harmonic components, and accepting that the (much smaller) contribution of station multipath and antenna phase center delays to the harmonic components, cannot be separated from the deformation signal in this particular case. We believe that, in all other cases, the estimated harmonic components and temperature influence are dominated by station dependent

effects, and, therefore that it is better to remove these components from the final series, as we did.

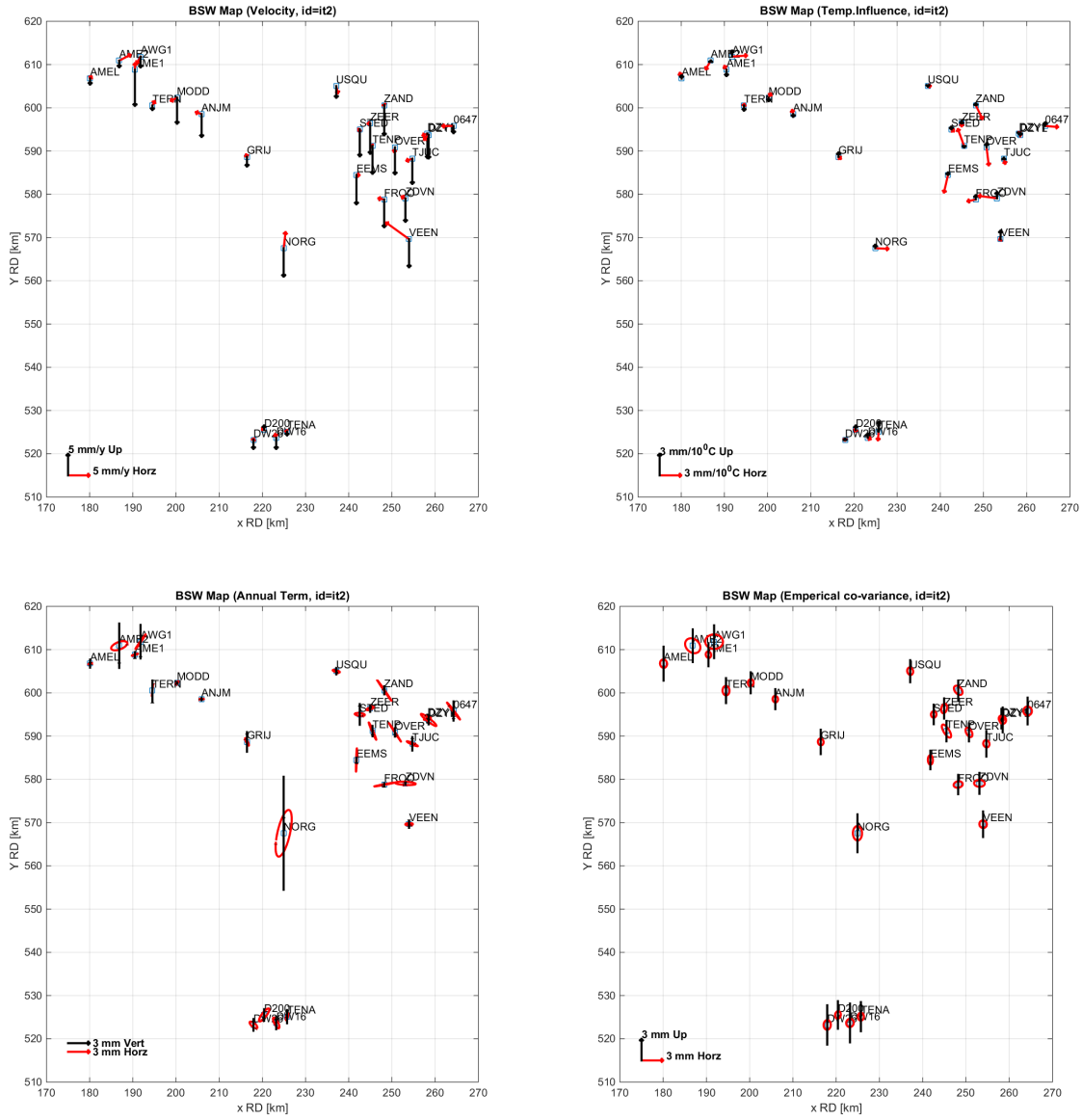

Figure 5.5: Map of the NAM monitoring stations with representation of estimated parameters: a) velocity vector, b) temperature influence parameter, c) annual harmonic component, and d) co–variance of the residuals.

The parameters of the time series decomposition can also be plotted on a map, as is shown in Figure 5.5. Figure 5.5a shows the estimated velocity component, computed from the spline fit at the center epoch, Figure 5.5b shows a representation of the estimated temperature influence parameter, while Figure 5.5c shows the estimated annual harmonic component, and Figure 5.5d shows the horizontal standard ellipse and vertical standard deviation as computed from the estimated co–variance matrix of the residuals. These figures provide a different, and more compact representation, of the time series decomposition results.

Figure 5.6 shows the periodogram of the de-trended signal and residuals for the BSW solution. The periodogram is computed for the stack of NAM monitoring stations (using the same stations as selected for estimating the common modes). On the x-axis is the frequency in cycles/year (cpy) in a logarithmic scale. On the y-axis the power spectral density is plotted in mm^2/cycle/year, also on a logarithmic scale. The y-scale is correct for the Up component. The East and North component are each shifted down by respective two and four octaves in power (factor 1/100 and 1/10000) to separate

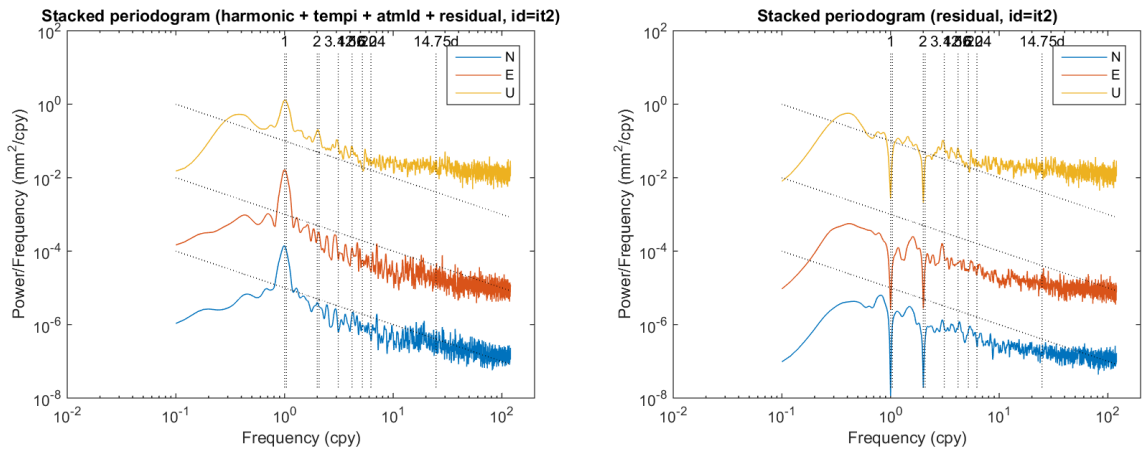

Figure 5.6: Lomb-Scargle periodogram of the NAM monitoring stations for the BSW solution. The plot on the left shows the periodogram for just the de-trended series. The plot in the right shows the periodogram of the residuals. See the text for an explanation of the figure.

them from the Up-series. The dotted vertical lines denote several important frequencies: namely 1 and 2 cycles per year, but also the draconitic period of 1.04 cycle/year and the first six harmonics of the draconitic period, and the frequency corresponding to the main tidal period of 14.75 days. The three slanted dotted lines represent a $0.1 f^{-1}$ mm^2/cpy power-law behavior typical for flicker noise (shifted by two and four octaves for the East and North component).

The periodogram on the left of Figure 5.6 shows the original signal, de-trended with the fitted trend function and corrected for steps. It has obvious peaks near 1 and 2 cycles/year that correspond to the annual and semi-annual terms. The periodogram on the right is for the residuals. Annual and semi-annual frequencies have disappeared As can be seen from Figure 5.6 the peaks near 1 and 2 cycles/year are quite broad. This is probably because several frequencies, with the draconitic year and solar year, are mixed together, and because of natural variations in the seasons that affect the atmospheric parameters.

In the periodogram of the residuals of Figure 5.6 three different noise regimes can be distinguished with two different cut-off frequencies. The middle part, between a low frequency cut-off of around 0.5 cpy, and a high frequency cut-off of around 10-20 cpy, has a typical flicker noise behavior parallel to the $0.1 f^{-1}$ mm^2/cpy lines. The low frequency cut-off, around 0.5 cpy, separates the upward slope in the periodogram from the middle part. The low frequency cut-off is related to our choice for the trend function, which consists of piece-wise linear polynomials with a length of about two years. The high frequency cut-off separates the middle part, with flicker noise behavior, from the high frequency noise, which has a different noise behavior. In case of the BSW solution, the periodogram becomes horizontal for frequencies above the high frequency cut-off, which is typical for white noise behavior. As we will see in Section 6 the exact spot of the high frequency cut-off is not the same for the SSR, BSW and PPP solutions. For the BSW and PPP solutions we have white noise above the high-frequency cut-off. In case of the SSR solution, above the high frequency cut-off, we have for the vertical component brown noise (random walk) instead of white noise, and flicker noise for the horizontal components. Our choice for the 21 day period in the moving median filter for outlier and step detection is related to the high frequency cut-off frequency, which is around 21 days (two to four weeks), as basically only want to reduce the white noise component by filtering.

For the final representation of the trend, which is composed of the estimated trend plus residuals, it would make sense to apply a 21 day moving average or median filter. The advantage of using a moving median filter is that it better preserves discontinuities in the signal, as we have seen in the station VEEN, and is less sensitive for outliers (though that make no difference as we have removed them). On the other hand, a moving average will be better in reducing the noise. In the current study we didn't apply a moving median or average to the estimated trend, composed of the trend function

plus residuals. In the next section we will compare the estimated trends for the three processing strategies without further filtering.

6

ANALYSIS OF THE NAM MONITORING STATION RESULTS

In this section the results of the decomposition on the NAM monitoring stations are presented for the three processing methods, and the results of the three processing centers are compared. For many of the figures in this section (and the next) we provide clickable links to high quality graphs. For these links to work, it is essential that the `figures` folder, that accompanies this report, is in the same folder as this report.

6.1. PERIODIC COMPONENT

The periodic components that are estimated in the decomposition are plotted in Figure 6.1. The harmonic components, temperature influence, and estimated atmospheric loading are all summed together, to form the periodic component of the signal. In each sub-figure the results of two solutions are plotted on top of each other. The first solution is plotted in a darker color than the second solution. The time series at the bottom of each plot is the common mode correction (CMC) for the periodic components. As explained in Section 5 the common mode is estimated in first iteration of the decomposition. To be more precise, two common modes are estimated. The one that is of interest here is the common mode in the periodic components, which is the average of the estimated harmonic, temperature influence and atmospheric loading parameters, computed from a subset of stations. The second common mode, which is discussed in later sections, is the average of the residuals, or residual stack, which mainly reduces the noise for the second iteration. The common modes are removed in the second iteration of the decomposition. The subset of stations from which the common mode is computed are the stations shown in Figure 6.1, except for the stations `AME2`, `AWG1`, `VEEN` and `NORG` which have not been used to estimate the common mode, residual stack and periodograms (but have been corrected in the second iteration). The stations `AME2` and `AWG1` have not been used because they are platforms, and may have a different behaviour; `NORG` was not used because the site is used to store gas, and `VEEN` was excluded because in 2018 there was a sudden change in deformation pattern possibly due to an expanding salt-cavern.

The plots of Figure 6.1 can be inspected in more detail through the following links BSW-PPP, SSR-BSW and SSR-PPP.

All stations have periodic components. Most of them are related to temperature influences on the structure and seasonal variations related to either the environment and/or GNSS processing artifacts. The station `NORG` is above an underground gas–storage which explains the large seasonal variations; it is also clear that this effect cannot be captured completely by annual and semi-annual harmonics.

The agreement between the estimated periodic components by the three processing chains is, in the second iteration (after removal of the common mode), very good. The standard deviation of the differences are below 0.3 mm for the horizontal components, and 0.4–0.5 mm for the vertical component. See also the first row of Table 6.1.

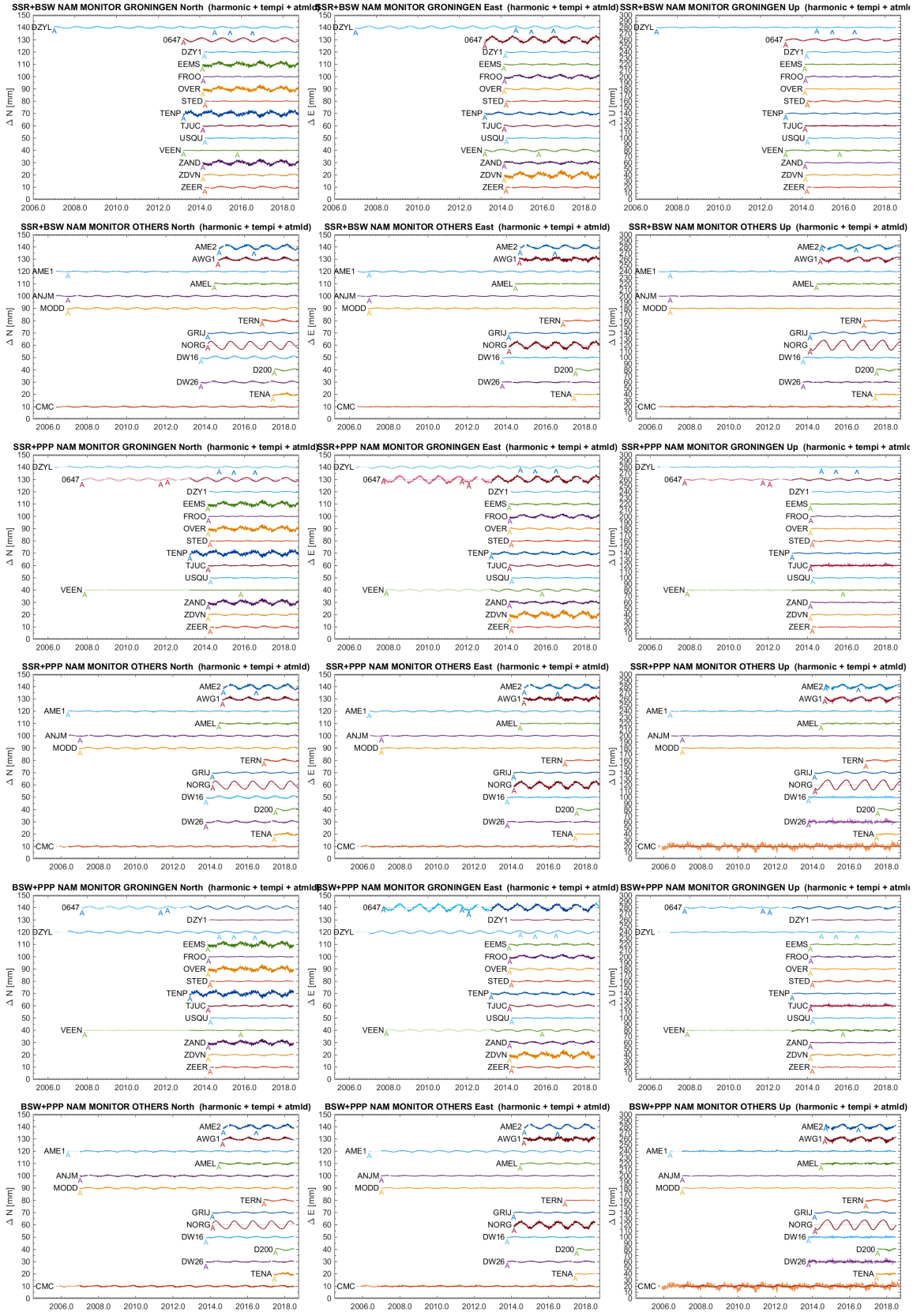

Figure 6.1: Periodic components for the NAM monitoring stations. Two solutions are plotted on top of each other: SSR-BSW (top), SSR-PPP (middle) and BSW-PPP (bottom). The first solution is in a darker color. The time series labeled CMC is the common mode correction that is applied. Antenna changes are marked by a letter "A" and other steps by a "∧".

Table 6.1: Standard deviation of the difference between two solutions for the stations in the Groningen area.

	North [mm]			East [mm]			Up [mm]		
	BSW SSR	PPP SSR	PPP BSW	BSW SSR	PPP SSR	PPP BSW	BSW SSR	PPP SSR	PPP BSW
Periodic	0.2	0.3	0.1	0.2	0.2	0.2	0.4	0.5	0.5
Trend	0.4	0.5	0.6	0.3	0.3	0.5	1.3	1.4	1.3
Residual	0.5	0.8	0.6	0.4	0.6	0.5	1.4	2.4	2.0
Trend+res	0.6	0.9	0.8	0.5	0.6	0.7	1.9	2.7	2.4

There is only agreement between the periodic components by the three processing chains after removal of a common mode signal. In the first iteration the common mode signal is different for each of the processing chains. This common mode signal from the first iteration is plotted also in Figure 6.1 at the bottom of each plot, with the label CMC (Common Mode Correction). The common mode signal is very significant, but different, for the BSW and PPP solution, whereby the common mode signal in the PPP solution is larger than the common mode in the BSW solution. There is hardly any common signal in the SSR solution. Note that in Figure 6.1the common mode signal (CMC) has been removed from all other time series.

In the second iteration also a (remaining) common mode signal is estimated, but the estimated values are negligible, which is proof that two runs (iterations) are sufficient to remove the common mode signal.

The conclusion from this subsection is that all three processing chains, after removal if the common mode in the periodic component, estimate the same annual signal, semi-annual signal, temperature influence and atmospheric loading for each station.

6.2. ESTIMATED STEPS

The steps that are estimated in the decomposition are given in Table 6.2. Whenever there is a change in antenna at a station an unknown step is introduced in the decomposition. The size of the step is estimated during the decomposition, along with the other parameters, but the start time of the step is given. Furthermore, the time series is checked for outliers and steps using a moving median filter. Apart from removing some outliers, this has led to the detection of a few steps that are not associated to an antenna change. Steps that were detected by the moving median filter were added, by hand, to the list of steps. These steps are called displacement (DPL) events. The size of the step was estimated in a subsequent decomposition run.

As can be observed from Table 6.2, for all steps associated to a displacement (DPL) event, there is a good agreement between the solutions. However, for the steps that are associated to an antenna replacement, the solutions do not agree, in particular for the height component. This probably has to do with the fact that the solutions may use different antenna models, with different phase center offsets and variations. It shows that, for a proper comparison between the solutions, it is essential to remove these steps. Table 6.2 also gives the estimated formal standard deviation of the steps, but the reader should be aware that these are too optimistic because in the estimation a simple diagonal co–variance matrix was used, and the time correlation in the input time series was not accounted for in the standard deviations.

6.3. TREND COMPONENT

The trends that are estimated in the decomposition are plotted in Figure 6.2. The trend is composed of two components: the estimated trend function (spline function or polynomial) with the residuals of the decomposition added to it. The rationale of adding the residuals to the estimated trend function is that the residuals may still contain a signal that has not been taken care of in the decomposition. The estimated trend, the trend function plus residuals, is the same as the original time

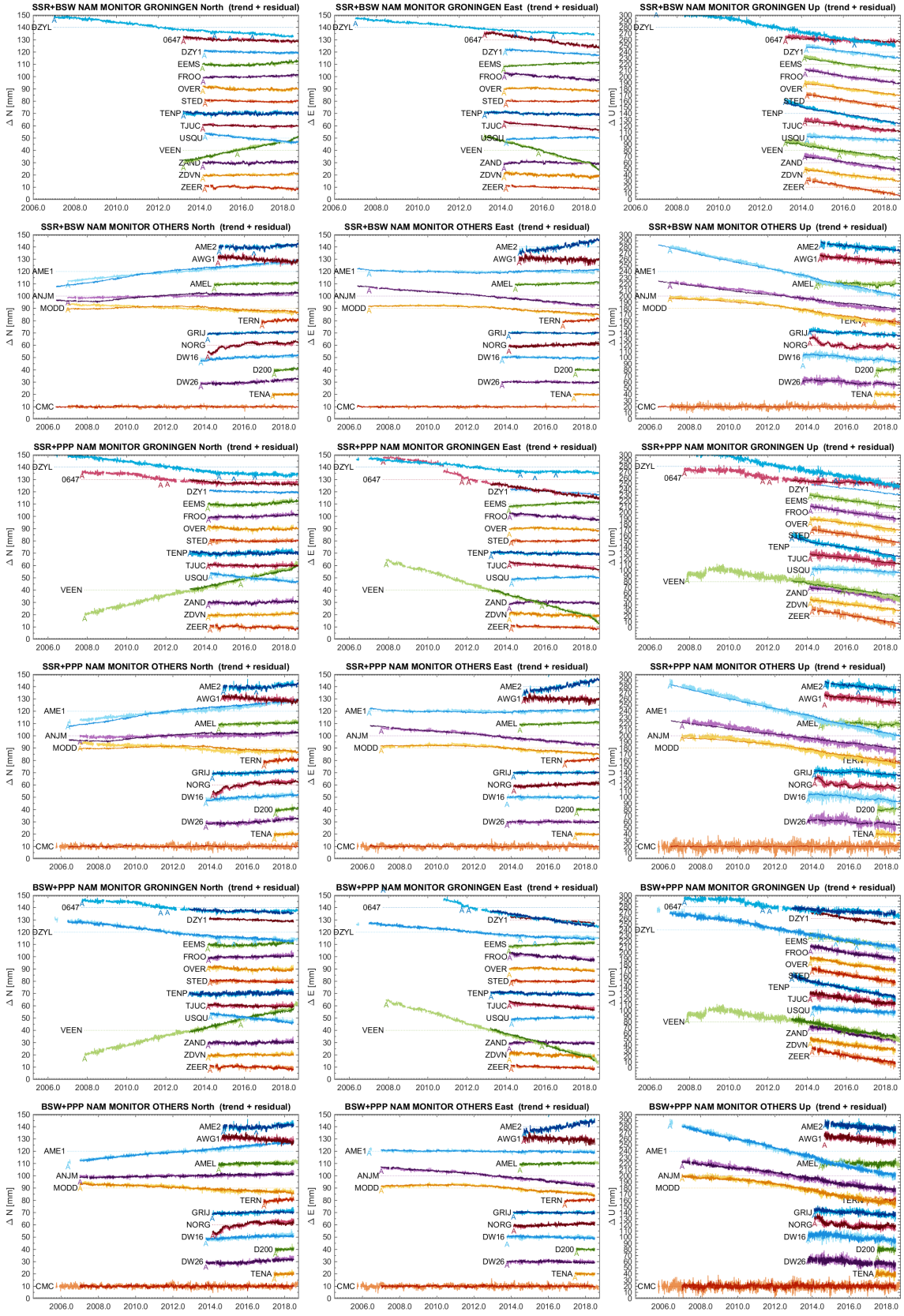

Figure 6.2: Trend plus residuals for the NAM monitoring stations. Two solutions are plotted on top of each other: SSR-BSW (top), SSR-PPP (middle) and BSW-PPP (bottom). The first solution is in a darker color. The time series labeled CMC is the common mode correction that is applied. Antenna changes are marked by a letter "A" and other steps by a "∧".

Table 6.2: Estimated steps in the SSR, BSW and PPP solutions (sol) with the estimated standard deviation. There a two events that cause the estimation of a step: an change of Antenna (ANT) or an apparent displacement (DPL).

station	dyear	event	sol	N[mm]	E[mm]	U[mm]	σN[mm]	σE[mm]	σU[mm]
AME2	2016.481	DPL	SSR	4.59	10.33	-3.21	0.10	0.10	0.12
			BSW	3.65	9.69	-2.18	0.12	0.13	0.27
			PPP	3.33	10.26	-2.87	0.14	0.15	0.34
VEEN	2015.804	ANT	SSR	0.25	-1.05	-1.09	0.08	0.10	0.12
			BSW	1.52	-1.33	-7.13	0.08	0.08	0.27
			PPP	1.49	-2.96	-4.39	0.11	0.10	0.38
DZYL	2014.713	ANT	BSW	-4.64	6.62	2.19	0.06	0.05	0.20
			PPP	-2.21	1.83	-62.21	0.09	0.07	0.27
DZYL	2015.463	DPL	BSW	-3.80	-6.62	-3.15	0.09	0.08	0.29
			PPP	-3.94	-6.73	-2.63	0.12	0.10	0.37
DZYL	2016.533	DPL	BSW	4.58	0.37	0.98	0.07	0.06	0.23
			PPP	4.40	0.48	1.63	0.09	0.08	0.30
0647	2011.719	ANT	PPP	1.30	3.09	3.33	0.10	0.12	0.32
0647	2012.070	ANT	PPP	-0.07	-0.09	1.27	0.09	0.11	0.29

series with (i) the periodic components of Section 6.1 removed, ii) the estimated steps of Section 6.2 removed , and iii) with the common modes (residuals stack and periodic common mode) removed. Whenever *estimated trend* or *trend solution* is mentioned we refer to the estimated trend function plus residuals.

In each sub-figure of Figure 6.2 the results of two solutions are plotted on top of each other. The first solution is plotted in a darker color than the second solution. The time series at the bottom of each plot is the common mode correction (CMC), or residual stack. The CMC has been estimated in the first iteration from the residuals, using the same subset of stations as for the periodic common mode, and is then subtracted from the data in the second iteration. The CMC in the trend (or actually residuals) only reduces the noise in the time series, in particular for the PPP, and to a lesser extend in the BSW solution. The CMC here has absolutely no effect on the estimated trend function. The plots of Figure 6.2 can be inspected in more detail through the following links BSW-PPP, SSR-BSW and SSR-PPP.

The station `VEEN` has a significant change in its horizontal velocity in the first half of 2018. This is well captured in the estimated trend (trend function plus residual). It is not captured in the trend function alone, as the change only occurred in the last half year, but it is visible in the residuals, and therefore also in the combination of trend function plus residual. Because this discontinuity in the velocity is not covered by the underlying model there is some overshooting in the residuals before the change. A possible improvement is to the decomposition is to introduce a discontinuity in the first derivative of the trend function at the epoch where the velocity change occurs, but this was not further explored in this study.

The station `NORG` is above an underground gas–storage which causes large seasonal variations; that cannot be captured completely by annual and semi-annual harmonics. On the other hand, some part of the seasonal deformations will be absorbed in the annual and semi-annual harmonics. So, for this station, where we know that a large part of the annual and semi-annual component has a real physical cause in the deep underground, it is not a good idea to remove the annual and semi-annual harmonics from the trend signal.

The agreement between the estimated trend of the BSW and PPP is in general good, however, there are some visible differences in the long term trend signal mostly between the SSR solution and the BSW and PPP solutions. The largest trend differences occur in the horizontal components, in particular in the North component for `AME1`, `ANJM` and `MODD` for 2006 until 2014. However, there seem also to be some differences in the up component between the solutions.

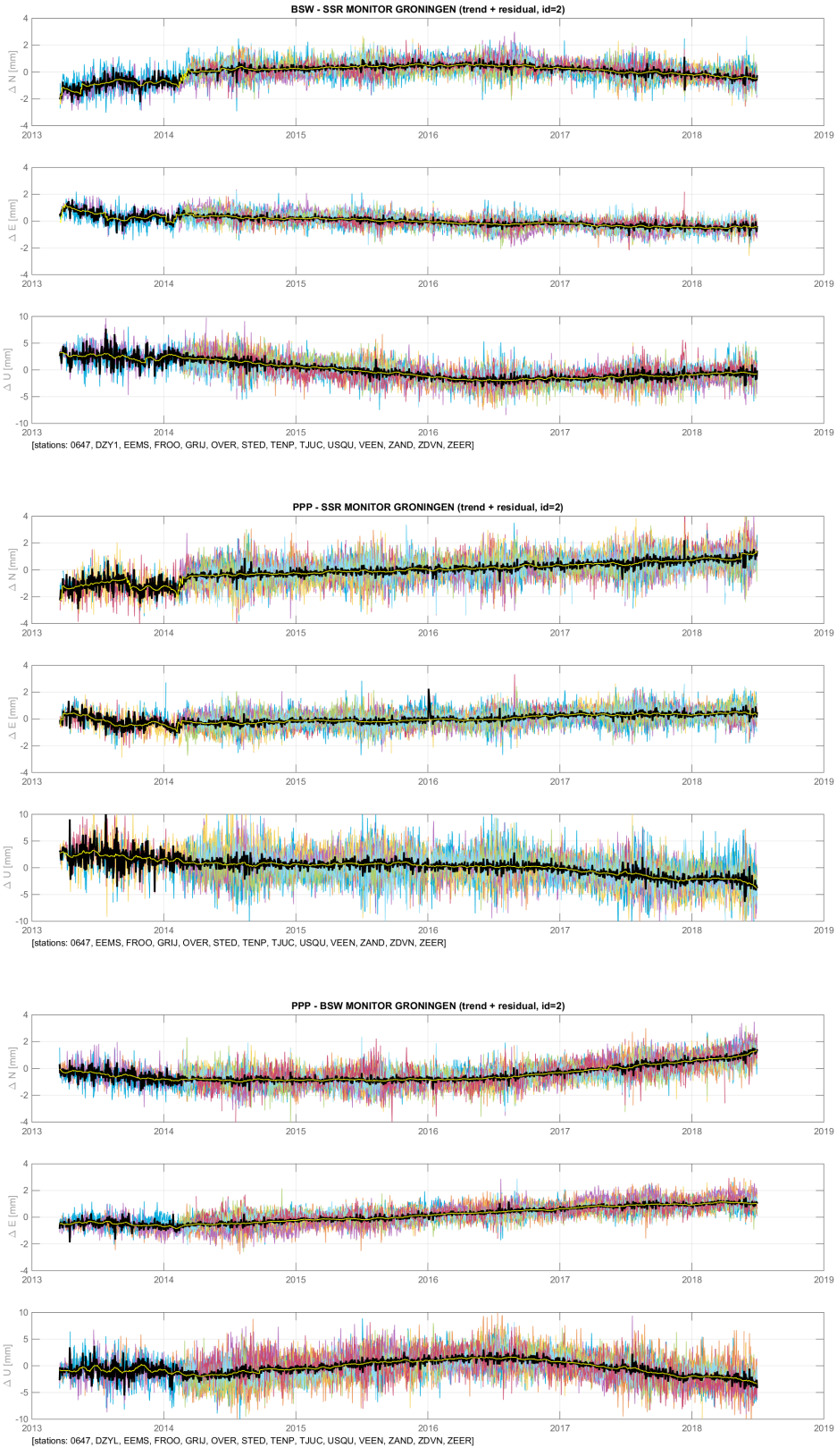

Figure 6.3: Trend difference for the Groningen monitoring stations: BSW-SSR (top), PPP-SSR (middle) and PPP-BSW (bottom). The colored lines in the background are the individual station differences, the thick black line is the time series of daily averages, and the yellow line is a moving 21 day median of the daily averages (with outlier and step detection).

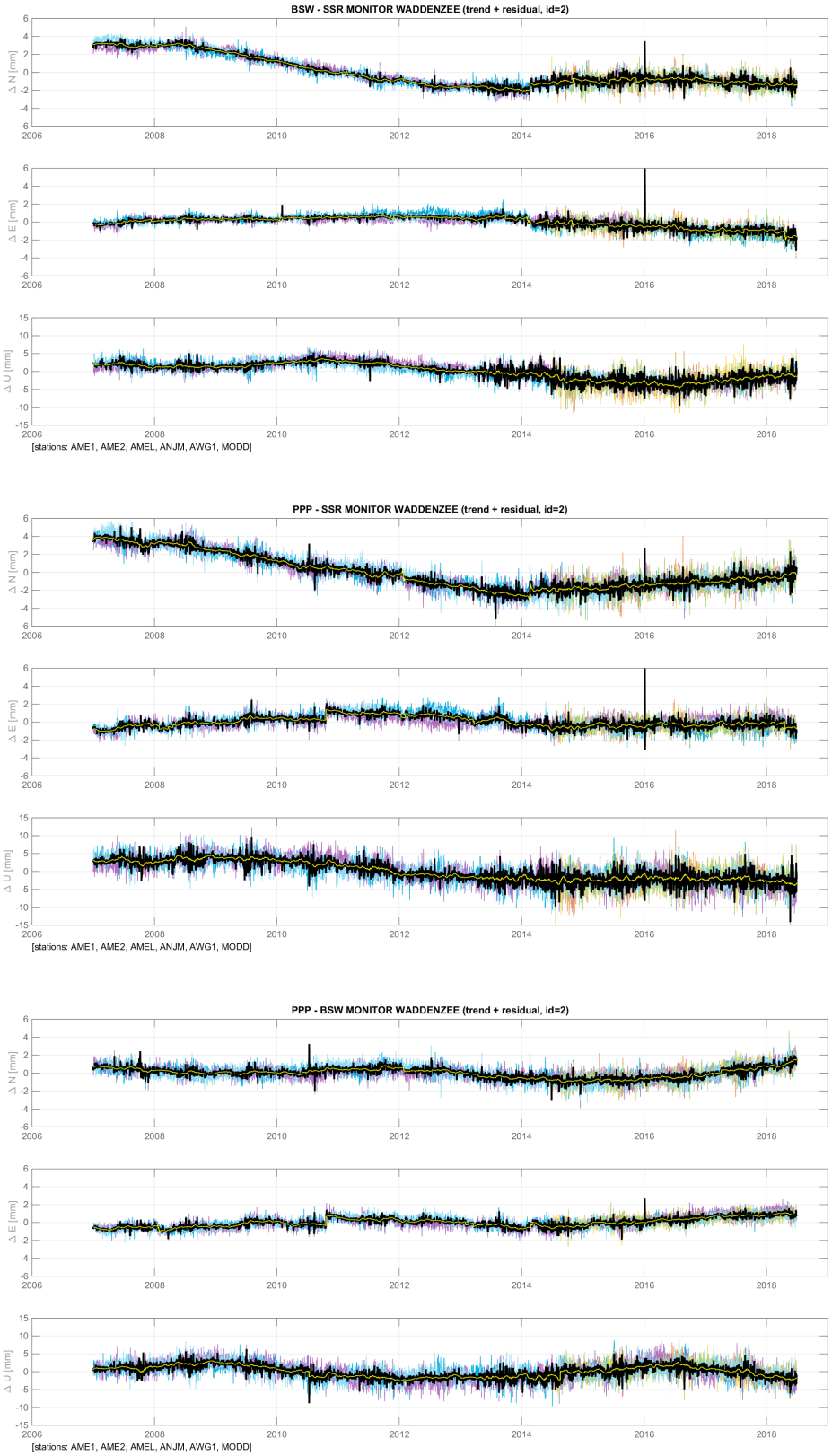

Figure 6.4: Trend difference for the Waddenzee monitoring stations: BSW-SSR (top), PPP-SSR (middle) and PPP-BSW (bottom). The colored lines in the background are the individual station differences, the thick black line is the time series of daily averages, and the yellow line is a moving 21 day median of the daily averages (with outlier and step detection).

In Figure 6.3 and 6.4 the differences in the estimated trends of the solutions are plotted for two groups of stations. Figure 6.3 shows the differences for the subset of station in the Groningen area, with stations 0647, DZYL, DZY1, EEMS, FROO, GRIJ, OVER, STED, TENP, TJUC, USQU, VEEN, ZAND, ZDVN and ZEER. Figure 6.4 shows the differences in the Waddenzee area, with stations AME1, AME2, AMEL, ANJM, AWG1 and MODD . For each group of stations a time series with the daily average difference is computed, using a simple Gauss-Seidel like iterative scheme with the daily averages and an unknown station offset such that the average difference between the station and daily average time series becomes zero. The colored lines in Figure 6.3 and 6.4 are the individual station differences, the thick black lime is the time series of daily averages, and the yellow line is a moving 21 day median of the daily averages (with outlier and step detection).

In 6.4 there a considerable differences for the horizontal components in the comparisons with the SSR solution, in particular for the North component. The reason for this is that, before 2014, the focus was on the vertical components and the horizontal coordinates of the NAM reference stations have not been adapted as they should have been, and some reference stations had a significant horizontal motion. Also, after 2014, new reference stations were added to the network, and two reference stations where ‘’demoted” to monitoring station.

The time series of daily averages and the 21 day moving medians are summarized in Figure 6.5 and 6.6 for the two groups of stations. Figure 6.7 shows the 21 day moving averages for the two groups in the same plot so that they are more easily to compare.

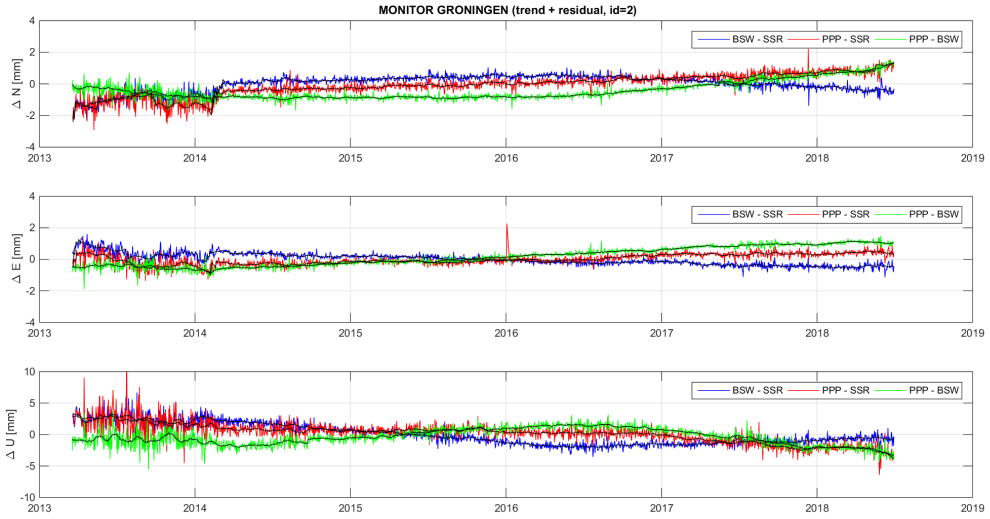

Figure 6.5: Trend differences for the Groningen monitoring stations for all combinations: SUM_TREND+RESIDUAL_GRO. The colored lines are time series of daily averages for the different combinations, the black lines are the moving 21 day median of the daily averages (with outlier and step detection).

There are differences in the average trend for any combination of solutions and station combination. The step in early 2014 in the differences with the SSR solution is related to the introduction of many new reference stations in the SSR solution, see the time line in Figure 1.2. The differences are summarized in Table 6.3, which gives the range (maximum minus minimum) of the trend differences for each combination. The range is computed from the moving 21 day median of the daily averages.

From Table 6.3 we conclude that, for the stations in the Groningen area, the difference in the North and East component are within a range (maximum minus minimum) of 3–4 mm and 2 mm respectively, and 5–7 mm for the height component, with the largest differences between the PPP and SSR solution. The differences between the BSW and PPP solution are the smallest. The largest differences are observed between the SSR and BSW, and SSR and PPP, solutions for the Waddenzee area over the period 2007.0-2013.3. As can be seen in Figure 6.7 and Table 6.3, the differences between

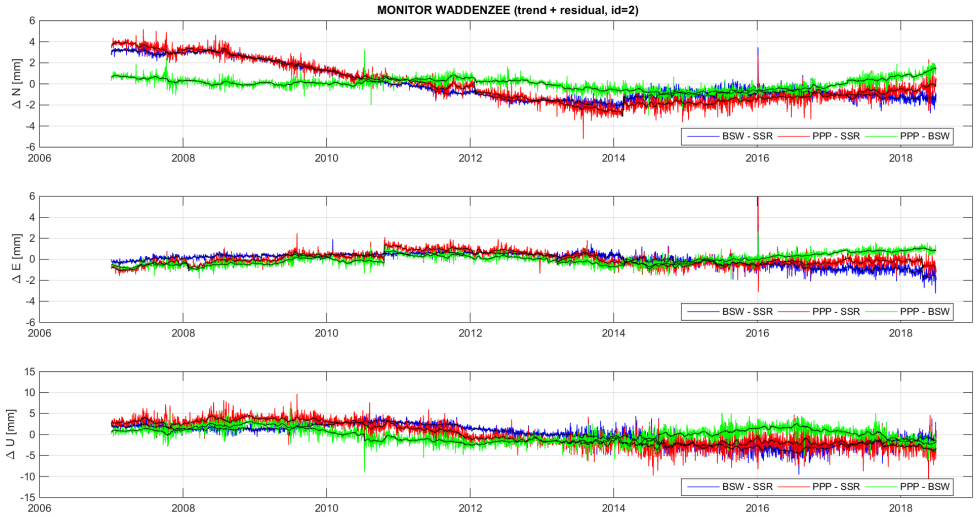

Figure 6.6: Trend differences for the Waddenzee monitoring stations for all combinations: SUM_TREND+RESIDUAL_WAD. The colored lines are time series of daily averages for the different combinations, the black lines are the moving 21 day median of the daily averages (with outlier and step detection).

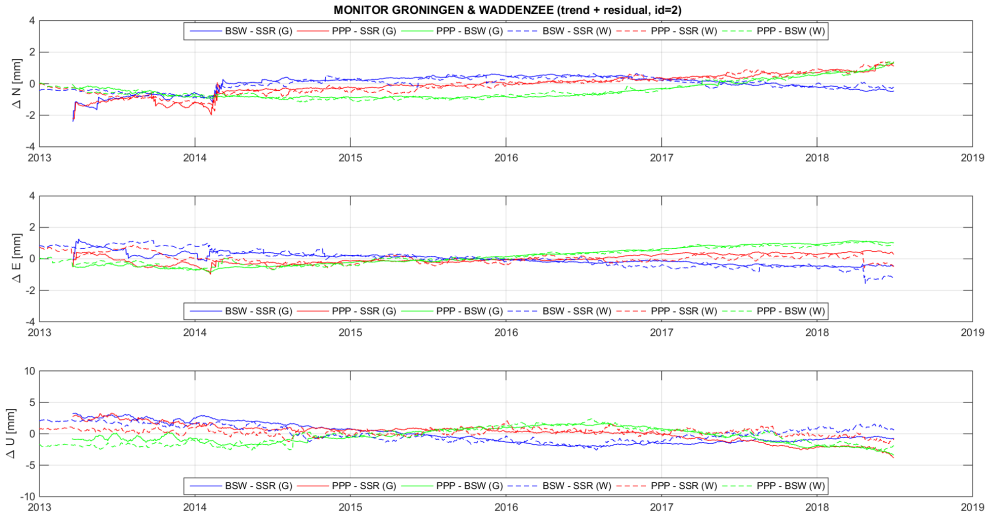

Figure 6.7: Trend differences for the Groningen (G) and Waddenzee (W) monitoring stations after 2013 for all combinations: SUM_TREND+RESIDUAL_NAM. The colored lines are time series of daily averages for the different combinations, the black lines are the moving 21 day median of the daily averages (with outlier and step detection).

Table 6.3: Range (maximum minus minimum) of the mean trend difference between two solutions computed from the moving 21 day median.

	North [mm]			East [mm]			Up [mm]		
	BSW SSR	PPP SSR	PPP BSW	BSW SSR	PPP SSR	PPP BSW	BSW SSR	PPP SSR	PPP BSW
Groningen (2013.3-2018.6)	3.02	3.63	2.33	1.82	1.52	2.01	5.35	7.11	5.05
Waddenzee (2013.3-2018.6)	1.57	3.13	2.58	2.77	1.57	1.86	4.95	3.73	5.15
Waddenzee (2007.0-2018.6)	5.31	7.06	2.58	2.86	2.50	2.25	8.25	8.61	5.73

Table 6.4: Mean velocity difference between two solutions.

	North [mm/y]			East [mm/y]			Up [mm/y]		
	BSW SSR	PPP SSR	PPP BSW	BSW SSR	PPP SSR	PPP BSW	BSW SSR	PPP SSR	PPP BSW
Groningen (2013.3-2018.6)	0.12	0.40	0.26	-0.21	0.15	0.37	-0.88	-0.84	-0.01
Waddenzee (2013.3-2018.6)	0.09	0.38	0.29	-0.34	-0.03	0.31	-0.30	-0.09	0.24
Waddenzee (2007.0-2018.6)	-0.42	-0.46	-0.04	-0.12	-0.03	0.09	-0.54	-0.68	-0.13

the BSW and PPP solutions for the Groningen and Waddenzee area are in good agreement, but this is not the case for the differences with the SSR solution. Therefore, the average trend for the Groningen and Waddenzee areas in the SSR solution is slightly different.

The trends for the PPP and BSW solutions show a slightly larger subsidence than the SSR solution, as can be seen also from Figure 6.7 and Table 6.4. This is very clear for the stations `AME1`, `ANJM` and `MODD` in the Waddenzee area that observed for a longer period, but the same can be observed for the stations in the Groningen area, which started observing after 2013. This is confirmed by Table 6.4 which gives the velocity difference between each pair of solutions. The larger differences are in the Groningen area, where the mean velocity difference in the up component between the SSR solution and BSW and PPP solutions is on average 0.86 mm/y lower. This is not alarming, remember, the vertical reference frame for the BSW and PPP solutions is ITRF2008, whereas for the SSR solution the reference frame is realized through reference station coordinates computed following a specific procedure (See Section 3.1.2). We come back to this in Section 7.3, where we will show that the NAM reference stations, which are kept fixed in the SSR solution, have a systematic vertical velocity of about -0.55 mm/y in the BSW and PPP solutions. In the same section we will connect the BSW and PPP solutions to a subset of the NAM reference stations. This gives a correction for the reference frame that affects the trend estimates of all stations in the same way. The new results, after correction for the reference frame, are discussed in Section 8.

6.4. PERIODOGRAMS

Figure 6.8 shows the periodograms for the three solutions. See also Figure 5.6 and the text in Section 5 related to this figure for an explanation. For the SSR solution there is hardly any improvement in the second iteration, this is because residual stack estimated after the first iteration does not have much power. However, for the BSW and PPP solutions, especially the PPP, there is a big improvement in the second iteration, resulting in a significant noise reduction in the estimated components. The final attained noise level is the smallest for the SSR solution, followed by the BSW and then the PPP solution. For frequencies larger than ten to twenty cycles per year the noise power for the BSW and PPP solutions become relatively flat. This is indicative for white (uncorrelated) noise. A small peak at about 70 cycles per year (5.2 day period) is visible in the PPP solution; the reason for this peak is not clear. The SSR solution has a completely different noise behavior. The two horizontal components more or less follow a flicker noise behavior as indicated by the dotted lines in the plots. However, after a period of 14 days, the up component follows an even more extreme power law behavior corresponding to a random walk (brown noise). The reason for this behavior is indicative for a low pass filter or smoothing of the high frequency component.

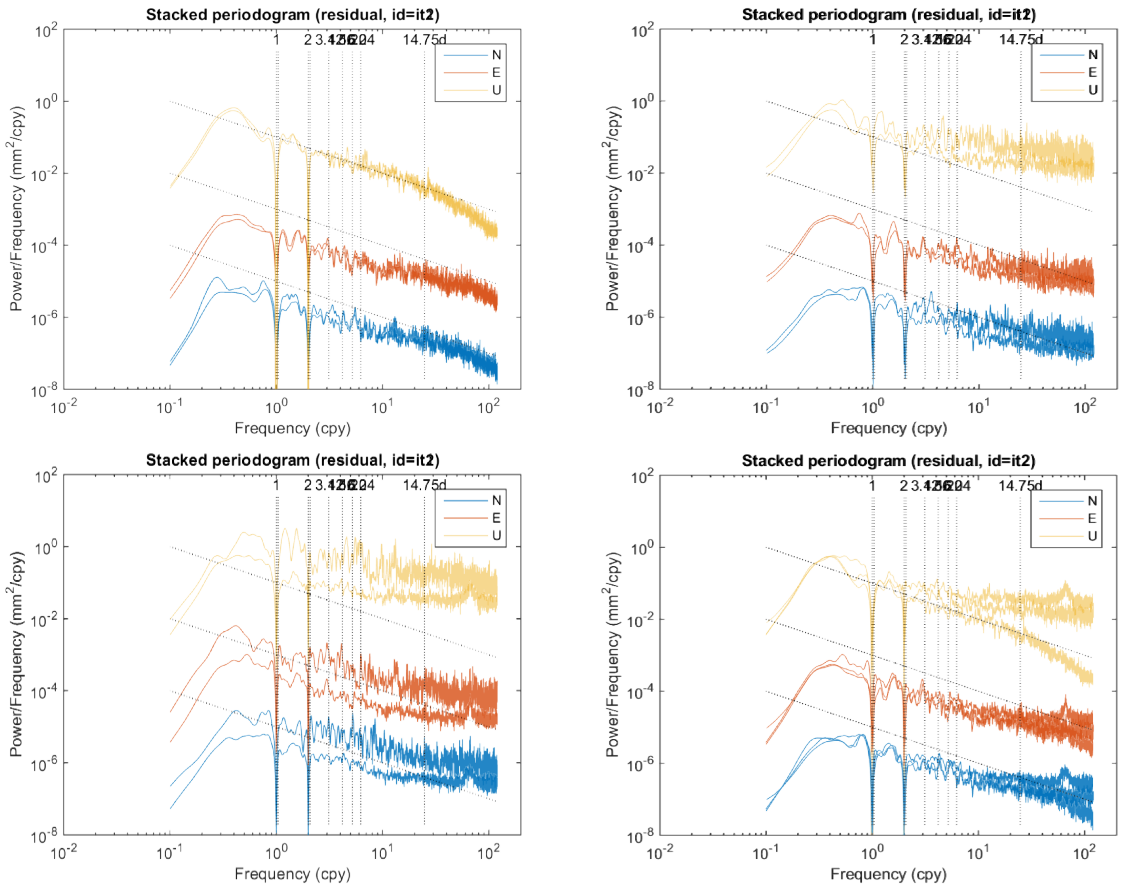

Figure 6.8: Periodograms for the first and second iteration, overlayed on each other, for the SSR solution (top left), the BSW solution(top right) and PPP solution (bottom left). The plot on the bottom right shows the periodograms for the SSR, BSW and PPP solutions overlayed on each other for the second iteration. The plots for the N, E and U component are offset; the slanted dotted lines represent the same power levels.

7

ANALYSIS OF NAM REFERENCE STATIONS

In the previous section the results for the NAM monitoring stations were analyzed. However, the BSW and PPP datasets also include the NAM reference stations in their solutions. In the SSR processing the coordinates for the NAM reference stations have been fixed (with incremental updates) and used as constraints for the solution. In this section, first, the BSW and PPP time series for the NAM reference stations are decomposed. Then the decomposed time series for the NAM reference stations are used to analyze the coordinates that have been used as constraints in the SSR processing. Finally, the BSW and PPP solutions are connected to a subset of the NAM reference stations, and a time series of shifts in the North, East and Up direction are computed for the BSW and PPP solutions. These shifts are applied to the NAM monitoring station in Section 8.

7.1. TIME SERIES DECOMPOSITION OF THE NAM REFERENCE STATIONS (BSW+PPP)

A time series decomposition of the NAM reference stations has been carried out for the BSW and PPP solutions. The decomposition includes the station SCHI, an AGRS station, just 2 m from the NAM reference station SCH1 at Schiermonnikoog. The decomposition also includes stations 0647 and VEEN which have been reference stations initially for GPS campaigns, but have never been used as reference stations for the continuously operating GPS stations, and which have been ‘’demoted” to monitoring stations in 2013. These decompositions are excluded from most analyses in this section. Figure 7.1 shows the estimated periodic components, the trend+residuals, and the trend function for both solutions, but without 0647 and VEEN, because no overlapping data was available in the period they were reference stations. The BSW solution is plotted in a darker color over the PPP solution. The time series have been corrected for a common mode, estimated in a first iteration from the periodic components and residuals, using a subset of reference stations. The stations VEEN (trend break in 2018), NIEU (station was relocated) and SCHI (not a NAM reference station) were excluded from the common mode computation. As can be seen from Figure 7.1 there is again a good agreement in the periodic components and also the estimated trends agree quite well, although there are some subtle differences which become more apparent later when the trend differences are analyzed in more detail. In Figure 7.1 both the trend+residual is plotted, as well as the underlying trend function itself. The trend function consists of piece-wise continuous line segments, with each segment covering a period of about 2 years, see also Section 5,

The difference in the estimated reference station trends for the BSW and PPP solutions is plotted in Figure 7.2, similar to what was done for the monitoring stations in the Waddenzee and Groningen areas in Figures 6.3 and 6.4. The colored lines in Figures 6.3, 6.4 and 7.2 are the individual station differences, the thick black line is the time series of daily averages, and the yellow line is a moving 21 day median of the daily averages (with outlier and step detection). The daily average difference is computed using a simple Gauss-Seidel like iterative scheme, with the daily averages and an unknown station offset, such that the average difference between the station and daily average time

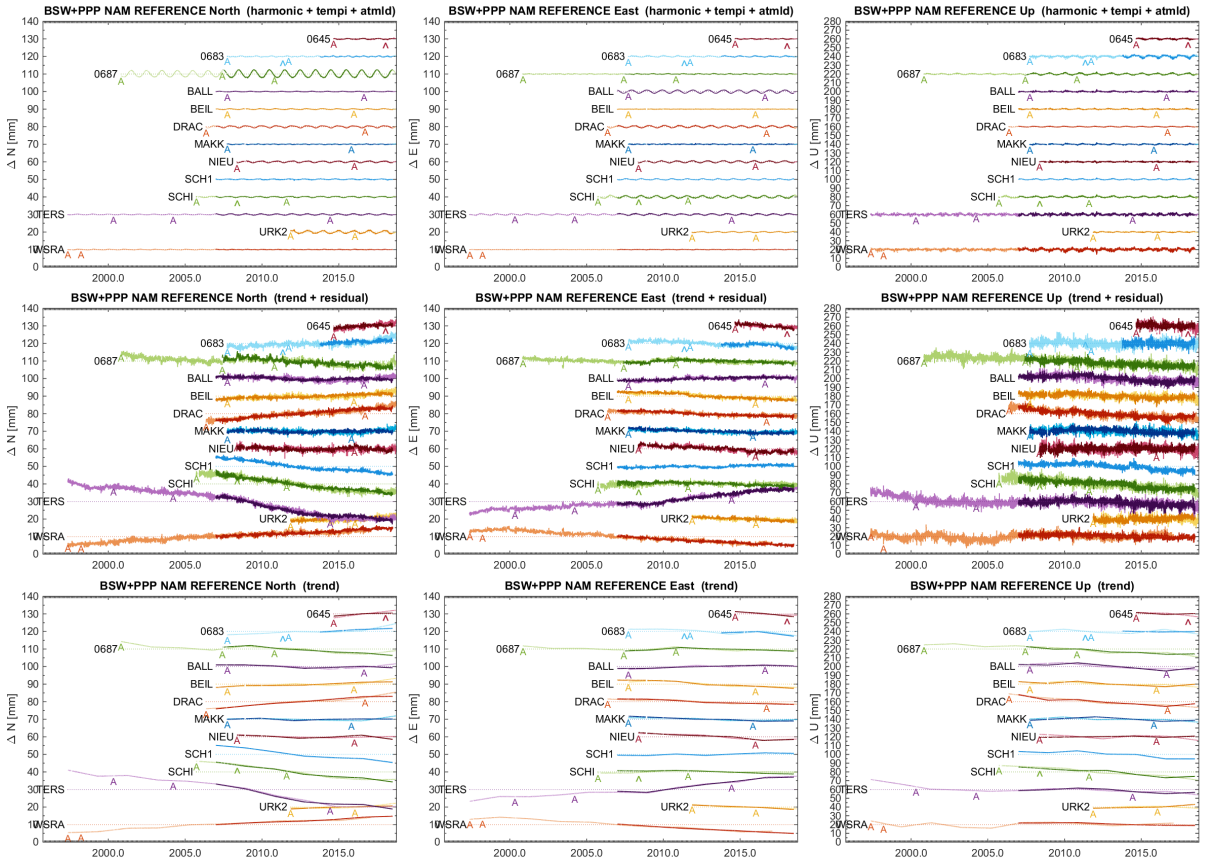

Figure 7.1: Decomposition of the NAM reference stations for the BSW and PPP solution: periodic components (top) trend+residual (middle) and trend only (bottom). The BSW solution is in a darker color plotted on top of the PPP solution in a lighter color. Antenna changes are marked by a letter "A" and other steps by a "∧". There is no overlapping data for the short period 0647 and VEEN have been reference stations.

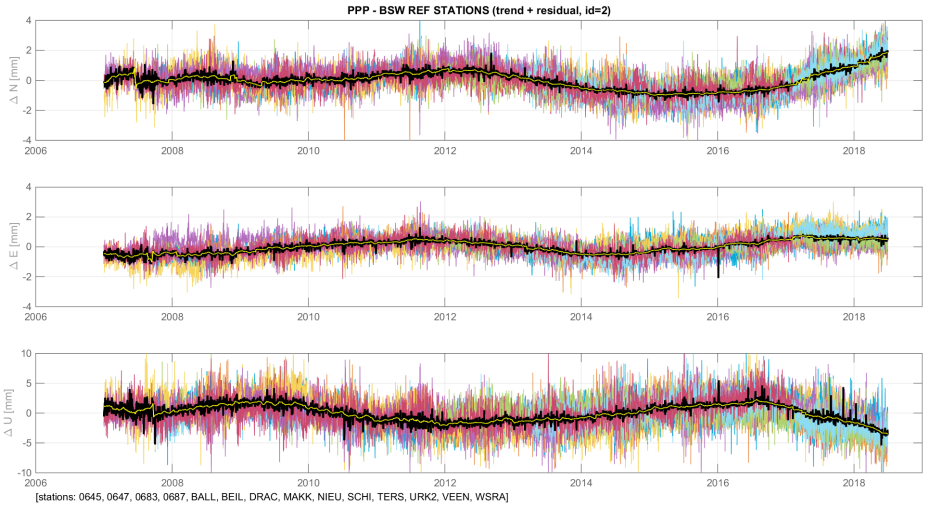

Figure 7.2: Trend difference for the reference stations for the period 2007.0 - 2018.6: PPP-BSW. The colored lines in the background are the individual station differences, the thick black line is the time series of daily averages, and the yellow line is a moving 21 day median of the daily averages (with outlier and step detection).

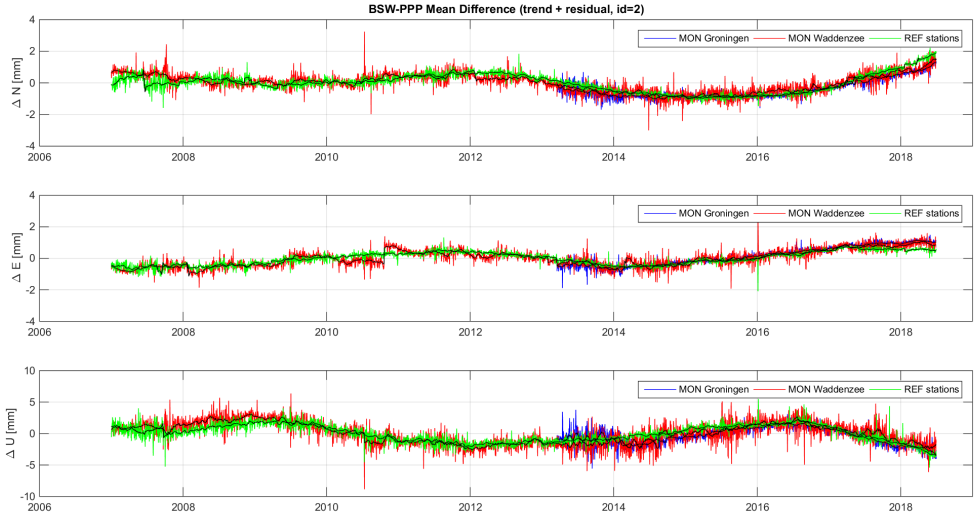

Figure 7.3: Average trend differences between the BSW and PPP solutions for the NAM monitoring and reference stations for the period 2007.0 - 2018.6 : SUM_TREND+RESIDUAL_BSW-PPP. The colored lines are time series of daily averages for respectively the NAM monitoring stations in the Groningen area, monitoring stations in the Waddenzee area and the NAM reference stations. The black lines are the moving 21 day median of the daily averages (with outlier and step detection).

series becomes zero. The offset has been subtracted from the individual series. The time series of daily averages and the 21 day moving medians are plotted together in Figure 7.3 so that they are more easily to compare. It confirms what was already observed in Figure 6.7 and Table 6.3, namely that, for various subsets of stations, the average daily differences between the BSW and PPP solutions are consistent.

7.2. COMPARISON WITH SSR REFERENCE STATION COORDINATES

The NAM reference station coordinates in the SSR solution are kept fixed (not adjusted) using coordinates determined by a special procedure described in Section 3.1.2. The reference station coordinates are checked by 06-GPS once per year, usually in the month of May, and only if the coordinates exceed certain limits (See Section 3.1.2) the reference station coordinates for subsequent runs are adjusted. In case there is an antenna change in one of reference stations the procedure is slightly different: the coordinates of that station are recomputed within the reference station network, keeping the reference station coordinates fixed, except for the station with the antenna change. The coordinates of the reference station with the antenna change are then fixed to the new coordinates in subsequent runs of the monitoring network.

The coordinates for the NAM reference stations have been provided by 06-GPS in a Microsoft Excel file [Dentz, 2019]. These have been used to generate a time series of reference station coordinates in the same format as used for the BSW and PPP solutions, as explained in Section 4.1.2. This reference station time series is labelled `SSRref`.

Figure 7.4 shows the SSRref reference station coordinates overlayed on top of the BSW and PPP trend+residual solutions of Figure 7.1. The results should be interpreted with great caution. The reference station time series contain effects from both reference station movement and antenna changes. The effect of an antenna change has been removed in the BSW and PPP series by estimating a step, but this is not the case for the reference station coordinates in SSRref.

Unfortunately, we are not able to separate the effect of antenna changes and reference station movement in the SSR reference station coordinates. In case there is an antenna change in one of reference stations, the coordinates of that station are recomputed immediately within the SSR reference station network, keeping the reference station coordinates fixed except for the station with the

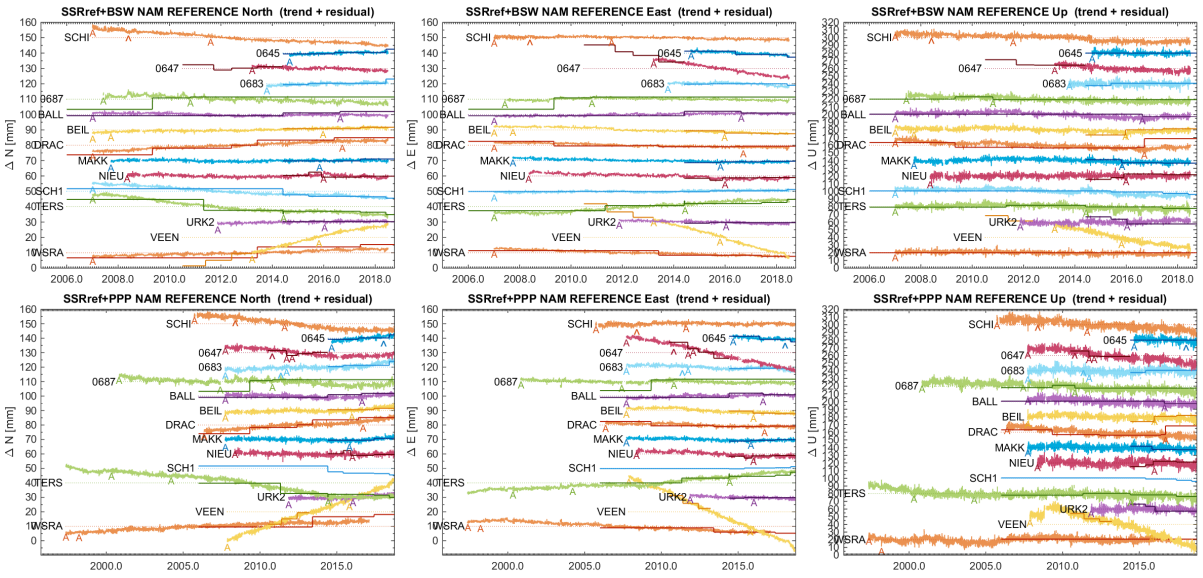

Figure 7.4: NAM reference station coordinates for the SSR solution plotted on top of the BSW and PPP solutions for the NAM reference stations: SSRef+BSW (top) and SSRef+PPP (bottom). The BSW and PPP solution are composed of the estimated trends plus residuals. Antenna changes are marked by a letter "A" and other steps by a "∧". Please note that steps due to antenna changes are still present in the SSR reference station coordinates, whereas, they have been removed in the BSW and PPP solutions.

antenna change. The time of the change and new coordinates are reported. But, the new station coordinates include the effect of both the antenna change as well as the accumulated reference station motion. To obtain only the effect of the antenna change it would be necessary to compute the coordinate in the week before, and in the week after, the change, and then take the difference. However, this is not part of the current procedure.

In the BSW solution `0647` and `VEEN` started to be processed only when they became monitoring stations in 2013, but not before, however, in the PPP solution they have also been processed before 2013. On the other hand, `SCH1` is included in the BSW solution, but not in the PPP solution.

Figure 7.5 shows the differences in the SSRref reference stations coordinates with the estimated trend for the BSW and PPP solutions. The colored lines in Figure 7.5 are the individual station differences, the thick black line is the time series of daily averages, and the yellow line is a moving 21 day median of the daily averages (with outlier and step detection). The daily average difference is computed using a simple Gauss-Seidel like iterative scheme, with the daily averages and an unknown station offset, such that the average difference between the station and daily average time series becomes zero. The offset has been subtracted from the individual series. The time series of daily averages and the 21 day moving medians are plotted together in Figure 7.6, together with the BSW-PPP difference of Figure 7.2, so that they are more easily to compare.

Figure 7.6 illustrates the difference between the reference frames for the three solutions quite well. For the height component we can conclude the agreement is within a centimeter, and even better for the horizontal components. However, there are some larger discontinuities in the horizontal coordinates for the SSR reference station coordinates. This could be related to the fact that in the procedure to check the reference station coordinates the same criterion is used for the horizontal and vertical components (Section 3.1.2), despite the fact that the horizontal and vertical coordinates have a different precision. Also, after 2011, we can observe a negative slope in the average of the SSRref reference station coordinates, compared to the BSW and PPP solutions, that is consistent with the velocity difference we observed in the previous section for the NAM monitoring stations. However, we cannot say (yet) if this is related to the SSRref reference station coordinates or the ITRF2008 reference frame used for the BSW and PPP solutions.

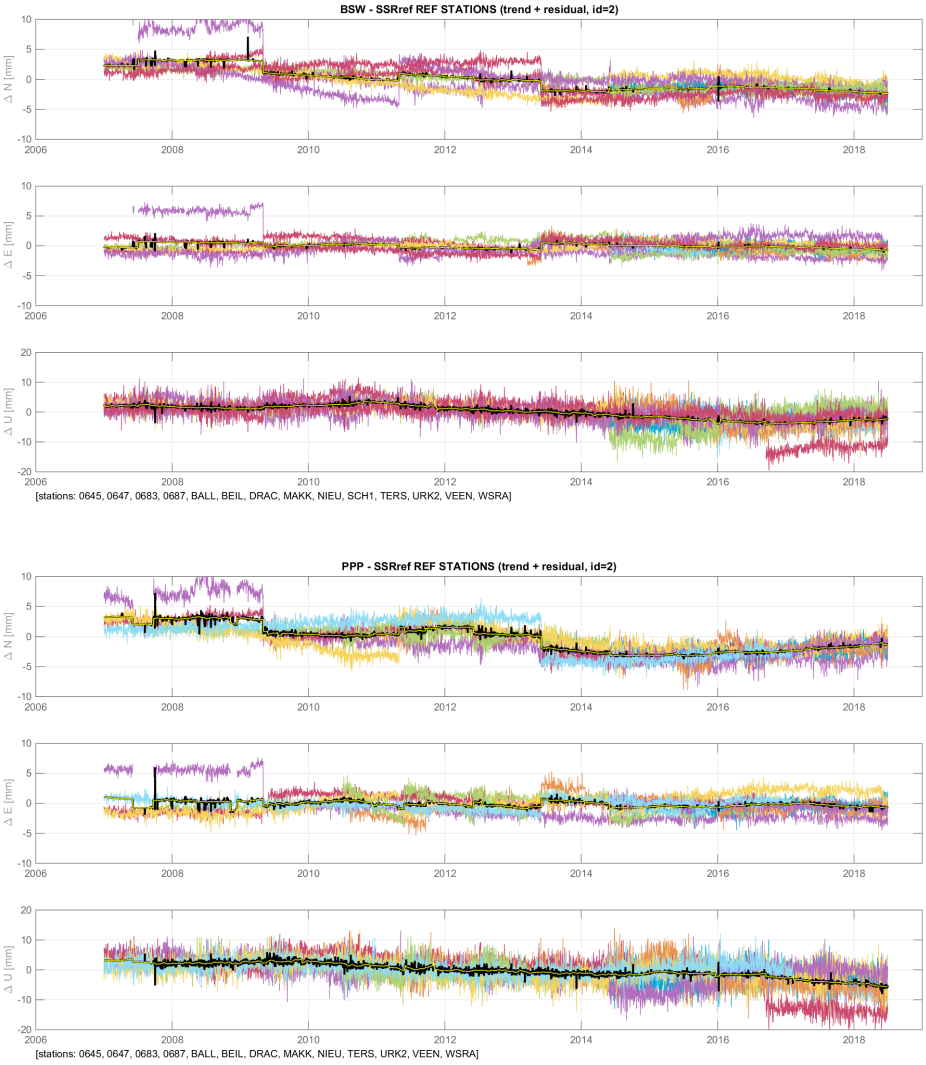

Figure 7.5: Trend difference for the reference stations for the period 2007.0 - 2018.6: BSW-SSRref (top) and PPP-SSRref (bottom). The colored lines in the background are the individual station differences, the thick black line is the time series of daily averages, and the yellow line is a moving 21 day median of the daily averages (with outlier and step detection). BSW and PPP are actual GPS solutions, SSRref are the reference station coordinates used for SSR solution. See also Figure 7.2 for the differences between the BSW and PPP solution. Please note that steps due to antenna changes are still present in the SSR reference station coordinates, whereas, they have been removed in the BSW and PPP solutions.

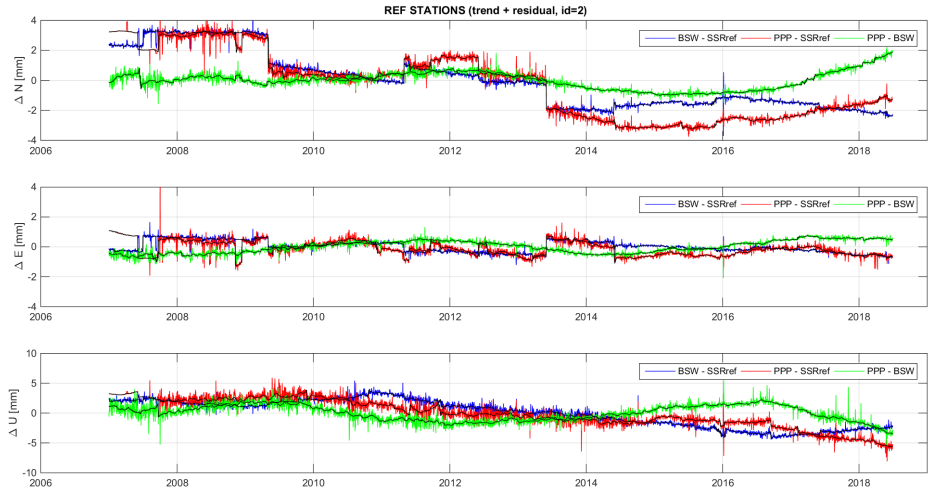

Figure 7.6: Average trend differences for the NAM reference stations for the period 2007.0 - 2018.6: SUM_TREND+RESIDUAL_REF. The colored lines are time series of daily averages for respectively BSW-SSRref, PPP-SSRref and BSW-PPP. The black lines are the moving 21 day median of the daily averages (with outlier and step detection). BSW and PPP are actual GPS solutions, SSRref are the reference station coordinates used for SSR solution. Please note that steps due to antenna changes are still present in the SSR reference station coordinates, whereas, they have been removed in the BSW and PPP solutions.

7.3. ANALYSIS OF REFERENCE STATION STABILITY

The BSW and PPP time series of reference station coordinates, for the period 2007.0-2018.6, is shown in Figure 7.7. The colored lines in Figure 7.7 are the individual station time series, the thick black line is the time series of daily median, and the yellow line is a moving 21 day average of the daily medians (with outlier and step detection). The daily median is used, because the daily median is a bit robust than the daily average. This is confirmed by runs which used daily averages instead of the median. The daily average (or median) difference is computed using a simple Gauss-Seidel like iterative scheme, with the daily averages (or medians) and an unknown station offset, such that the average difference between the station and daily average (median) time series becomes zero. The offset has been subtracted from the individual station time series. Figure 7.7 uses 11 reference stations: 0645, 0683 0687, BALL, BEIL, DRAC, MAKK, NIEU, SCHI, URK2 and WSRA. The stations 0647 and VEEN have not been used because they have not been used as reference stations for the continuously operating GPS receivers, and because they became (part-time) monitoring stations in March 2013. Furthermore, the AGRS station TERS is known (from local surveys) to move in the direction of the nearby harbor channel, is also not used. The island station SCHI is used instead of SCH1, as both SCH1 and SCHI are located on the same building, and only SCHI is used by the PPP solution.

As can be seen from Figure 7.7 there are big differences between the stations. Apparently, the reference stations move with respect to each other. The idea is to remove reference stations successively, starting with the one that has the largest deviations, until a satisfactory selection is obtained. The largest differences are 7 mm with respect to the time series of daily averages and 21 day moving median, with the largest deviations are for the station SCHI. When we remove SCHI, and repeat the computation with 10 selected reference stations, the differences are within 5 mm. Next the station DRAC is removed from the selection, which happens to be close to a gas-reservoir. Also, reference station coordinates of SCH1 and DRAC have undergone several small coordinate adaptions in the SSR solution in the recent years, which is another reason to remove them. Finally, after removing the next stations BALL and 0687 (Borkum), a more or less satisfactory result is obtained. The final selection of 7 reference stations, 0645, 0683, BEIL, MAKK, NIEU, URK2 and WSRA, is shown in Figure 7.8. For the final selection of reference stations the daily average is used instead of the median. The final differences are now within a few mm.

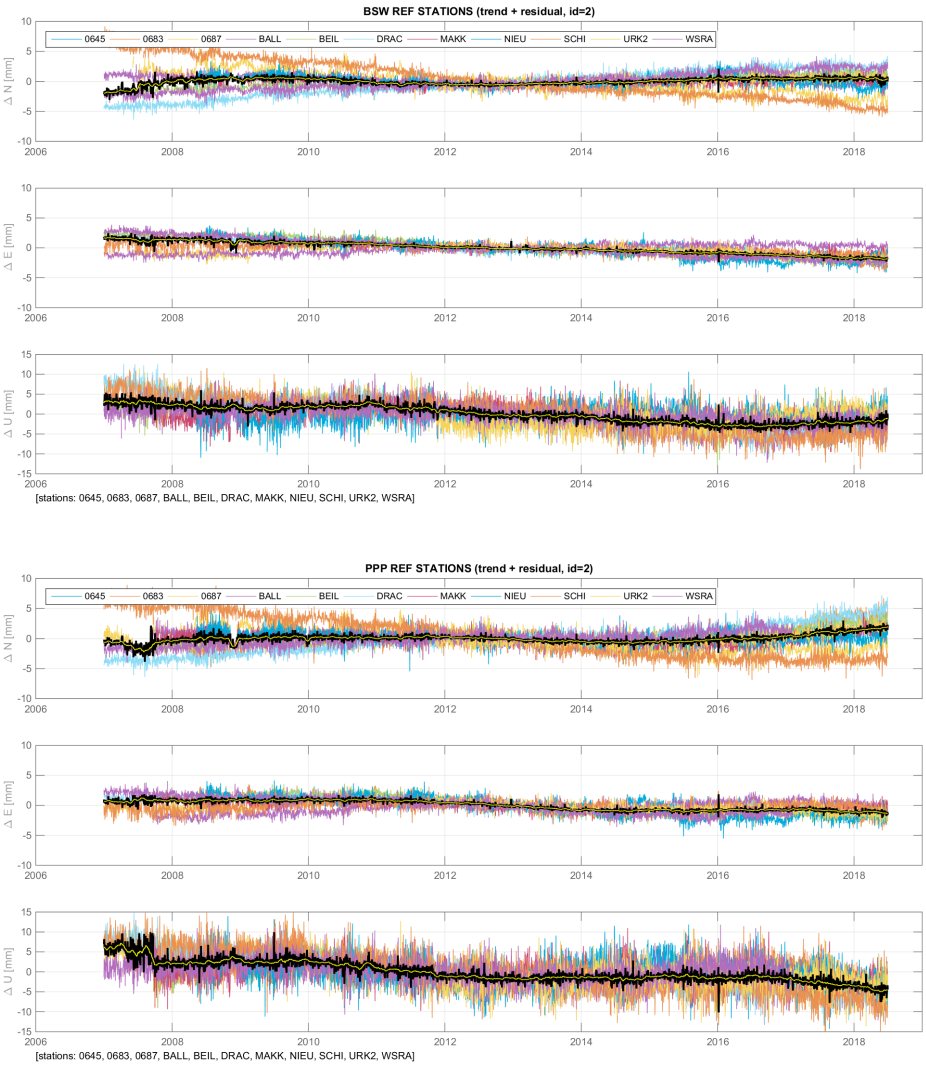

Figure 7.7: Reference station coordinate time series for the period 2007.0 - 2018.6: BSW (top) and PPP (bottom). The colored lines in the background are the individual station time series (trend+residual), the thick black line is the time series of daily median, and the yellow line is a moving 21 day average of the daily median (with outlier and step detection).

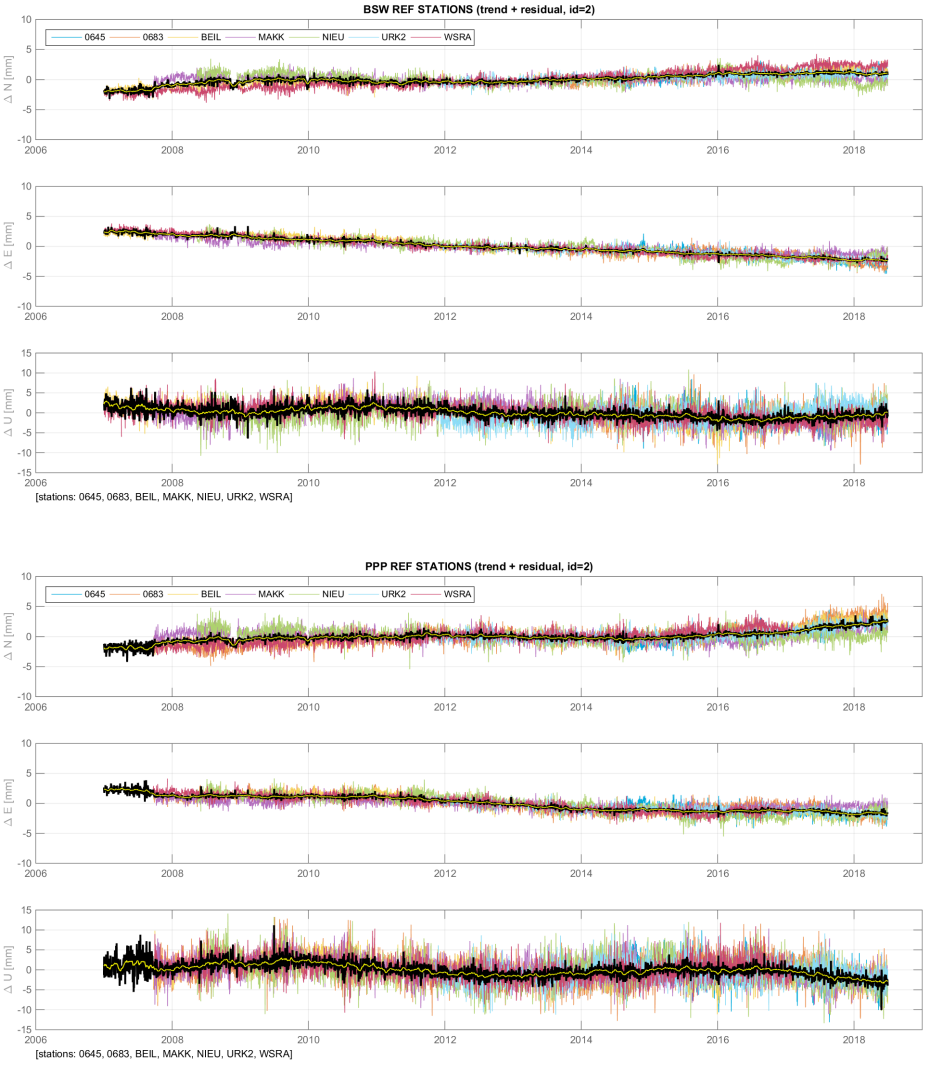

Figure 7.8: Reference station coordinate time series for the period 2007.0 - 2018.6: BSW (top) and PPP (bottom). The colored lines in the background are the individual station time series (trend+residual) for the final selection of 7 reference stations. The thick black line is the time series of daily average, and the yellow line is a moving 21 day average of the daily average (with outlier and step detection).

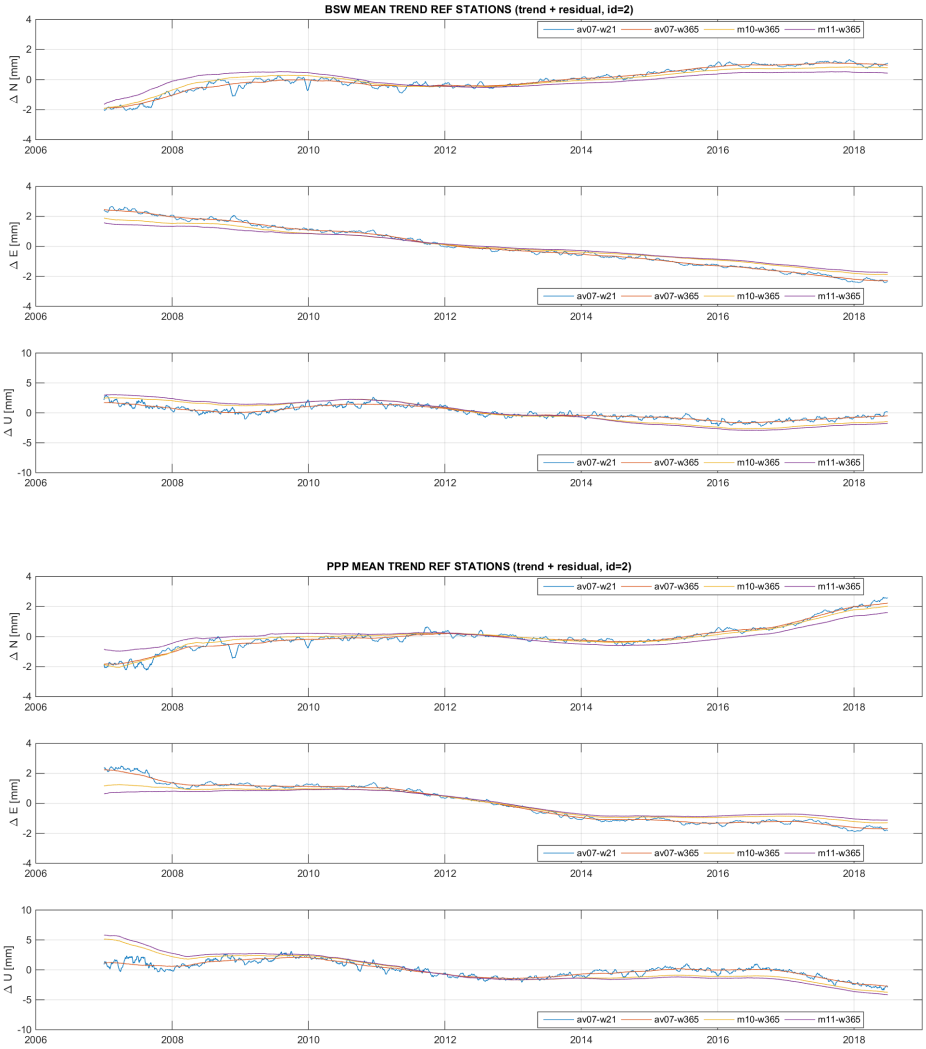

Figure 7.9: Average trend for various selections of NAM reference stations for the period 2007.0 - 2018.6: BSW (top) and PPP (bottom). Results are show for selections of 11, 10 and 7 reference stations. For the selection with 11 and 10 stations the 365 day moving average of the daily medians is showns. For the final selection with 7 stations the 365 and 21 day moving averages of the daily averages are shown.

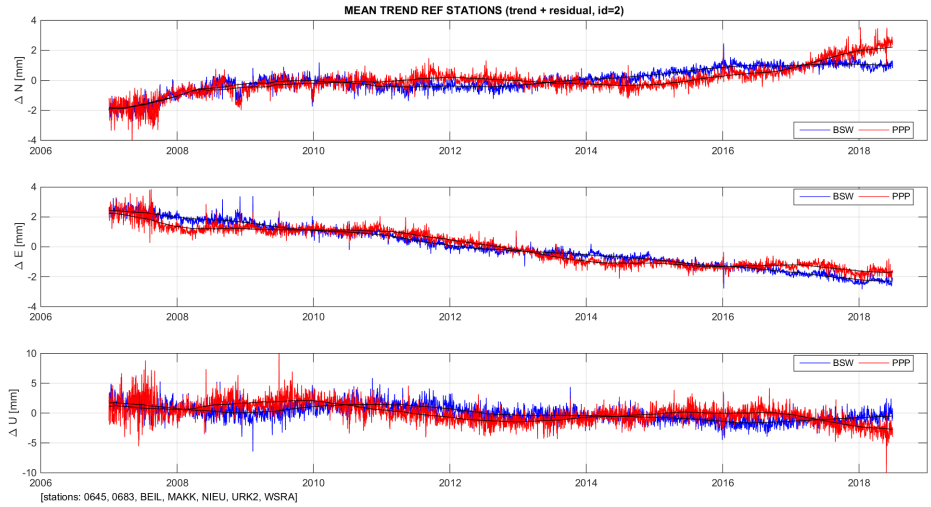

Figure 7.10: Average trend for the NAM reference stations in the period 2007.0 - 2018.6 for the BSW and PPP solutions: SUM_TREND+RESIDUAL_REF_av07_w365. The red and blue lines are time series of daily averages for respectively BSW and PPP solutions using 7 selected reference stations. The black lines are the moving 365 day average of the daily averages that will be used as reference frame corrections.

The various options and reference station selections are compared in Figure 7.9. We have not plotted all the combinations that were investigated. Figure 7.9 shows results for the selections with 11, 10 and 7 selected stations. For the selections with 11 and 10 stations the daily medians are used and smoothed by a moving average filter of 365 days. For the final selection with 7 references stations the daily means (instead of median) are used, and the results are shown for a 21 and 365 moving average filter.

The whole process of eliminating reference station is not very satisfactory and to some extent rather subjective. Our objective is to compute the average trend with respect to an ensemble of reference stations, which each may have some autonomous motion. Therefore, we should use as many reference stations as possible, and only deselect stations when there are good grounds to do so, so that the effect of autonomous reference station motion is randomized and averaged out. Despite the fact that no formal testing was done on the suitability as reference station, we believe our overall objective is achieved with the final selection of 7 reference stations.

The time series of daily averages and the 365 day moving average for the BSW and PPP solutions are plotted together in Figure 7.10 so that they are more easily to compare. The estimated velocity in the average North, East and Up components is 0.20, −0.42 and −0.25 mm/y for the BSW solutions, and 0.21, −0.35 and −0.27 mm/y for the PPP solution. If we look at these numbers we see that they are similar for the both solutions. If we take the average for the vertical component, we can conclude that the average vertical velocity of the selected 7 reference stations is about −0.26 mm/y with respect to ITRF2008.

7.4. CHOICE OF REFERENCE FRAME

The BSW and PPP solutions are in ITRF2008, but with the plate motion removed for the horizontal components. As explained in Section 4.2 the plate motion correction is computed using the transformation from ITRF2008 to ETRF2000[1]. The nominal station velocity in ITRF2008 with respect to ETRF2000 is shown in Figure 7.11. Only the horizontal velocities have been used to correct the BSW and PPP time series, the Up component is not corrected. The vertical component of the BSW and

[1] In the actual conversion actually ITRF2014 is used instead of ITRF2008, but since only the horizontal coordinates are corrected, it does not affect our analysis of the vertical components in this paragraph.

PPP solutions are therefore in IGb08 (ITRF2008). The difference in vertical velocity for the ITRF2008 and ETRF2000 reference frame is about 0.91 mm/y for the North of the Netherlands. Therefore, if we take the average vertical velocity of the selected reference stations, which is about −0.26 mm/y with respect to ITRF2008, subtract the 0.91 mm/y between ITRF2008 and ETRF2000, we find that the average vertical velocity of the selected reference stations is about −1.17 mm/y in ETRF2000. So, we an conclude that not correcting the vertical velocities from ITRF2008 to ETRF2000 was the correct choice in Section 4.2.

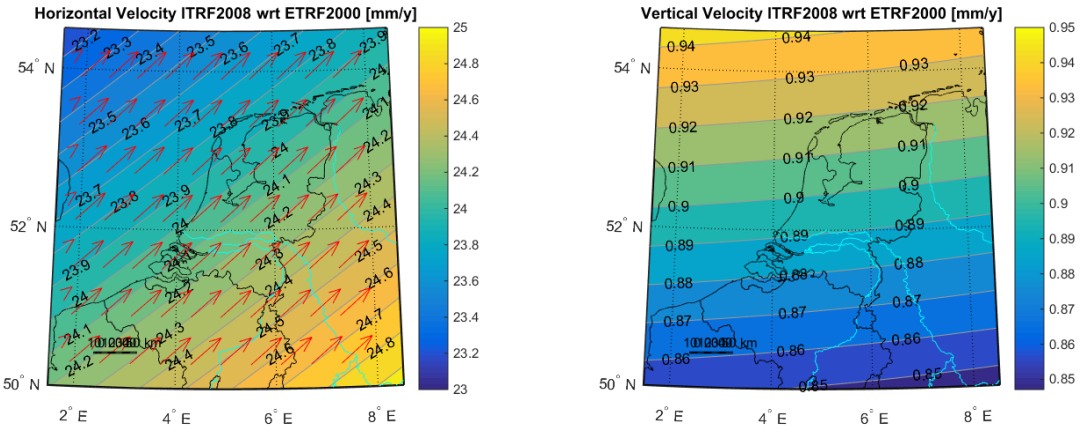

Figure 7.11: Nominal station velocity in ITRF2008 with respect to ETRF2000. The horizontal velocities are shown in the plot on the left, the vertical velocities are shown in the plot on the right.

The actual behavior of the reference stations in the vertical is actually closer to ITRF2008 than ETRF2000, but nonetheless, the ITRF2008 reference frame is not perfect. The observed −0.26 mm/y systematic velocity for the reference stations of Figure 7.10 is something worth correcting for. This is something that can be done in multiple ways: the North, East and Up components in the BSW and PPP solutions can be shifted using either (i) the daily average (or median) of the selected reference stations, (ii) one of the moving averages (21, 365 or any other number of days), or (iii) using the estimated average velocity. We selected to use the 365 day moving average. The main reason for this is that we believe that only the estimated trend functions should be affected; we don't want to change the periodic components, steps and residuals from the decomposition. This is also the reason that in black lines in Figure 7.10 are the 365 day moving averages: this is what will be used in the next section as reference frame correction.

8

SYNTHESIS

In this section the trend series analysis for the NAM monitoring stations of Section 6.3 is repeated, but now using the BSW and PPP trend series that have been corrected for the reference frame motion, a.k.a. reference frame correction. The reference frame correction for the BSW and PPP solution was computed in Section 7.3, using the trend series for 7 stable NAM reference stations as input. It minimizes the average displacements for the selected reference stations, using the mean over the reference stations, and smooths the reference frame correction by taking a moving average with a period of one year so that only the estimated trend functions are impacted. The reference frame correction should not affect the periodic components, steps and residuals of the NAM monitoring stations, that were analyzed in Section 6, only the trend series is affected.

The reference frame correction, sort of, acts like a third ''common" mode term. The periodic components and residuals for the NAM monitoring station in Section 6 were already corrected for a common mode each, estimated from the monitoring stations themselves, whereby we made certain that the estimated trend function was not affected by these two common modes. The reference frame correction is different, it is computed from *another* set of stations, the selected 7 NAM reference stations in Section 7.3. It is a time series, smoothed using a yearly moving average so that only the trend function is affected, which shifts the solution in the North, East and Up component. The reference frame correction is similar to a common mode in the sense that the North, East and Up time series for each monitoring station is shifted by the same amount.

The trend series of the SSR is not corrected, this is because the SSR solution of Section 6.3 has already been connected to reference stations, and because we have no time series estimates for the NAM reference stations in the SSR solution. But, of course, the SSR solution is compared (again) with the modified BSW and PPP solutions.

The trend series of Figure 6.2 are plotted again in Figure 8.1 after the reference frame correction for the BSW and PPP solutions. The trend is composed of two components: the estimated trend function (spline function or polynomial) with the residuals of the decomposition added to it, except for `NORG`, where the harmonic component is added. In each sub-figure of Figure 8.1 the results of two solutions are plotted on top of each other. The first solution is plotted in a darker color than the second solution. The SSR solution is the same as in Figure 6.2, only the BSW and PPP solutions are different. The time series at the bottom of each plot is the common mode correction (CMC), or residual stack, with the reference frame correction included. The CMC has been estimated in the first iteration from the residuals, using the same subset of stations as for the periodic common mode, and is then subtracted from the data in the second iteration. The CMC in the trend (or actually residuals) only reduces the noise in the time series, in particular for the PPP, and to a lesser extend in the BSW solution. The CMC in Figure 8.1 includes the reference frame correction with opposite sign, so that the sum of the individual series and CMC in Figure 6.2 and 8.1 is the same.

As mentioned before in Section 6.3, the station `VEEN` has a significant change in its horizontal velocity in the first half of 2018. This is well captured in the estimated trend (trend function plus

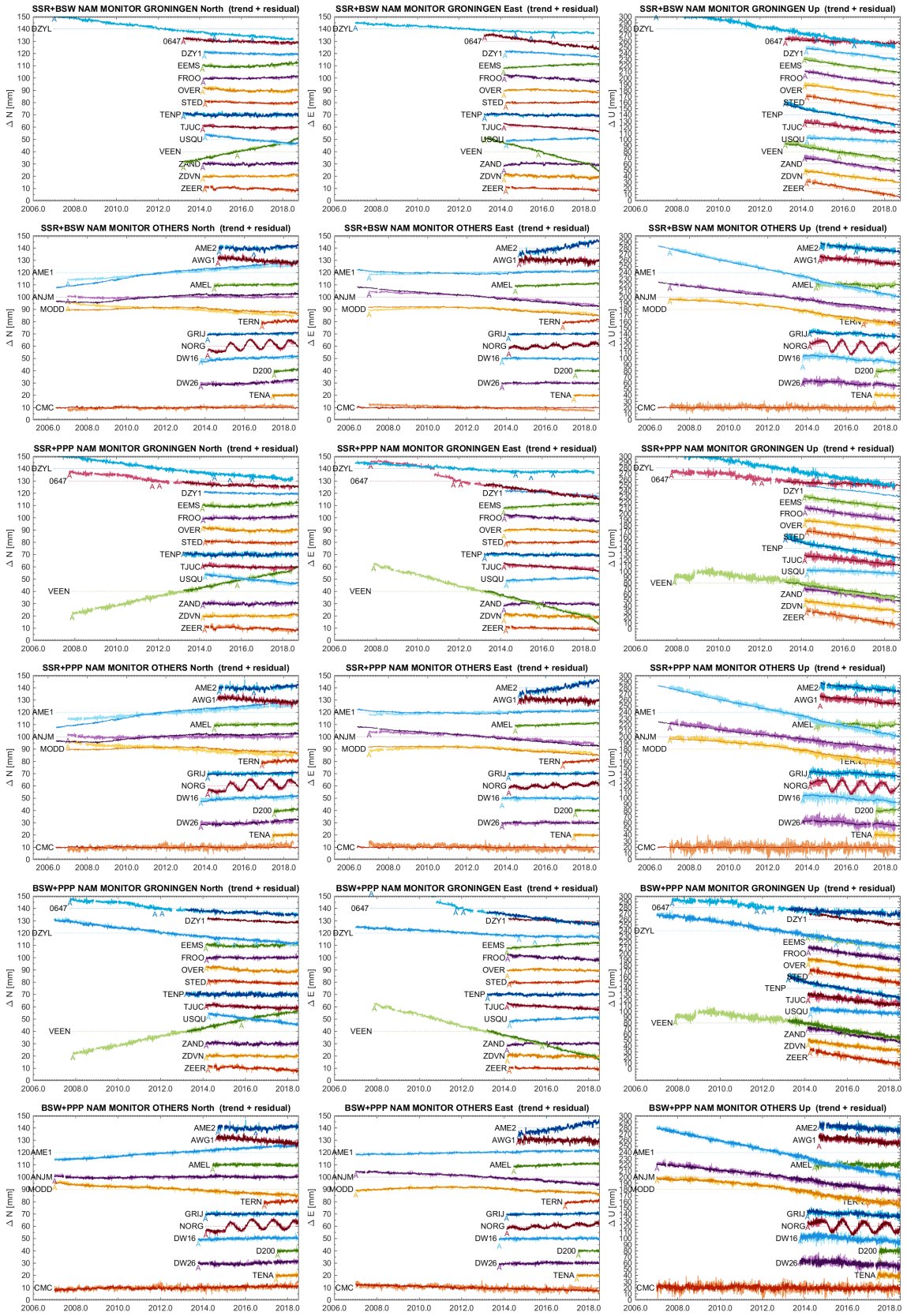

Figure 8.1: Trend plus residuals for the NAM monitoring stations after reference frame correction for the BSW and PPP solutions. Two solutions are plotted on top of each other: SSR-BSW (top), SSR-PPP (middle) and BSW-PPP (bottom). The first solution is in a darker color. The time series labeled CMC is the common mode correction that is applied. Antenna changes are marked by a letter "A" and other steps by a "∧". For NORG the harmonic component is added, see the text.

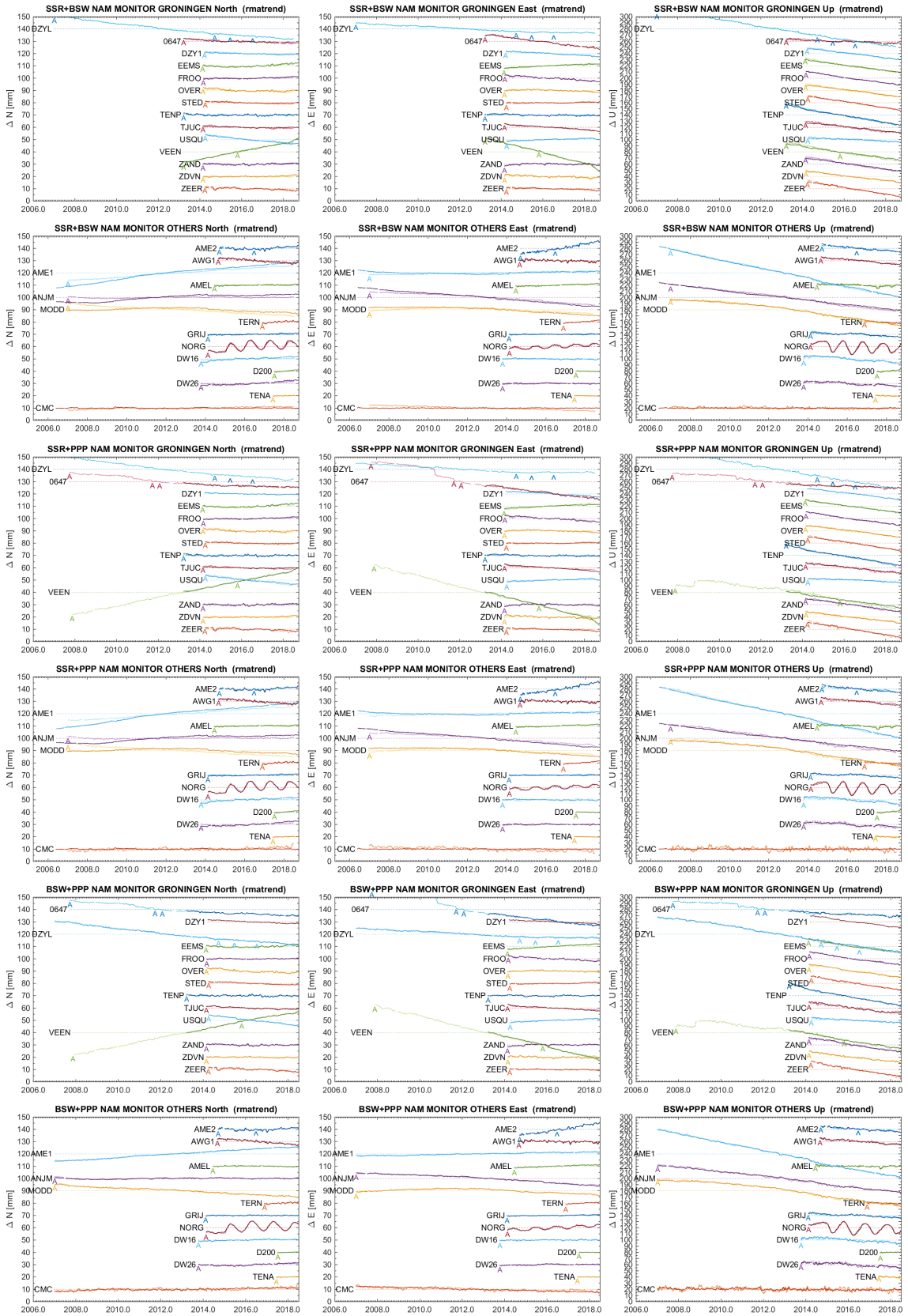

Figure 8.2: Trend plus residuals for the NAM monitoring stations after reference frame correction for the BSW and PPP solutions, smoothed using a 21 day moving average filter. Two solutions are plotted on top of each other: SSR-BSW (top), SSR-PPP (middle) and BSW-PPP (bottom). The first solution is in a darker color. The time series labeled CMC is the common mode correction that is applied. Antenna changes are marked by a letter "A" and other steps by a "∧". For NORG the harmonic component is added, see the text.

Table 8.1: Standard deviation of the difference between two solutions for the stations in the Groningen area, copied in part from Table 6.1, with the reference frame corrected results (Trend-rfc, Trend-rfc+res) added. The non reference frame corrected results are shown in gray for comparison.

	North [mm]			East [mm]			Up [mm]		
	BSW SSR	PPP SSR	PPP BSW	BSW SSR	PPP SSR	PPP BSW	BSW SSR	PPP SSR	PPP BSW
Periodic	0.2	0.3	0.1	0.2	0.2	0.2	0.4	0.5	0.5
Trend-rfc	0.5	0.5	0.2	0.3	0.5	0.2	1.1	0.9	0.7
Trend	0.4	0.5	0.6	0.3	0.3	0.5	1.3	1.4	1.3
Residual	0.5	0.8	0.6	0.4	0.6	0.5	1.4	2.4	2.0
Trend-rfc+res	0.7	0.9	0.6	0.5	0.7	0.5	1.8	2.5	2.1
Trend+res	0.6	0.9	0.8	0.5	0.6	0.7	1.9	2.7	2.4

residual). On the other hand, the station NORG is above an underground gas–storage which causes large seasonal variations. A significant part of the seasonal deformations will be absorbed in the annual and semi-annual harmonics. So, for this station, it is better not to remove the annual and semi-annual harmonics from the trend signal, and so this is included in the trend series of Figure 8.1.

The standard deviation of the differences for the Groningen stations is given in Table 8.1, which borrows some results from Table 6.1.

Comparing Figure 8.1 to Figure 6.2, and also from Table 8.1, we see that the agreement between the estimated trend of the BSW and PPP, which was already quite good, is further improved. You can also see that the visible differences in the Up component between the SSR solution and the BSW and PPP solutions is improved. However, where we had the largest trend differences between the SSR and the BSW and PPP solutions, in the North component for AME1, ANJM and MODD for 2006 until 2014, we see that the differences have increased, and there is now also a visible difference in the East component .

In Figure 8.3 and 8.4 the differences in the estimated trends of the solutions are plotted for two groups of stations after reference frame correction. Compare these to Figure 6.3 and 6.4 before reference frame correction. Figure 8.3 and 6.3 shows the differences for the subset of station in the Groningen area, with stations 0647, DZYL, DZY1, EEMS, FROO, GRIJ, OVER, STED, TENP, TJUC, USQU, VEEN, ZAND, ZDVN and ZEER. Figure 8.4 and 6.4 shows the differences in the Waddenzee area, with stations AME1, AME2, AMEL, ANJM, AWG1 and MODD . For each group of stations a time series with the daily average difference is computed, using a simple Gauss-Seidel like iterative scheme with the daily averages and an unknown station offset such that the average difference between the station and daily average time series becomes zero. The colored lines in Figure 8.3 and 8.4 are the individual station differences, the thick black lime is the time series of daily averages, and the yellow line is a moving 21 day median of the daily averages (with outlier and step detection).

The time series of daily averages and the 21 day moving medians are summarized in Figure 8.5 and 8.6 for the two groups of stations. Figure 8.7 shows the 21 day moving averages for the two groups in the same plot so that they are more easily to compare. Compare these also to Figure 6.5, 6.6 and 6.7 before the reference frame correction. The step in early 2014 in the differences with the SSR solution is related to the introduction of many new reference stations in the SSR solution, see the time line in Figure 1.2. The differences are summarized in Table 8.2, which gives the range (maximum minus minimum) of the trend differences for each combination. The range is computed from the moving 21 day median of the daily averages. Compare this to Table 6.3 before the reference frame correction.

From Figure 8.5, 8.6 and 8.7 and Table 8.2, and comparing these to the results without reference frame correction, we see that the differences between the BSW and PPP solutions for the Groningen and Waddenzee area are not only in good agreement for both area's, as we had before reference frame correction, but are now, after reference frame correction, also much closer to zero and some the long period deviations we had before have disappeared. This also implies that the BSW-SSR and PPP-

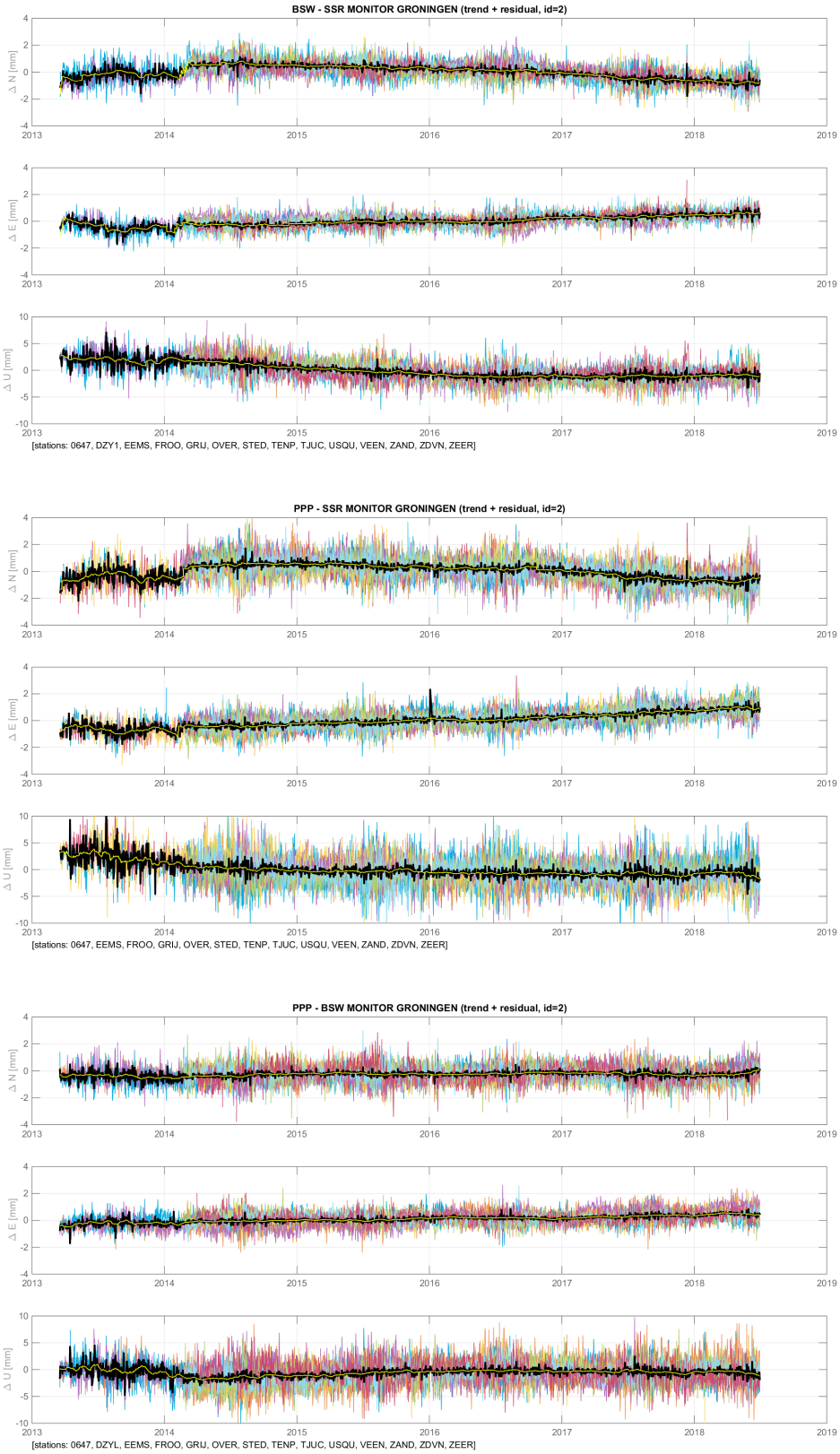

Figure 8.3: Trend difference for the Groningen monitoring stations after reference frame correction: BSW-SSR (top), PPP-SSR (middle) and PPP-BSW (bottom). The colored lines in the background are the individual station differences, the thick black line is the time series of daily averages, and the yellow line is a moving 21 day median of the daily averages (with outlier and step detection).

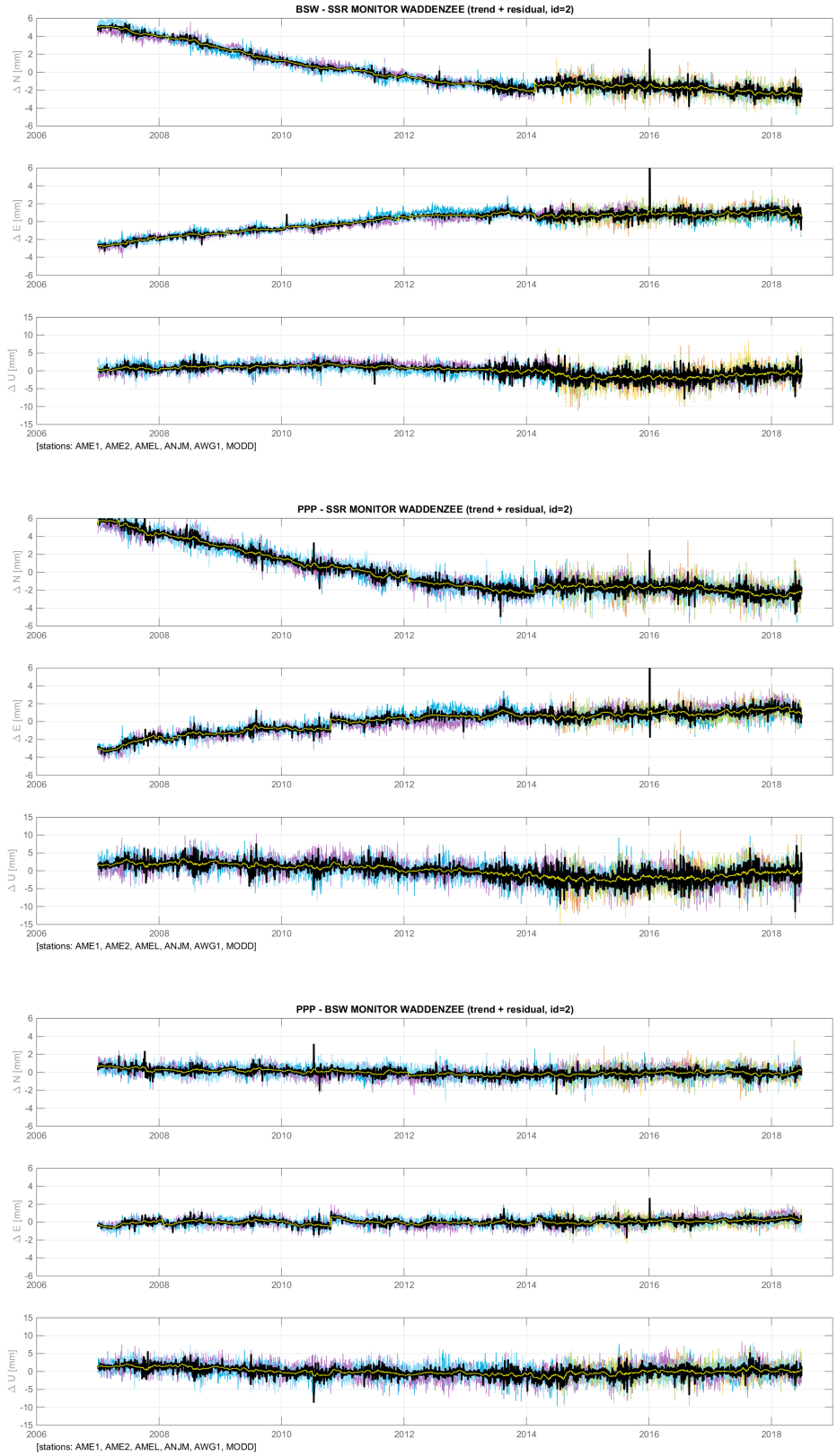

Figure 8.4: Trend difference for the Waddenzee monitoring stations after reference frame correction: BSW-SSR (top), PPP-SSR (middle) and PPP-BSW (bottom). The colored lines in the background are the individual station differences, the thick black line is the time series of daily averages, and the yellow line is a moving 21 day median of the daily averages (with outlier and step detection).

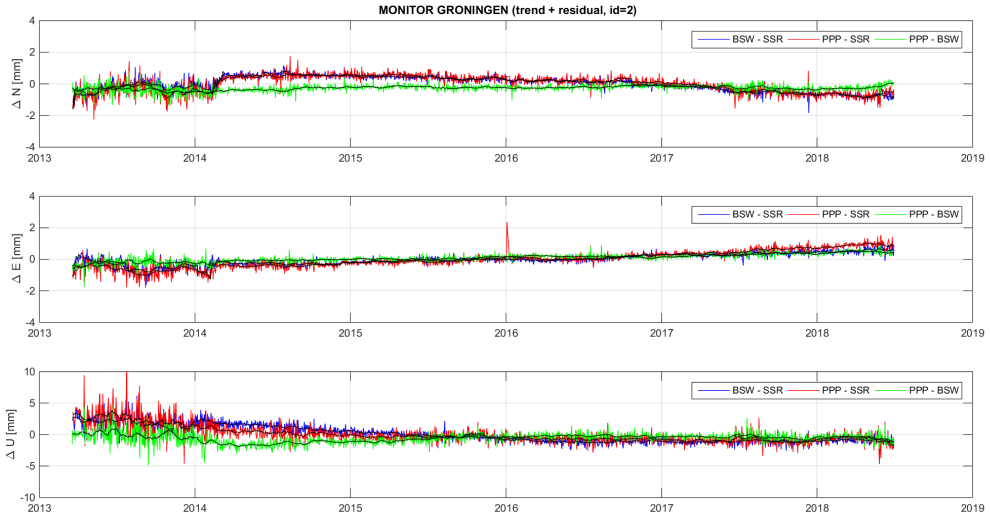

Figure 8.5: Trend differences for the Groningen monitoring stations after reference frame correction for all combinations: SUM_TREND+RESIDUAL_GRO. The colored lines are time series of daily averages for the different combinations, the black lines are the moving 21 day median of the daily averages (with outlier and step detection).

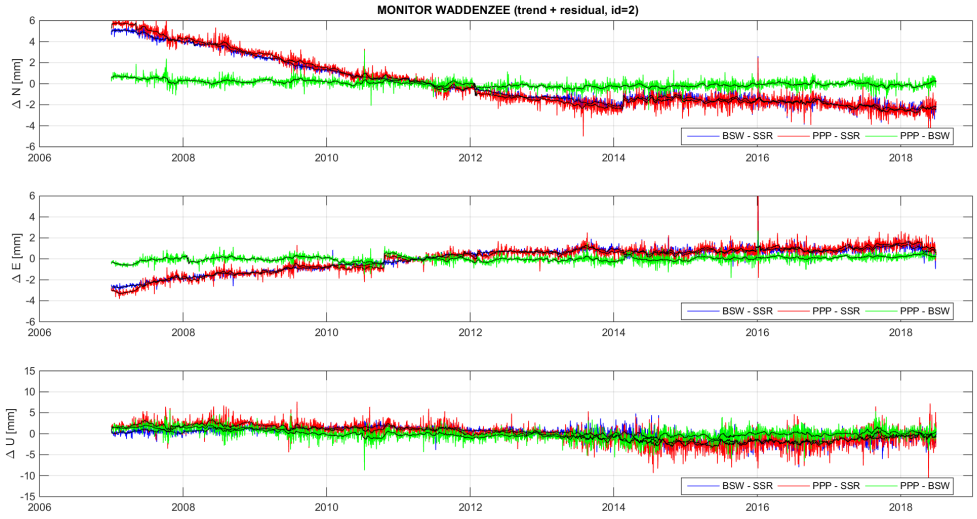

Figure 8.6: Trend differences for the Waddenzee monitoring stations after reference frame correction for all combinations: SUM_TREND+RESIDUAL_WAD. The colored lines are time series of daily averages for the different combinations, the black lines are the moving 21 day median of the daily averages (with outlier and step detection).

Table 8.2: Range (maximum minus minimum) of the mean trend difference between two solutions computed from the moving 21 day median after reference frame correction.

	North [mm]			East [mm]			Up [mm]		
	BSW SSR	PPP SSR	PPP BSW	BSW SSR	PPP SSR	PPP BSW	BSW SSR	PPP SSR	PPP BSW
Groningen (2013.3-2018.6)	2.42	2.01	0.67	1.72	2.29	1.06	4.15	5.55	2.90
Waddenzee (2013.3-2018.6)	1.60	1.68	0.88	1.05	1.51	0.85	3.40	3.96	4.03
Waddenzee (2007.0-2018.6)	7.70	8.60	1.29	4.16	4.99	1.21	4.90	6.62	4.45

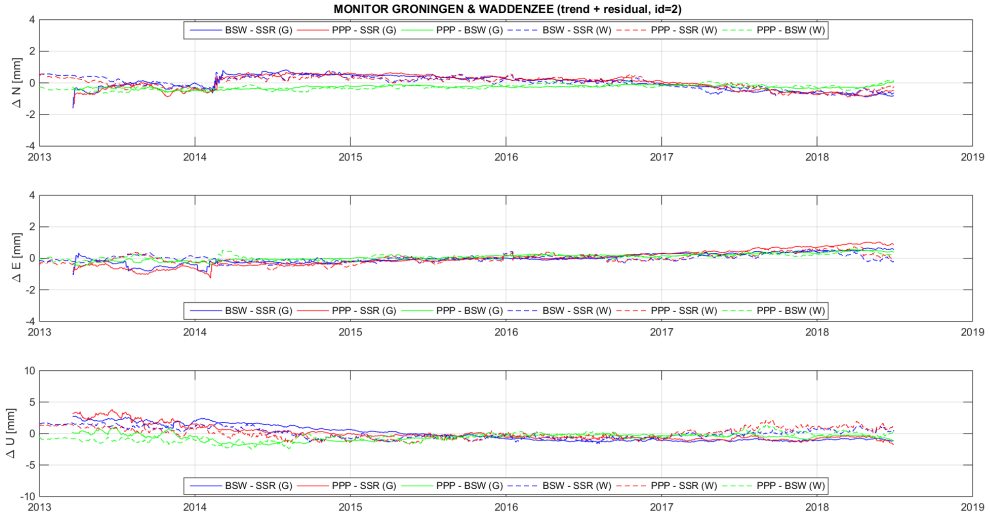

Figure 8.7: Trend differences for the Groningen (G) and Waddenzee (W) monitoring stations, after reference frame correction, for all combinations after 2013: SUM_TREND+RESIDUAL_NAM. The colored lines are time series of daily averages for the different combinations, the black lines are the moving 21 day median of the daily averages (with outlier and step detection).

SSR differences are now much closer together (for each area) than before the reference frame frame correction. However, the BSW-SSR and PPP-SSR differences, are not the same both area's. Therefore, the average trend for the Groningen and Waddenzee areas in the SSR solution is slightly different.

From Table 8.2 we conclude that, after 2013.3, the differences in the North and East component are within a range (maximum minus minimum) of 1–2.5 mm, and 3–5 mm for the height component, with the smallest differences for the horizontal components between the BSW and PPP solutions. Before the reference frame correction, see Table 6.3, these numbers were 3–4 mm for the North component, 2 mm for the East, and 5–7 mm for the Up component.

But, the largest differences are observed for the Waddenzee area over the period 2007.0-2013.3, between the SSR and BSW, and SSR and PPP, solutions. These differences became even larger after the reference frame correction for the BSW and PPP solutions. The differences between the SSR and BSW, and SSR and PPP, solutions for the Waddenzee area over the period 2007.0-2013.3, are 8-9 mm in the North, 4-5 mm in the East, and $5-7$ mm in the Up component. This can also be seen in Figure 8.6, where there a considerable differences for the horizontal components in the comparisons with the SSR solution, in particular for the North component. Compared to Figure 6.6, we can see now after the reference frame correction an almost linear trend in the North component of about 1 mm/y until early 2014. The reason for this is that, before 2014, the focus was on the vertical components and the horizontal coordinates of the NAM reference stations have not been adapted as they should have been, and some reference stations had a significant horizontal motion. Also, after 2014, new reference stations were added to the network.

Table 8.3: Mean velocity difference between two solutions after reference frame correction.

	North [mm/y]			East [mm/y]			Up [mm/y]		
	BSW SSR	PPP SSR	PPP BSW	BSW SSR	PPP SSR	PPP BSW	BSW SSR	PPP SSR	PPP BSW
Groningen (2013.3-2018.6)	-0.15	-0.09	0.04	0.19	0.31	0.14	-0.74	-0.62	0.06
Waddenzee (2013.3-2018.6)	-0.17	-0.11	0.07	0.06	0.14	0.08	-0.18	0.13	0.31
Waddenzee (2007.0-2018.6)	-0.62	-0.66	-0.05	0.30	0.32	0.03	-0.30	-0.42	-0.12

The trends for the PPP and BSW solutions show a slightly larger subsidence than the SSR solution, as can be seen also from Figure 8.7. Compared to the results before reference frame correction, see Figure 6.7, this is now even clearer for the Groningen area. This is confirmed by Table 8.3 which gives the velocity difference between each pair of solutions. The larger differences are in the Groningen area, where the mean velocity difference in the up component between the SSR solution and BSW and PPP solutions is on average 0.68 mm/y lower. Before the reference frame correction this number was 0.86 mm/y, so there is a slight improvement, but the effect remains. This means, that the SSR solution, compared to the BSW and PPP solutions, is underestimating subsidence in Groningen area by about 0.7 mm/y. We suspect this is caused by the stricter selection of reference stations for the BSW and PPP solutions, excluding some reference stations that are used in the SSR solution that have shown some subsidence themselves.

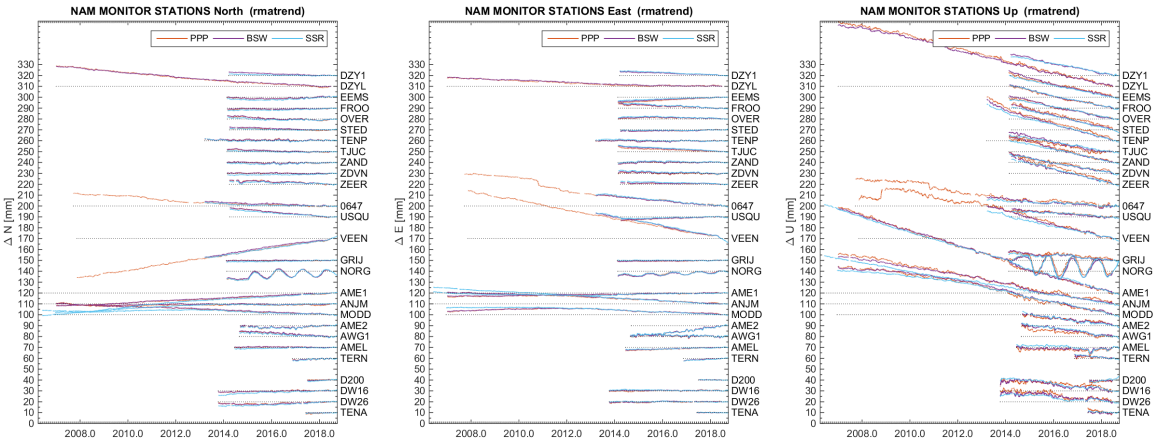

Figure 8.8: Final time series for the NAM monitoring stations, using the 21 day moving average of the trend plus residuals, with common modes removed, and after a reference frame correction for the BSW and PPP solutions: North (left), East (middle) and Up (right). For NORG the harmonic component is added.

Figure 8.2 shows the final trend series overlayed on top of each other. It is based on the same data as Figure 8.1, but the daily solutions have been smoothed using a robust 21 day moving average filter. Figure 8.8 shows the final trend series with all three solutions overlayed.

9

DISCUSSION AND CONCLUSIONS

The goal of this project is to compare existing GNSS processing methodologies, to investigate potential biases in the solutions and to obtain through the decomposition of signals transparent time series estimates for the NAM monitoring stations in the North of the Netherlands, with the final aim to detect deformation trend changes with predefined confidence levels. Three GNSS processing methods have been investigated: State–Space modeling (SSR), regional network processing with the Bernese GNSS Software (BSW), and Precise Point Positioning (PPP).

Data from the NAM monitoring stations is processed routinely by 06-GPS, on behalf of NAM, for reporting subsidence in the study area, using the SSR method implemented in the Geo++ GNSMART software [Wübbena, Bagge, and Schmitz, 2001; Henry and Dentz, 2016; Dentz and Henry, 2019]. The same network, with some additional stations, including NAM reference stations, was processed for this project also by the Dutch Kadaster, using the Bernese GNSS Software (BSW), following the guidelines from EUREF for standard regional network processing [Dach et al., 2015; Hoentjen and Huisman, 2019]. The third dataset was provided by Nevada Geodetic Laboratory (NGL), who uses the Precise Point Positioning (PPP) method, implemented in the Gipsy/Oasis software from JPL [Zumberge et al., 1997; Blewitt, Hammond, and Kreemer, 2018]. Each of the processing methods thus involves a different data provider and processing software. This resulted in three completely independently processed GNSS time series datasets that were used as input for this study.

A description of each of the processing methodologies is given in Section 3. The main characteristics were summarized in Table 1.1. There are considerable differences between the methodologies, but also similarities. Some of the underlying (physical) models are the same, or differ only in the fine details. There are substantial differences in how ionosphere delay is handled (state-space representation/ionosphere free linear combination), in the handling of troposphere delay (state-space representation/station parameters), in the estimation method (Kalman filter/batch least squares) and handling of observations and clock parameters (un-differenced/double-differences), but these differences had little impact on the final time series, except maybe for the smoothness, but the biases – if any – were not different. The most important difference, and the one that affected the final time series most, is how the reference frame is realized, and for that matter, which stations are used as reference stations. In this respect, an important influence is also the scope of the processing; local, regional or global.

The SSR processing only includes data from the NAM monitoring and reference stations, but only the coordinates of the NAM monitoring stations are estimated. The coordinates of the NAM reference stations are fixed to ''known" values. The NAM reference station coordinates are computed in a separate processing step, which is explained in Section 3.1.2. On the other hand, in the BSW and PPP processing the NAM monitor and reference stations are processed in the same way and there is no fundamental difference between them from the processing point of view. Furthermore, in the BSW processing a set of ten IGS stations is included in the processing. These stations are used to align the daily BSW solutions to the International Terrestrial Reference Frame 2008 (ITRF2008/IGb08). The

connection is made using the minimum number of constraints possible, only three shifts are estimated for each daily solution. In the PPP processing the reference frame is fully defined by the satellite orbit and clock products that are used. NGL uses satellite orbit and clock products from JPL, which have been computed by JPL using a global network of IGS stations, using a subset of selected IGS reference stations to align the products to – at the time of the project – ITRF2008.

The scope of the SSR processing is the North of the Netherlands, with a few stations over the border in Germany, whereas the scope of the BSW processing, with the IGS reference stations included, is the Western part of Europe. The PPP processing is truly global, here it doesn't matter on which continent the stations are processed, the satellite orbit and clock products that are used are determined from a global network. The way in which the reference frame is realized, and the scope of the network, has a big impact on the noise properties of the GNSS time series computed by each of the processing methods. From the results in this report we find that the global PPP solution is noisier than the SSR method, and that the regional BSW solution is somewhere in between. But also, for nearby stations, like the North of the Netherlands, the errors in the PPP and BSW solutions are strongly correlated. The spatial correlation is largest for the PPP, followed by the BSW, and the smallest for the SSR. Therefore, the errors in the PPP and BSW solution can be reduced significantly by removing the spatially correlated, or common mode, errors, and thus improving the noise properties of these methods.

Each time series is the result of different physical processes that are related to the deep-underground, shallow sub-surface, or the construction with the GNSS antenna (monument motion). There are also effects from tidal and atmospheric loading on the time series. Other components in the time series are the result of observational processes or artifacts from the processing that have no physical meaning in the sense of deformation or subsidence. These effects are mainly caused by model imperfections, which, in combination with a satellite constellation that has a repeat period of one draconitic year (351 days), results in spurious signals with frequencies of one year and higher. Ideally, these effects should be removed from the time series in order to obtain clean and transparent time series. How, and what, to remove, depends on the application at hand. In this project, the aim is to produce transparent time series that represent processes related to the deep underground. But, although components associated to monument motion and loading effects, as well as some artifacts from the processing, can be removed quite well, it is not possible to separate between deformation processes from the deep underground and shallow sub-surface.

The time series decomposition is key to understanding the time series, as well as for dealing with common mode errors and separating the different processes (See Section 5). The time series in each input dataset is decomposed into several components: long term trend using a spline function, annual and semi-annual components, temperature influence, atmospheric loading, time series steps, and residuals of the fit. Temperature and pressure data is used to estimate the temperature influence and atmospheric loading. In the first iteration also two common mode components are estimated: the common mode in the residuals (residual stack), and common mode of the periodic parameters (harmonics, temperature influence, and atmospheric loading). Common modes are signals that are the same for the region of interest, or, have a common cause, and are present in all the stations. For the estimation of the common mode a subset of well behaving stations is used. In the second iteration the common mode is removed, providing the final decomposition. Removing these two common modes reduces the noise in the time series, but it does not affect the estimated long term trends. After removing the common modes it becomes also possible to compare the periodic components in the solutions.

In dealing with several datasets it is necessary to harmonize the station names, so that the different datasets use the same names for stations. This happened with the NAM stations `DZYL` and `SCHI`, which were renamed to respectively `DZY1` and `SCH1`. In this report the stations `DZYL` and `SCHI` refer to the nearby NETPOS and AGRS.NL stations, that have also been used in the analysis.

The results of the decomposition are given in Section 6 and 7 for respectively the NAM monitoring and reference stations. The main findings and conclusions from the time series decomposition are

Outlier and step detection Outliers were successfully removed using a moving median filter on the residuals of the decomposition. No user intervention, apart from selecting the rejection level and filter length, was needed. Most outliers were removed in a single iteration.

Several, formerly unknown steps, were also identified by the moving median filter (using step detection algorithms). The newly detected steps, if confirmed by the author, were added to the list of events in the meta data, and the decomposition was runs again including the newly detected steps.

Steps The decomposition was successful in estimating the size of each step in the time series. Steps occur every time an antenna is changed, but also, a few other steps were detected in the processing (see previous point). The start time of a step was taken from the meta data. The estimated size of the step, for steps associated to an antenna replacement, was slightly different in the three solutions, especially in the height coordinate. We believe this is related to the fact that the solutions may have used different antenna models, with different phase center offsets and variations. For steps associated to other events the agreement between the solutions was much better.

Common mode signal The common modes in the three processing chains are very different; this is the case for the residual stack as well as for the periodic common mode parameters. The common mode in the PPP solution is the largest of the three. The common mode observed in the BSW is smaller than the PPP common mode. There is hardly any common mode in the SSR solution. After removing the common mode in the harmonic, temperature influence and atmospheric loading parameters, the periodic component of the three solutions are virtually the same (see next point).

Removing the residual stack improves the noise in the solutions, as can be observed from the residuals and periodograms. The biggest impact was for the PPP solution, followed by the BSW, and there was hardly any improvement for the SSR solution. After removing the residual stack, the noise figures of the PPP and BSW were reduced, but the noise figure in the PPP was still slightly larger than the noise figure of the BSW, and the BSW larger than the noise figure of the SSR solution.

One iteration was enough to remove all of the common modes.

Periodic component (Harmonics, temperature influence and atmospheric loading) The agreement between the three processing chains in the periodic components (after removal of the common modes) is very good. The standard deviation of the differences are below 0.3 mm for the horizontal components, and 0.4–0.5 mm for the vertical component. All three processing chains, after removal of the common mode in the periodic component, estimate the same annual signal, semi-annual signal, temperature influence and atmospheric loading for each station.

Periodograms Removing the residual stack after the first iteration resulted in an improvement in the periodograms for the PPP and BSW solutions.

The final attained noise level is the smallest for the SSR solution, followed by the BSW and then the PPP solution. The three periodograms are dominated by flicker noise for frequencies between 0.5 and 10-20 cycles/year. For frequencies above 10-20 cycles/year, the BSW and PPP solutions basically are white noise, whereas the SSR solution has flicker noise in the horizontal components and brown (random walk) noise in the up component.

Composition of the trend signal The trend is composed of two components: the estimated trend function (spline function) with the residuals of the decomposition added to it. The reason for adding the residuals is that the residuals may still contain a signal that has not been taken care of in the decomposition. This is illustrated clearly by the station `VEEN`, which had a significant change in its horizontal velocity in early 2018. This would be missed completely if only the

trend function is considered, but, is captured well in the composite signal. The temperature influence and atmospheric loading are not considered to be part of the trend signal in this project, because they are not related to the deep underground.

What to do with the annual and semi-annual harmonics is something more open to debate. For almost all stations, except NORG, the periodicity can be modeled by annual and semi-annual harmonic, temperature influence and atmospheric loading. It is a different story for station NORG, which is above an underground gas–storage which causes large seasonal variations. Here we see that the annual and semi-annual harmonics do not capture the variations very well, and that a significant part of the variations remain in the residuals. This leads us to believe that, for all stations except NORG, the annual and semi-annual terms are not real motions of the stations, but rather artifacts from the processing, related to multipath and unmodelled effects, which cause biases with periods close to the solar year. However, if there is a real annual and semi-annual motion in the station, this cannot be separated from the above mentioned artifacts. On the other hand, for NORG, which has, compared to other stations, relatively large harmonic components, and variations that are not fitted by the model, we believe that the best trend model is the composite of the trend function, the estimated annual and semi-annual components, and the residuals. That some part of the periodicity, caused by station multipath and other effects is leaked into the trend, is something that we have to accept in this case.

Trend differences In a general sense the solutions agree well in the estimated trend signal (the composite of the trend function and residuals). However, looking to the series in more detail, subtle differences can be observed.

Most of the differences can be explained by a common trend difference between the solutions, computed by taking the average over a subset of the stations, which are discussed in the next point. The remaining differences, after removal of an average trend common to all stations, are less than 1 mm for the horizontal components and 2 mm for the vertical components (95% reliability interval, computed from the standard deviations in Table 8.1).

Average trend differences Although both the BSW and PPP solutions are computed in a similar (ITRF2008 based) reference frame, the average trend difference between the BSW and PPP solution is not negligible. But, the average trend difference between the BSW and PPP solution is basically the same for three different subsets of stations: NAM monitor stations in Groningen, NAM monitor stations in the Waddenzee area, and the NAM reference stations. This is not the case for the SSR-BSW and SSR-PPP differences: here the difference in the average trend is not only larger, it is also not the same for the Groningen and Waddenzee area. This learns us that there are subtle differences in the reference frame realization for the SSR, BSW and PPP solution. For the BSW and PPP solutions these affect all the stations in a similar way (homogeneous), but this is not the case for the SSR solution.

The average trend differences have been analyzed before and after connecting the BSW and PPP solutions to a selected set of 7 NAM reference stations. For stations in the Groningen area, the differences (maximum minus minimum value) in the North and East component before the reference frame correction are in the range of 3–4 mm and 2 mm respectively, and 5–7 mm for the height component, with the largest differences between the PPP and SSR solution. After the reference frame correction, the differences in the North and East component over the period 2013.3-2018.6 are within a range (maximum minus minimum) of 1–2.5 mm, and 3–5 mm for the height component, with the smallest differences for the horizontal components between the BSW and PPP solutions. Larger differences are observed between the SSR and BSW, and SSR and PPP, solutions for the Waddenzee area over the period 2007.0-2013.3: 8-9 mm in the North, 4-5 mm in the East, and $5-7$ mm in the Up component. There is an almost linear trend in the North component of about 1 mm/y until early 2014.

The reason for this is that, before 2014, the focus was on the vertical components and the horizontal coordinates of the NAM reference stations have not been adapted as they should have been, and some reference stations had a significant horizontal motion. Also, after 2014, new reference stations were added to the network, and two reference stations where ''demoted" to monitoring station.

Average subsidence rate The SSR solution shows a slightly lower subsidence rate than the BSW or PPP solutions. The average subsidence rate of the SSR solution in the Groningen area is 0.68 mm/y lower than the subsidence rates for the reference frame corrected BSW and PPP solutions. With respect to ITRF2008 the average subsidence rate difference is 0.86 mm/y (with the same sign). This means, that the SSR solution, compared to the BSW and PPP solutions, is underestimating subsidence in Groningen area by a small amount. We suspect this difference is caused by a few reference stations in the SSR solution that have shown some subsidence themselves (either by deep or shallow causes), but which have been excluded as reference stations for the reference frame corrected BSW and PPP solutions.

The NAM reference stations are processed in the BSW and PPP processing, and have been compared with each other, as well as the reference station coordinates used by the SSR processing. They have also been used to analyze the stability of the NAM reference stations and to connect the BSW and PPP solutions to a selected subset of reference stations (the so called reference frame correction). The results have been discussed in Section 7. The impact of the reference frame corrections was analyzed in Section 8, from which some results have already been mentioned earlier in this section. The main findings and conclusions from the reference station analysis are:

SSR reference station coordinates The SSRref reference station coordinates have been compared to the BSW and PPP trend+residual solutions. The results should be interpreted with great caution. The effect of an antenna change has been removed in the BSW and PPP series by estimating a step, but this is not the case for the reference station coordinates in SSRref. Unfortunately, the current procedure did not allow to separate the effect of antenna changes from reference station movement in the SSR reference station coordinates. So it was not possible to do a proper analysis of the SSR reference station coordinates. We recommend to change the procedure for computing new reference station coordinates after an antenna change, by including data both directly before and after the change in antenna, so that is becomes possible to separate the effect of antenna changes from reference station motion.

Connection of the BSW and PPP solution to reference stations Although both the BSW and PPP solutions are computed in a similar (ITRF2008 based) reference frame, the average trends for the NAM reference stations is not the same, which implies that there are subtle differences in the realization of the reference frame. Therefore, in order to obtain a fair comparison, and to obtain realistic trend estimates and subsidence rates with respect to stable reference stations in the Netherlands, it is necessary to connect the the BSW and PPP solutions to a subset of stable reference stations.

For every day a shift in the North, East an Up components is computed by taking the average (or median) over the decomposed trend series (trend function plus residuals) for a subset of reference stations. The main challenge is to select the proper subset of stable reference stations. The approach we used in this report is to start with an initial selection and to remove reference stations successively, starting with the one that has the largest deviations, until a satisfactory selection is obtained. Initially the median is used to obtain the time series of daily shifts, but in the final selection the average is used. The final selection of 7 reference stations consisted of `0645`, `0683`, `BEIL`, `MAKK`, `NIEU`, `URK2` and `WSRA`. All stations on the wadden islands in the North have been removed, but this is not a problem, because an uniform translation is computed for all stations without deforming the station network.

The average velocity in the North, East and Up components for the selected reference stations is 0.20, −0.42 and −0.25 mm/y for the BSW solutions, and 0.21, −0.35 and −0.27 mm/y for the PPP solution. If we take the average for the vertical component, we can conclude that the average vertical velocity of the selected 7 reference stations is about −0.26 mm/y with respect to ITRF2008.

The time series of daily shifts can be used as reference frame corrections for the other stations. All stations are shifted by the same amount. However, the shifts are not the same for the BSW and PPP solutions. For the actual reference frame correction we further advise to smooth the daily shifts. We selected to use a 365 day moving average. The main reason for this is that we believe that only the estimated trend functions should be affected; we don't want to change the periodic components, steps and residuals from the decomposition.

Applying the reference frame corrections resulted in a significant improvement in the average observed trends for the BSW and PPP solutions.

The goal of this project, compare GNSS processing methodologies, investigate potential biases and to obtain transparent time series estimates through time series decomposition, we believe, has been achieved. However, did we achieve the final aim, to be able to detect deformation trend changes with predefined confidence levels?

The set up of our trend model, which consists of spline functions with the residuals added, which is identical to removing the common modes in the residuals, annual and semi-annual harmonics, temperature influence, atmospheric loading, steps, and outliers, takes trend changes explicitly into account. The model can accommodate slow changes in the trends through the spline function, but also discontinuities in the velocity are not lost because of the residuals. To be able to give confidence values for the trend series the stochastic model is needed. The stochastic model follows from the estimated periodograms: the temporal correlation at the mid range frequencies can be described by a flicker noise, whereas the higher frequency component, above a certain cutoff frequency, is either white noise, flicker noise or brown noise, depending on the type of coordinate and the processing method. The lower frequencies in the periodogram can be ignored as these are absorbed in the trend function.

Trend changes can be detected in principle by hypothesis tests that involve the estimated trend series, using confidence levels that follow from the stochastic model of the trend series. The implementation for detecting sudden changes might not be straightforward: for the null-hypothesis we have our original model, the alternative hypothesis would be the same model, but with an additional break-point (at the time of suspected change) added, but then, what if this is close to an already existing break-point. Maybe a higher order spline function would help. Detecting slow changes (over a time period of two years) may be easier: this would simply amount to computing the velocity difference between two spline segments with its confidence parameters. This is something that needs further investigation.

Furthermore, it is also possible to down-sample the trend series using moving medians or averages. A good choice for the window length would be 21 days, as this is around the high frequency cut-off of the flicker noise component.

Finally, we observed that the SSR solution is very sensitive to the choice of reference station coordinates. In the first part of the dataset there weren't so many changes in the reference station coordinates, and maybe not enough so far the horizontal components are concerned. In later years we see that coordinate changes become more frequent.

Since the coordinates of the NAM reference stations are a critical aspect in the whole SSR processing we recommend a review of the procedure. Aspects that should be taken into consideration are the 2 mm level threshold that is used for the coordinates, whether the threshold should be the same for both the horizontal and vertical coordinates, or should there be a threshold at all, why not simply update the coordinates once per year, or even more often. From an analysis point of view it would be good to be able to separate between changes in the reference station coordinates due to

an antenna change, and changes due to actual movement of the station. For this we recommend a change in procedure as well, by including data both directly before and after the change in antenna, in order to separate the effect of antenna changes from reference station motion.

The whole process of selecting subsets of reference station for the BSW and PPP solutions is not very satisfactory and to some extent rather subjective. Our objective is to compute the average trend with respect to an ensemble of reference stations, which each may have some autonomous motion. Therefore, we should use as many reference stations as possible, and only deselect stations when there are good grounds to do so, so that the effect of autonomous reference station motion is randomized and averaged out. Despite the fact that no formal testing was done on the suitability as reference station, we believe our overall objective is achieved with the final selection of 7 reference stations. However, we recommend that a more formal and less subjective procedure, using statistical testing, for selecting the subset of reference stations is developed. Having such a procedure in place it becomes possible to use many more candidate reference stations, such as AGRS.NL, NETPOS and other 06-GPS stations that are part of the BSW and/or PPP solutions. It might also be possible to apply the same procedure for selecting reference stations in the SSR solutions.

ACKNOWLEDGMENTS

The studies described in this report have been made possible by the contributions from the following parties: placement and processing of GNSS receivers by 06-GPS B.V.; GNSS regional network processing by the Dutch Kadaster, and GNSS Precise Point Positioning processing by Nevada Geodetic Laboratory.

REFERENCES

Altamimi, Zuheir, Xavier Collilieux, and Laurent Métivier (2011). "ITRF2008: an improved solution of the international terrestrial reference frame". In: *Journal of Geodesy* 85.8, pp. 457–473. DOI: 10.1007/s00190-011-0444-4.

Altamimi, Zuheir et al. (2016). "ITRF2014: A new release of the International Terrestrial Reference Frame modeling nonlinear station motions". In: *Journal of Geophysical Research: Solid Earth* 121.8, pp. 6109–6131. DOI: 10.1002/2016jb013098.

Blewitt, Geoffrey, William Hammond, and Corné Kreemer (2018). "Harnessing the GPS Data Explosion for Interdisciplinary Science". In: *Eos* 99. DOI: 10.1029/2018eo104623.

Bruyninx, C. et al. (2009). "The European Reference Frame: Maintenance and Products". In: *Geodetic Reference Frames*. Springer Berlin Heidelberg, pp. 131–136. DOI: 10.1007/978-3-642-00860-3_20.

Bruyninx, Carine et al. (2019). "GNSS metadata and data validation in the EUREF Permanent Network". In: *GPS Solutions* 23.4. DOI: 10.1007/s10291-019-0880-9.

Dach, R. et al. (2015). *Bernese GNSS Software Version 5.2. User manual*. University of Bern, Bern Open Publishing.

Dentz, Frank (2019). *Private communication*. E-mail, 15 July 2019, 20 January 2020.

Dentz, Frank and Jean-Paul Henry (2019). *Check reference station coordinates NAM*. Tech. rep. Version 1.11, Jun 24, 2019. 06-GPS.

Dow, John M., R. E. Neilan, and C. Rizos (2009). "The International GNSS Service in a changing landscape of Global Navigation Satellite Systems". In: *Journal of Geodesy* 83.3-4, pp. 191–198. DOI: 10.1007/s00190-008-0300-3.

Fokker, Peter A. et al. (2018). "Subsidence in the Dutch Wadden Sea". In: *Netherlands Journal of Geosciences* 97.3, pp. 129–181. DOI: 10.1017/njg.2018.9.

GeoService (2006a). *Continuous Object Monitoring with GPS at ANJM*. Tech. rep. GeoService, Gesellschaft für satellitengestützte Vermessungen mbH, Garbsen Germany.

— (2006b). *Continuous Object Monitoring with GPS at ANJM - Extension 1* -. Tech. rep. GeoService, Gesellschaft für satellitengestützte Vermessungen mbH, Garbsen Germany.

Hanssen, Ramon (2019). "A radar retroreflector device and a method of preparing a radar retroreflector device." English. Pat. Patent No. 2019103 (IPC No. P115850NL00).

Henry, Jean-Paul and Frank Dentz (2016). *GPS Survey NAM Waddenzee*. Tech. rep. Version 1.20, Jan 14, 2016. 06-GPS.

Hoentjen, Kees and Lennard Huisman (2019). *GNSS-Processing in context with the ´Study and Data Acquisition Plan´ related to the Production plan ´Winningsplan´ Groningen*. Tech. rep. Kadaster, Geo- en Vastgoedinformatie en Advies, Materiebeleid GRS.

Kamphuis, Jurjen C. (2019). "Co-location of geodetic reference points: On the design and performance of an Integrated Geodetic Reference Station". MA thesis. Delft University of Technology.

Leijen, Freek van et al. (2017). *Uniformization of Geodetic data for deformation analysis. Contribution to the research project: Second phase of the long-term subsidence study in the Wadden Sea region (LTS2)*. Tech. rep. Final Report, v1.0, 19 January 2017. Geoscience and Remote Sensing, Delft University of Technology.

Marel, H. van der et al. (2016). *Na-ijlende gevolgen steenkolenwinning Zuid-Limburg, Final report on the results of the working group 5.2.1 - ground movements*. Tech. rep. Projectgroup Na-ijlende gevolven van de steenkolenwinning in Zuid-Limburg (GS-ZL). Delft University of Technology / GeoControl / Ingenieurburo Heitfeld Schetelig GmbH.

Marel, Hans van der (2015). *GNSS Processing Groningen – Rapport voor Staatstoezicht op de Mijnen (SodM)*. Tech. rep. Versie 1.1 (29 Oktober 2015; herzien 8 November 2015. Geoscience and Remote Sensing, Technische Universiteit Delft.

Teunissen, Peter J.G. and Oliver Montenbruck, eds. (2017). *Springer Handbook of Global Navigation Satellite Systems*. Springer International Publishing. DOI: 10.1007/978-3-319-42928-1.

Williams, Simon (2015). *Description of GPS uncertainties within the Long Term Study on Anomalous Time-Dependent Subsidence*. Tech. rep. Literature Review of the Major Signals in GPS Coordinate Time Series. Nat. Oceanographic Centre, Liverpool.

Wübbena, G., A. Bagge, and M. Schmitz (2001). "RTK networks based on Geo++ GNSMART - concepts, implementation, results". In: *Proceedings of ION GPS*.

Zumberge, J.F. et al. (1997). "Precise point positioning for the efficient and robust analysis of GPS data from large networks". In: *Journal of Geophysical Research, Solid Earth* 102.B3, pp. 5005–5017.

A

RECEIVER AND ANTENNA META DATA

Table A.1, Table A.2 and Table A.3 give the meta data for respectively the NAM monitoring stations, NAM reference stations and the additional stations DZYL, SCHI and WSRT. In each Table the receiver and antenna type is given, with the date of the change. If a cell is empty, the antenna or receiver type is the same as above (has not been changed). If the same antenna type, or receiver type, appears for a station, it means that the antenna or receiver was changed for an identical type, or that the antenna height was changed.

All antenna changes correspond to a step in the time series. The magnitude of the steps have been estimated in the processing. However, during the processing a few steps have been identified which didn't correspond to a documented antenna change. These events have been indicated in the last column of the tables (STEP). The reason for these steps is unknown. Receiver changes usually do not result in a step. If there was some other reason for a step this is also indicated in the last column.

A.1. MONITORING STATIONS

Table A.1: Receiver and antenna types used by the NAM monitoring stations. A step in the time series is introduced at every antenna change and at indicated events in last column.

Id	Start date	Receiver type	Antenna type	Other
0647	2013-03-19T00:00Z	LEICA GRX1200+GNSS	LEIAR25.R4 LEIT	REF → MON
	2015-06-25T00:00Z	SEPT POLARX4		
AME1	2006-05-09T00:00Z	TPS GB-1000	TPSCR3_GGD CONE	
	2017-04-26T08:28Z	TPS EG3_OEM		
AME2	2014-09-12T13:28Z	TPS EG3_OEM	TPSCR.G5 TPSH	
	2016-06-25T00:00Z			STEP
AMEL	2014-06-16T00:00Z	LEICA GR25	LEIAR25.R4 LEIT	
	2016-07-14T00:00Z	TRIMBLE NETR9		
ANJM	2006-06-01T00:00Z	TPS GB-1000	TPSCR3_GGD CONE	
	2015-10-29T00:00Z	TPS EG3_OEM		
AWG1	2014-08-27T12:03Z	TPS EG3_OEM	TPSCR.G5 TPSH	
D200	2017-07-05T10:18Z	TPS EG3_OEM	TPSCR.G3 TPSH	
DW16	2013-10-10T11:30Z	TPS EG3_OEM	TPSCR.G5 TPSH	
DW26	2013-10-10T11:38Z	TPS EG3_OEM	TPSCR.G5 TPSH	
DZY1	2014-03-19T00:00Z	TPS EG3_OEM	TPSCR.G5 TPSH	
EEMS	2014-02-18T11:42Z	TPS EG3_OEM	TPSCR.G5 TPSH	
FROO	2014-02-28T10:27Z	TPS EG3_OEM	TPSCR.G5 TPSH	
GRIJ	2014-02-11T14:15Z	TPS EG3_OEM	TPSCR.G5 TPSH	
MODD	2006-12-14T00:00Z	TPS GB-1000	TPSCR3_GGD CONE	
	2013-04-18T00:00Z	TPS EG3_OEM		
NORG	2014-02-17T15:08Z	TPS EG3_OEM	TPSCR.G5 TPSH	
OVER	2014-02-24T10:43Z	TPS EG3_OEM	TPSCR.G5 TPSH	
STED	2014-03-31T12:38Z	TPS EG3_OEM	TPSCR.G5 TPSH	

Continued on next page

Table A.1 – *Continued from previous page*

TENA	2017-06-08T11:48Z	TPS EG3_OEM	TPSCR.G3 TPSH	
TENP	2013-03-18T14:26Z	TPS EG3_OEM	TPSCR.G5 TPSH	
TERN	2016-11-17T12:06Z	TPS EG3_OEM	TPSCR.G5 TPSH	
TJUC	2014-02-21T10:58Z	TPS EG3_OEM	TPSCR.G5 TPSH	
USQU	2014-04-04T00:00Z	TPS EG3_OEM	TPSCR.G5 TPSH	
VEEN	2013-03-19T00:00Z	TPS GB-1000	TPSCR.G3 TPSH	REF → MON
	2015-10-22T00:00Z		TPSCR.G5 TPSH	
ZAND	2014-02-21T10:23Z	TPS EG3_OEM	TPSCR.G5 TPSH	
ZDVN	2014-02-25T10:06Z	TPS EG3_OEM	TPSCR.G5 TPSH	
ZEER	2014-03-30T00:00Z	TPS EG3_OEM	TPSCR.G5 TPSH	

A.2. REFERENCE STATIONS

Table A.2: Receiver and antenna types used by the NAM reference stations. The steps indicated in the last column have been detected by the BSW and PPP processing.

Id	Start date	Receiver type	Antenna type	Other
0645	2013-05-13T00:00Z	UNKNOWN	UNKNOWN	
	2014-09-01T00:00Z	LEICA GRX1200+GNSS	LEIAR25.R4 LEIT	
	2015-06-24T00:00Z	SEPT POLARX4		
	2018-01-24T00:00Z			STEP
0647	2002-11-19T00:00Z	GNREF	GPPNULLANTENNA	
	2007-09-23T00:00Z	LEICA GRX1200GGPRO	LEIAT504GG LEIS	
	2010-08-27T00:00Z			
	2010-10-22T00:00Z			STEP
	2011-09-21T00:00Z		LEIAR25.R4 LEIT	
	2013-03-19T00:00Z			REF → MON
	2015-06-25T00:00Z	SEPT POLARX4		
0683	2003-02-01T00:00Z	UNKNOWN	UNKNOWN	
	2007-09-23T00:00Z	LEICA GRX1200GGPRO	LEIAT504GG LEIS	
	2010-06-24T00:00Z	LEICA GRX1200+GNSS		
	2011-05-19T00:00Z			STEP
	2011-09-21T00:00Z		LEIAR25.R4 LEIT	
	2015-06-24T09:38Z	SEPT POLARX4		
0687	2000-11-01T00:00Z	GNREF	GPPNULLANTENNA	
	2007-06-05T00:00Z	LEICA GRX1200GGPRO	LEIAT504GG LEIS	*)
	2010-08-27T00:00Z	LEICA GRX1200+GNSS		
	2010-10-22T00:00Z		LEIAR25.R4 LEIT	
	2015-06-26T00:00Z	SEPT POLARX4		
BALL	2002-12-06T00:00Z	GNREF	GPPNULLANTENNA	
	2006-05-14T00:00Z	TPS GB-1000	TPSCR3_GGD CONE	*)
	2010-08-27T00:00Z	TPS LEGACY		
	2016-08-18T10:53Z		TPSCR.G5 TPSH	
	2017-05-18T00:00Z	TPS NET-G5		
	2017-07-01T00:00Z	TPS LEGACY		
BEIL	2002-11-18T00:00Z	GNREF	GPPNULLANTENNA	
	2007-09-23T00:00Z	TPS GB-1000	TPSCR3_GGD CONE	
	2014-09-20T00:00Z	TPS E_GGD		
	2015-12-23T00:00Z		TPSCR.G5 TPSH	
	2018-10-08T00:00Z	TPS NET-G5		
DRAC	2005-04-28T00:00Z	GNREF	GPPNULLANTENNA	
	2006-05-14T00:00Z	TPS GB-1000	TPSCR3_GGD CONE	*)
	2016-09-16T00:00Z		TPSCR.G5 TPSH	
MAKK	2007-09-23T00:00Z	TPS GB-1000	TPSCR.G3 TPSH	
	2015-10-29T00:00Z	TPS E_GGD	TPSCR.G5 TPSH	
NIEU	2008-05-09T10:37Z	TPS ODYSSEY_E	TPSCR.G3 TPSH	
	2014-09-20T00:00Z	TPS EG3_OEM		
	2015-12-31T00:00Z	TPS E_GGD	TPSCR.G5 TPSH	Re-located **)
	2016-03-22T00:00Z	TPS NET-G5		
	2016-08-02T00:00Z	TPS E_GGD		
	2016-12-17T00:00Z	TPS NET-G5		

Continued on next page

Table A.2 – *Continued from previous page*

	2018-01-27T00:00Z	TPS E_GGD		
	2018-10-08T00:00Z	TPS NET-G5		
SCH1	2006-05-02T00:00Z	TPS GB-1000	TPSCR3_GGD CONE	
	2012-01-29T00:00Z	TPS EG3_OEM		
TERS	1996-10-30T14:00Z	ROGUE SNR-12 RM	AOAD/M_T DUTD	
	2000-04-27T10:50Z	TRIMBLE 4700	TRM29659.00 UNAV	
	2004-03-24T14:30Z		TRM29659.00 UNAV	
	2008-09-16T07:30Z	TPS ODYSSEY_E		
	2013-08-30T00:00Z	SEPT POLARX4		
	2014-06-07T14:30Z		LEIAR25.R4 LEIT	
URK2	2011-11-13T00:00Z	TPS GB-1000	TPSCR.G3 TPSH	
	2016-01-13T00:00Z		TPSCR.G5 TPSH	
VEEN	2007-11-13T00:00Z	TPS GB-1000	TPSCR.G3 TPSH	
	2009-10-31T00:00Z	TPS GB-1000		
	2013-03-19T00:00Z			REF → MON
	2015-10-22T00:00Z		TPSCR.G5 TPSH	
WSRA	1997-05-16T00:00Z	ROGUE SNR-12	AOAD/M_T DUTD	
	1998-03-17T15:09Z		AOAD/M_T DUTD	
	2000-01-06T00:00Z	AOA SNR-12 ACT		
	2000-04-28T00:00Z	TRIMBLE 4700		
	2015-02-11T00:00Z	TRIMBLE NETR9		

*) For the NAM dataset. For the 06-GPS dataset the change occurs at 2007-09-23T00:00Z.
**) NIEU was re-located on 2015-12-31T00:00Z (2015-11-29T00:00Z according to refcheck document).

A.3. OTHERS

Table A.3: Receiver and antenna types for the stations DZYL (Netpos), SCHI (AGRS) and WSRT (IGS). These stations are not part of the SSR solution, but are included in the BSW and PPP solutions. DZYL is near the NAM monitoring station DZY1 and SCHI is located on the same building as the NAM reference station SCH1. WSRT (IGS) shares the antenna with the AGRS station WSRA (which is used as reference station in the SSR solution). WSRT has been processed instead of WSRA in the PPP processing.

Id	**Start date**	**Receiver type**	**Antenna type**	**Other**
DZYL	2005-09-20T00:00Z	TPS ODYSSEY_E	TPSPG_A1+M NONE	
	2014-09-18T06:02Z	LEICA GR25	LEIAR20+S10 LEIM	
	2015-06-19T06:02Z			STEP
	2016-07-14T00:00Z			STEP
	2016-07-14T00:00Z	TRIMBLE NETR9		
SCHI	2005-09-20T00:00Z	TPS ODYSSEY_E	TPSPG_A1+M NONE	
	2008-05-30T00:00Z			STEP
	2011-08-04T00:00Z		TPSCR.G3 TPSH	
	2014-09-03T00:00Z	LEICA GR25		
	2016-07-13T00:00Z	LEICA GR50		
WSRT	1997-06-01T12:00Z	ROGUE SNR-12 RM	AOAD/M_T DUTD	
	1998-03-17T15:09Z		AOAD/M_T DUTD	
	2000-01-05T14:46Z	AOA SNR-12 ACT		
	2017-11-27T17:00Z	TRIMBLE NETR9		
	2018-12-17T00:00Z	SEPT POLARX5		